WIRELESS POWER TRANSMISSION BASED ON RETRO-REFLECTIVE ANTENNA ARRAY

by

SHAOSHU SHA

Presented to the Faculty of the Graduate School of

The University of Texas at Arlington in Partial Fulfillment

of the Requirements

for the Degree of

DOCTOR OF PHILOSOPHY

THE UNIVERSITY OF TEXAS AT ARLINGTON

December 2013

Acknowledgements

First of all, I would like to express my sincere gratitude to Dr. Mingyu Lu. He was my advisor for 5 years. Not only did he impart knowledge to me, but also the way of thinking. He always asked me to think about the fundamentals and said if you really understand a thing you can always explain it in a very simple way. Without his advices and encouragement I wouldn't be able to get so far in my PhD study.

Secondly, I owe thanks to Dr. Sungyong Jung, my co-advisor, for his guidance and support throughout my dissertation. His opinion and suggestions were invaluable to the completion of the the dissertation. Also I want to thank Dr. Jonathan Bredow, Dr. Robert Magnusson, Dr. Saibun Tjuatja and Dr. Haiying Huang for their consent and time to be my committee members.

I would also like to thank Dr. Xin Wang, Li Fang, Lisheng Guo, and Jinmei He for their help of simulation and collecting the experimental data.

I also owe thanks to Shan Shen, the general manager of Ayia Electronic Tech Co., LTD, for their help of fabricating the antennas and rectifiers.

Also, I would like to thank my laboratory colleague Sunil Govardhan and Jay Jen for the help.

I also give thanks to all my friends who help me in my life. They make my life rich and memorable.

Most importantly, I am grateful to my parents and family for their unconditional love and support of my studies, especially during hard times. They always back up my decisions and encourage me to pursuit what I like.

November 22, 2013

Abstract

WIRELESS POWER TRANSMISSION BASED ON

RETRO-REFLECTIVE ANTENNA ARRAY

Shaoshu Sha, PhD

The University of Texas at Arlington, 2013

Supervising Professor: Sungyong Jung

In recent years, there is a lot of research on wireless power transmission (WPT) for various applications, such as mobile devices, electric vehicles, implanted medical devices, sensors, RFID, etc. Compared to wired power transmission, WPT is more convenient and allows the devices to move more freely. Microwave beamforming WPT has been investigated extensively because its fast tracking capability, multiple target tracking capability and so on.

A retro-reflective antenna array based on novel phase-conjugate method is proposed in this dissertation. The phase of the received signal is detected individually and simultaneously at each antenna and the conjugated phase is applied to the corresponding phase shifter of each antenna. Using this method, the antenna element of the array can be placed arbitrarily, which offers high construction flexibility. The single frequency WPT experimental results verify that the proposed retro-reflective antenna array is able to track and focus microwave beam on the receiver. Experiments also show that the transmission efficiency can be improved by increasing the antenna number. A rectenna is also designed to convert received RF energy into DC energy. Measured results show excellent agreement with simulations.

The sidelobe level in the single frequency WPT can be reduced by using ultra-wideband (UWB) retro-reflective beamforming. The system design of the UWB retro-reflective antenna array is improved in this dissertation by using sub-band technique. An impulse receiver is also designed to extract the spectrum of UWB signal. The UWB signal is decomposed into several narrower sub-bands with overlapping regions. An algorithm is developed to seamlessly merge the sub-band spectra into a complete wideband spectrum. Experimental results show that the proposed impulse receiver is able to extract the wideband spectrum with little distortion.

Table of Contents

List of Illustrations

List of Tables

Chapter 1

Introduction

Nowadays, modern people are relying on electronic devices, such as mobile phones, laptops, and tablets more than ever. As they become more powerful, they also consume more power. However, the battery technology has not made breakthroughs to meet the ever-increasing demand, and thus people have to plug their devices into power source frequently. In the recent years, there is a lot of research on wireless power transfer/transmission (WPT), or wireless charging for various applications, including mobile electronics [1] [2], electrical vehicles [3] [4], implanted devices [5] [6], RFID [7] [8], etc. Compared to wired charging or transmission, WPT is more convenient and allows the devices under charging to move more freely.

Nicola Tesla was the pioneer of WPT. He proposed two ideas of WPT in 19th century to realize his dream of World of Wireless [9] [10]. Even though Tesla did not succeed, his early work still influences recent mid-range wireless power transfer. Not only did Tesla create “the idea of inductive coupling between the driving and the working circuits”, he also pointed out “the importance of tuning both circuits, that is, the idea of an ‘oscillation transformer’” [11]. The “oscillation transformers” combined the magnetic induction principle and magnetic resonance between two coil-resonators, and the combination is a common theme in recent short-range and mid-range wireless power transfer.

Besides Tesla’s ideas, there are five methods currently under development for WPT; there are (1) ultrasonic, (2) inductive coupling, (3) magnetic resonance coupling, (4) microwave beamforming, and (5) laser. Except ultrasonic, all other methods use electromagnetic (EM) wave.

Ultrasonic WPT utilizes piezoelectric materials to convert electrical power to acoustic wave, and vice versa [12]. The biggest advantage of ultrasonic WPT is that its wavelength is much smaller than the EM wave for the same frequency, because its propagation speed is much slower than the EM wave's. Smaller wavelength permits smaller transducer size to achieve high directivity compared to the EM counterpart. But ultrasonic WPT is not efficient through air [12]. The reason is that air has very low acoustic impedance (about 400 Pa·s/m) while piezoelectric material's acoustic impedance is around 30 MPa·s/m. The impedance mismatch causes big reflections, thus reduces the transfer efficiency dramatically.

Inductive coupling WPT uses magnetic near field to transfer energy between two coils. The principle is Faraday's Law of Induction. A time-varying current driving the primary coil generates time-varying magnetic field, which in turns induces time-varying current in the secondary coil. The two coils must place very close to each other in order to achieve high efficiency. As the distance between coils increases, the efficiency drops exponentially. However the distance can be increased by tuning both transmitter and receiver coils resonating at the same frequency [13]. Even though inductive coupling WPT has very short range – about the same as coils diameter, it is very simple and the efficiency is every high (up to 95% [14]).

Magnetic resonance coupling further extends the transmission distance by adding a power driving coil and a load coil to the inductive coupling system [15]. The addition of the two coils offers two more mutual coupling coefficients for impedance matching. when the transmission distance is changed, the two extra mutual coupling coefficients are tuned to match the load impedance to source impedance. However, the extension of transmission distance does not come without its price compared to inductive coupling method. Because it is based on maximum power transfer theorem (inductive

coupling is based on maximum efficiency theorem), the total efficiency cannot exceed 50%, no matter how high the transfer efficiency is between the Sending and Receiving resonator coils [16].

While the inductive coupling and magnetic resonance coupling use the near field of EM waves, microwave beamforming WPT utilizes the far field component of EM waves. The disadvantage is that far field radiates in all directions and the power is inversely proportional to the square of distance. However, the transmission efficiency can be improved to 100% theoretically, by increasing the gain of the antenna or antenna array. The benefit of using antenna array is that the direction of the microwave beam can be electronically steered, thus provides fast tracking capability.

When the frequency of the EM waves is in the region of visible light (several hundred of terahertz), power can be transmitted using a laser beam and collected by photovoltaic cells [17]. Compared to microwave beam, laser has much better directional property because of its collimated monochromatic wavefront propagation. This allows very narrow beam cross-section area for transmission over long distances [18]. However, laser radiation is hazardous, even low power level can blind people or animals. High power level can even kill through localized spot heating. So laser beam power transmission is mostly explored in military weapons [19] [20] and aerospace [21].

Table 1-1 summarizes and compares different technologies of WPT in terms of range, efficiency, complexity, and so on. Safety is a very important issue for all the technologies, however, not much research is done in this area yet [22] [23], so it is not compared in the table. But procedures must be taken to meet the regulations for each technology [24-28].

Table 1-1 Comparisons Between Different WPT Technologies

	Ultrasonic	Inductive Coupling	Magnetic Resonance Coupling	Microwave Beamforming	Laser
Principle	Acoustic Waves	Magnetic Near field	Magnetic Near field	EM Far field	Laser
Range	Short to medium	Short	Medium	Medium to Long	Long
Overall Efficiency	Low to high	High	Medium	Low to medium	Medium
Transmitter Size	Small	Large	Large	Large	Small
Receiver Size	Small	Large	Large	Small to large	Small to medium
Receiver Power Level	Low to High	Medium to high	Medium	Low to high	Low to high
System Complexity	Medium	Simple	Medium	High	High
Receiver Mobility	Low	Low	Low	High	Medium
Cost	Medium	Low	Low	High	High

In this dissertation, the microwave beamforming method is used for WPT. There are several benefits of microwave beamforming method, such as fast tracking capability, multiple receivers tracking capability, good penetration through objects and multipath environment compatibility. Fast tracking capability is the most important one. With the assistance of pilot signal from the receiver, the microwave beam can automatically focus on the receiver even it is moving. Ultrasonic transducer array has the similar beamforming capability, but the impedance mismatch between transducer and air limits the transmission efficiency [12]. With active impedance matching [29] and frequency tracking technique [30], Inductive coupling and magnetic resonance coupling is able to maintain high efficiency for different receiver's locations, but the receiver's mobility is very limited. Laser system can also steer the beam towards the receiver, but the receiver has

to adjust its photovoltaic panel to the beam direction mechanically, which makes the receiver system complicated and bulky. Using some techniques, the microwave beamforming can also create a separate beam for each receiver. Another benefit of microwave beamforming WPT is that microwave at RF frequency has good penetration through non-metal objects such as woods and walls. With time-reversal or phase-conjugate techniques, microwave beamforming method can also work in complex environments [31]. Actually, the multipath effect improves the focusing effect, even beyond the diffraction limit [32].

There are many microwave beamforming methods. Traditional phased antenna array can steer microwave beam towards the receiver, but it needs to know the receiver's location. But more often the retro-reflective (also called retro-directive) antenna array is used, because it automatically focuses the microwave beam on the receiver. The principle of retro-reflective antenna array is retro-reflection. In contrast to mirror reflection, retro-reflection reflects the wave back to the direction of incidence.

Van Atta array is one type of retro-reflective antenna array. It has pairs of antennas interconnected by transmission lines of the same length [33]. The wave received by one antenna is reradiated by its pair. Because the transmission lines have the same length, the phase difference between the pair is flipped. The reverse of phase difference creates the outgoing wavefront same as the incoming one, so that the reradiated wave is retro-reflected back to the incident direction. However, the Van Atta array is restricted to planar wavefront and planar arrangement, thus not very spatially efficient [34].

Phase-conjugate array using heterodyne scheme is a more popular way to realize retro-reflection [35]. It reverses the phase at each antenna, so the antenna elements are not restricted to planar placement and equal spacing. There are two major

heterodyne schemes of phase-conjugate array: (1) using local oscillator (LO) at twice of the radio frequency (RF) [36], and (2) using a small intermediate frequency (IF). The first scheme achieves phase conjugate using only one LO and one mixer, but it suffers from RF-to-IF isolation problem because the RF and IF signals have the same frequency. The second scheme uses two LOs and two mixers to solve the RF-to-IF isolation problem. It is also capable of full-duplex communication by modulating the retransmitted signal [37]. But adding more LO and mixer makes the system bulky and costly.

All the methods mentioned above have one common limitation, that is they only response to incoming signal, but cannot transmit power by themselves.

Phase detection and phase shifting is another technique to realize retro-reflection [38]. The angle of arrival (AoA) is detected by a two-element antenna array and the angle information is used to control of the phase shifters of the transmitting antenna array. The progressive phase difference between adjacent elements steers the beam back to the direction of incidence. The advantage of this idea is that it can maintain a constant retransmitted power. However, similar to Van Atta array, this method also requires planar wavefront, planar arrangement and equal spacing of antenna elements.

Another idea is try-and-error brute force. The transmitting antenna array keeps adjusting the phase shifter of each antenna until the receiver reports maximum power is received [39]. When the receiver moves, or the environment changes, the synchronization procedure has to be performed again. This method guarantees that the received power is maximized with little communication overhead. But it is not efficient. If the receiver keeps moving, the method takes a lot of time to synchronize, especially when the number of antennas is large, and a large number of antennas is required to achieve high transmission efficiency.

A new phase-conjugate method is used in this dissertation to realize the retro-reflective antenna array. The phase of the received pilot signal at each antenna element is detected simultaneously using heterodyne receiver, then the conjugated phase is applied to the phase shifter of each antenna for retransmission. Because the phase-conjugate is performed at each antenna individually, the antenna element can be fplaced arbitrarily, which offers high construction flexibility. Also, the phase shifters enable the antenna array transmit power to the receiver continuously, so the receiver only need to send pilot signal when it moves or at a low repetition rate. Single-frequency WPT experiments are conducted to demonstrate the auto-focusing and tracking capability of the retro-reflective antenna array. Also, a 2-element array and a 4-element array are compared in the experiments to show that the focusing effect and the transmission efficiency can be improved by increasing the number of antennas. To convert the received RF energy into DC energy, a rectenna is designed too. It is based on 6-stage voltage multiplier architecture to boost the output DC voltage.

Sidelobe is another consideration in wireless power transmission. It is not only a waste of energy, but also potential interference to other wireless technologies. In single frequency power transmission, beam shaping techniques are usually adopted to reduce sidelobes [40], but the maximum gain of the antenna array remains the same, instead the main beam width is increased. In other words, the focal area is larger. In some applications, this could improve the transmission efficiency if the receiving antenna or array is large enough. Another way to reduce the sidelobe is to use ultra-wideband (UWB) retro-reflective beamforming [41]. In this method, the main beam width and maximum gain remain the same, but the sidelobes are smaller because their energy goes to the nulls in the radiation pattern. The numerical simulation in [41] shows that the sidelobes (or multiple focal points) are greatly reduced when 30 frequencies in an ultra-

wideband are used. A hardware system based on frequency-domain approach is proposed in [31] that can implement the UWB retro-reflective antenna array in [41], but it is a little bit complicated. In this dissertation, an improved hardware system is proposed to reduce the number of local oscillator and mixer, thus reduce the system complexity. The new system consists of two subsystems, one of which is the power receiver (which is missing in [31]) and the other is power transmitter, which is the retro-reflective antenna array. The power receiver is relatively simple. It has an impulse transmitter that sends the wideband pilot signal, and a rectenna that receives and converts RF energy into DC energy. On the other hand, the power transmitter consists of three functional blocks: an impulse receiver, a DSP and a waveform generator. The impulse receiver analyzes the received pilot signal and extracts the spectrum together with a DSP. Then the DSP processes the spectrum and controls the waveform generator to synthesize the waveform for retransmission.

Impulse receiver for UWB signal faces challenges. The time-domain method using sampling and Fourier transform is straightforward, but it requires a high speed ADC, which is very expensive. Frequency-domain sampling method has been investigated to extract the spectrum of UWB signal to avoid high-speed ADC [31]. But it requires a LO, a mixer and a filter for each frequency sample [31]. Sub-band technique [104] combines several frequency samples together to reduce the number of LO, mixer and filter, even though the ADC speed is required to be higher. But the sub-band technique is designed to estimate the information bit carried in the UWB signal, not to perfectly extract the spectrum. However, the spectrum, especially the phase information is very important in the retro-reflective antenna array to focus the beam automatically on the receiver. In this dissertation, the sub-band technique is improved by assigning overlapping regions to the adjacent sub-bands. The sub-band spectra are obtained first.

Then an algorithm is developed to seamlessly merge the sub-band spectra into a wideband spectrum.

The single-frequency WPT experiment results verify that the retro-reflective antenna array can automatically track and focus the microwave beam to the receiver. When the antenna number is increased from 2 to 4, the average transmission efficiencies for different receiver's positions are improved by 70%, 91% and 168% for frequency 2.06GHz, 2.08GHz and 2.108GHz respectively. With 4-element antenna array, the total received powers for different positions and different frequencies is between 7dBm and 12dBm. The measured rectenna conversion efficiency for 10dBm input power at 2.08GHz is 47.4% and the DC output voltage is 2.92V on a resistance load of 1.8kΩ. The measurement results show excellent agreement with simulation results.

The impulse receiver using the improved sub-band technique is implemented and tested. The measurement results show that our impulse receiver can extract the spectrum of periodic short impulses with little distortion. The measurement error for signal-to-noise ratio SNR=32dB is 3.73% and the performance of the impulse receiver does not deteriorate substantially when the SNR reduces. The measurement error for SNR=2dB is only 6.08%.

The organization of the dissertation is as follows:

Chapter 1 introduces the need for wireless power transmission and compares different WPT technologies. The contributions and structure of this dissertation are also summarized.

Chapter 2 reviews all wireless power transmission technologies, their working principle, applications, advantages and disadvantages. Different microwave beamforming methods for WPT are reviewed too.

Chapter 3 shows the numerical simulation results of the ultra-wideband retro-reflective antenna array for WPT. The system design of retro-reflective antenna array and each functional block of the system is explained in details.

Chapter 4 explains the details of the single-frequency microwave beamforming WPT experiments and impulse receiver design. Simulation and experimental results are presented and compared in this chapter.

Chapter 5 gives conclusions and future works.

Chapter 2

Background of Wireless Power Transmission

2.1 Early Work of Tesla's Wireless Power Transmission

Wireless power transmission (WPT) has a long history. Nicolas Tesla was the pioneer of WPT. He proposed two ideas in 19th century and did several experiments to verify them [9] [10]. The first idea is to ionize the air between transmitter/receiver and ionosphere so that a conducting path is formed between transmitter and receiver [9]. The earth itself offers the returning path from receiver to transmitter. For short distance WPT, the conducting path can be formed directly by ionizing the air between transmitter and receiver, as shown in **Error! Reference source not found.**. However, this idea is not practical because both transmitter and receiver need to maintain extremely high potentials (millions of volts) to sustain the conducting path and the high potentials are harmful to surrounding electronic appliances.

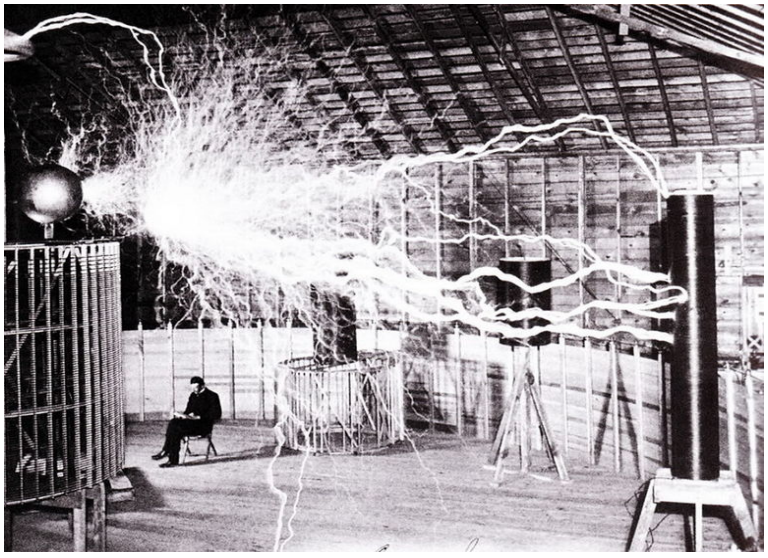

Figure 2-1 Nikola Tesla sitting in his laboratory in Colorado Springs in December 1899.

Later, Tesla found it did not require the conducting path in the air to transmit electrical energy [10]. The earth itself can be used to transmit power over long distance.

A Transverse Magnetic (TM) mode surface wave is excited and propagates along the earth-air interface, as shown in Figure 2-2 [42]. The surface wave is similar to surface plasma. Free electrons move back and forward creating a “longitudinal current wave” (Figure 2-3) [43]. Large plates of several wavelength or horns are usually used to excite and receive the surface wave. In Tesla’s idea, the “Magnifying Transmitter” (Figure 2-4) [44] [45] was used as launching devices. Tesla also stated that when the oscillating earth current was coupled with the earth resonance, his method could transmit power all over the globe with little loss [10]. In 1952, the earth resonance was discovered by Winfried Otto Schumann [46], and was named “Schumann Resonances”. However, Schumann Resonances are in extremely low frequencies (ELF) below 100Hz, while Tesla’s system was operating at tens of kilohertz [10]. Also the quality factor of the Schumann Resonances is too low (about of 5 [47]) to support strong resonance.

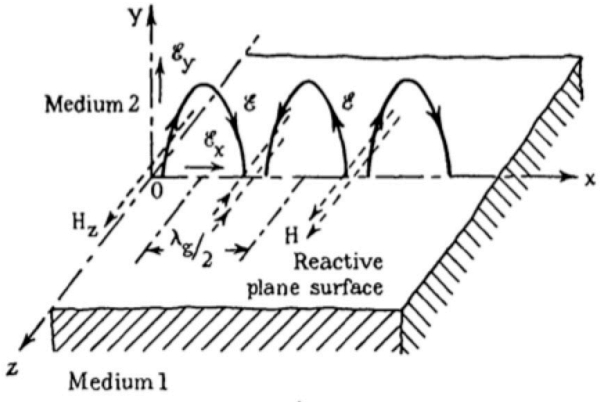

Figure 2-2 TM mode surface wave along interface between Medium 1 and Medium 2. Medium 1 is conductor and Medium 2 is dielectric [42].

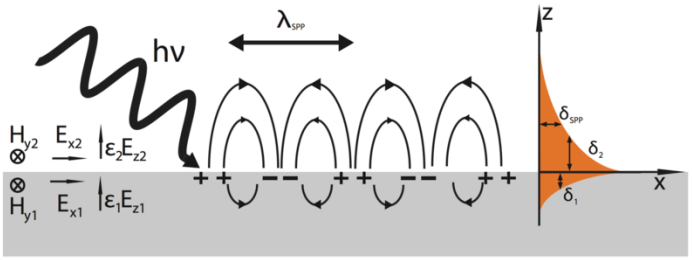

Figure 2-3 Surface plasmon-polariton waves propagating along a metal-dielectric interface [43].

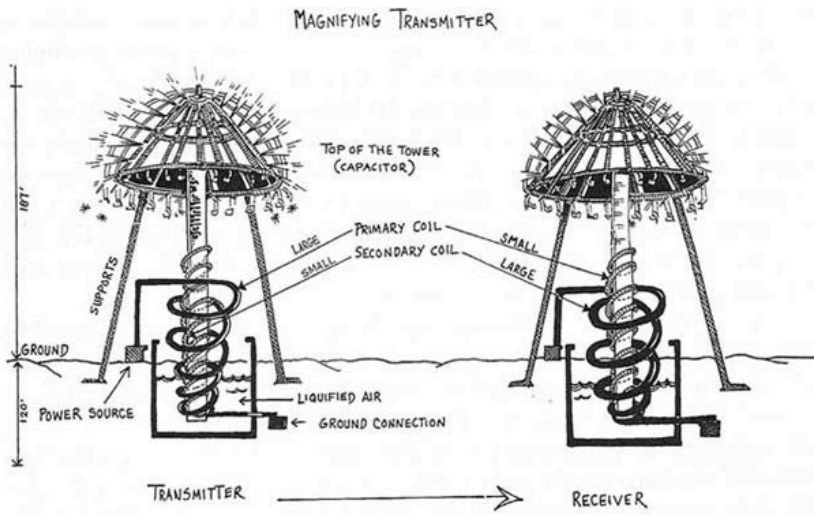

Figure 2-4 Tesla's magnifying transmitter [45].

Even though Tesla did not realize his dream of "World System of Wireless", his early work on non-radiative wireless power still influences recent mid-range wireless power transfer. A diagram of Tesla's wireless power transfer experiment is shown in Figure 2-5 [48]. Not only did Tesla create "the idea of inductive coupling between the driving and the working circuits", he also pointed out "the importance of tuning both circuits, that is, the idea of an 'oscillation transformer'" [11]. The "oscillation transformers" combined the magnetic induction principle and magnetic resonance between two coil-

resonators, and the combination is a common theme in recent short-range and mid-range wireless power transfer.

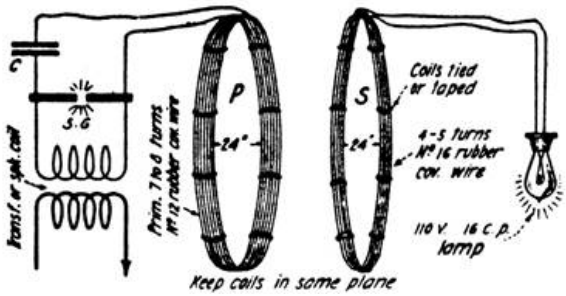

Figure 2-5 A diagram of Tesla's wireless power experiment [48].

2.2 Current Technologies of Wireless Power Transmission

Currently, there are five WPT methods under development; there are (1) ultrasonic, (2) inductive coupling, (3) magnetic resonance coupling, (4) microwave beam, and (5) laser.

2.2.1 Ultrasonic

Ultrasonic wave is an acoustic wave at frequency above 20KHz. It utilizes piezoelectric materials to convert electrical power to mechanical power, and vice versa [12]. The typical ultrasonic WPT system is shown in Figure 2-6. The transmitter consists of a power source, a pulse generator, power amplifier and an ultrasonic transducer. The receiver is composed of an ultrasonic transducer and a rectifier that converts high frequency electrical power to DC power.

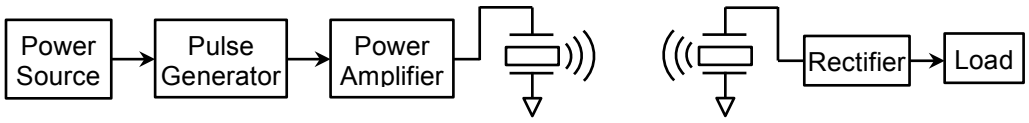

Figure 2-6 Schematic diagram of ultrasonic wireless power transmission.

Most research on ultrasonic WPT focuses on biomedical implants charging and through-wall energy transfer for metal enclosures, but not so much on WPT through air

[12]. The reason is that air has very low acoustic impedance (about 400 Pa·s/m) while piezoelectric material's acoustic impedance is around 30 MPa·s/m. The impedance mismatch causes big reflections, thus reduces the transfer efficiency dramatically. However, metals have similar acoustic impedance (about 45 MPa·s/m for steel) to piezoelectric materials. Lawry *et al.* [49] demonstrated a through-wall system that delivers 50W at 51% efficiency. Bao *et al.* [50] even achieved an efficiency of 84% at 1kW by using prestressed piezo actuator. In biomedical applications, the maximum efficiency measured in publications is 39.1% [51] at 5mm distance for 100mW, but reduces to 17.6% at 40mm for 45mW. Arra *et al.* [52] were able to transfer 80mW at a maximum efficiency of 25% over a distance of 100mm. They also found that the reflection between two transducers influences the transfer efficiency, leading to maxima and minima as a function of distance.

2.2.2 Inductive Coupling

Inductive coupling WPT uses magnetic near field to transfer energy between two coils. A typical system consists of a primary coil on the transmitter side and a secondary coil on the receiver side, as shown in Figure 2-7. The principle of transformer is Faraday's Law of Induction. A time-varying current driving the primary coil generates time-varying magnetic field, which in turns induces time-varying current in the secondary coil. The two coils must be placed very close to each other in order to achieve high efficiency. As the distance between coils increases, the efficiency drops exponentially.

The power transmission distance can be increased by tuning both transmitter and receiver coils resonating at the same frequency [13] [53], as Tesla had done it a hundred years ago. Another way to increase the distance is to design the transmitter and receiver coils with high Q factor. Pinuela *et al.* [54] demonstrated an overall system efficiency of 77% over a distance 30cm. In his system, the transmitter coil has a diameter

of 30cm and a Q factor of 1270, and the receiver coil has a diameter of 20cm and a Q factor of 1100.

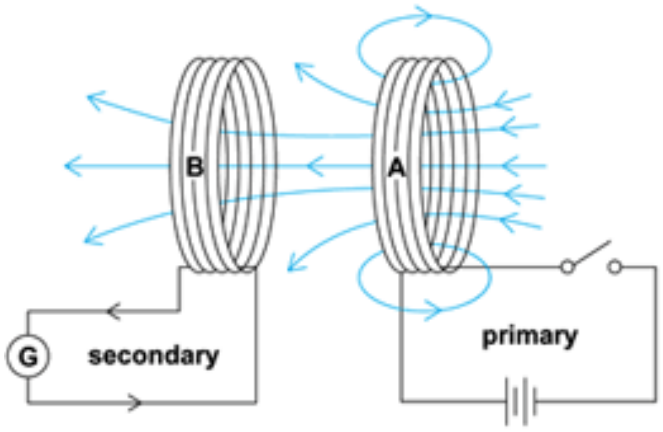

Figure 2-7 Inductive coupling wireless power transmission.

Lately, relay- or domino-resonators between transmitter and receiver coils are investigated in order to increase the transmission distance and improve the system efficiency [55-58]. The domino-resonators can be placed in various forms so the system has more flexibility. Some examples of domino-resonator arrangements are shown in Figure 2-8.

Even though inductive coupling WPT has very short range – on the order of coils diameter without relay resonators, it is the simplest form of wireless power transmission and has very high efficiency [16]. It is also the only commercially available WPT technology so far. The applications include wireless toothbrush and Qi inductive power standard for mobile devices [59]. There is also a lot of research focusing on wireless charging for implanted devices [60] [61] and electrical vehicles [3] [4].

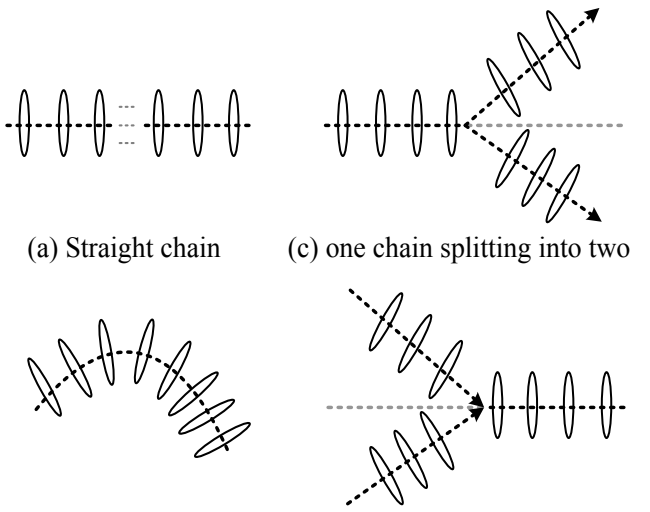

Figure 2-8 Some examples of domino-resonator arrangement [57].

2.2.3 Magnetic Resonance Coupling

In 2007, an MIT professor Marin Soljačić and his group demonstrated a new idea to extend the transmission distance by adding a power driving coil and a load coil. In their experiment 60W power was transferred with 40% efficiency over distances of 2 meters [15]. While the coupled mode theory was used in [15], Cheon *et al.* [62] explained the experiment using electric circuit theory, which is more easily understood by electrical engineers, as shown in Figure 2-9. The addition of power driving and load coils offers two extra mutual coupling coefficients κ_{PS} (between driving coil and sending resonator) and κ_{RD} (between receiving resonator and load coil) for impedance matching besides the mutual coupling coefficient κ_{SR} (between sending resonator and receiving resonator). The maximum power transfer condition is:

$$\frac{\kappa_{PS}\kappa_{RD}}{\kappa_{SR}} = 1 \tag{2.1}$$

All the coupling coefficients are inversely proportional to the distance between coils. So when the transmission distance is increased, the mutual coupling coefficient κ_{SR} becomes smaller. By reducing mutual coupling coefficients κ_{PS} and κ_{RD}, condition (2.1) can still be met. Compared with inductive coupling where only two resonator coils are used, the 4-coil magnetic resonance coupling system provides extra freedom for extending transmission distance by adjusting 3 mutual coupling coefficients [16].

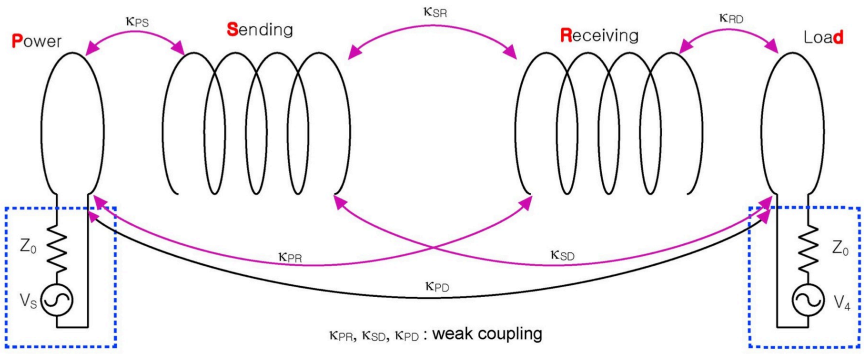

Figure 2-9 Schematic of magnetic resonant coupling WPT [33].

However, the resonant frequency and coupling coefficient depend on load impedance matching [63], alignment and the distance between two coils [64]. A phenomenon called “frequency splitting” is observed in both 2-coil inductive coupling and 4-coil magnetic resonance coupling WPT. It occurs when the condition (2.1) cannot be met at the resonant frequency within the over-coupled region [64]. Figure 2-10 shows an example of frequency splitting phenomenon in a 4-coil WPT system [64]. Adaptive matching methods based on frequency tracking have been developed to overcome the issues mentioned above [65] [66]. Also, Lee *et al.* [67] shows that antiparallel resonant structure formed by forward and reverse loops can stabilize the transfer efficiency by eliminating the distance-related frequency splitting.

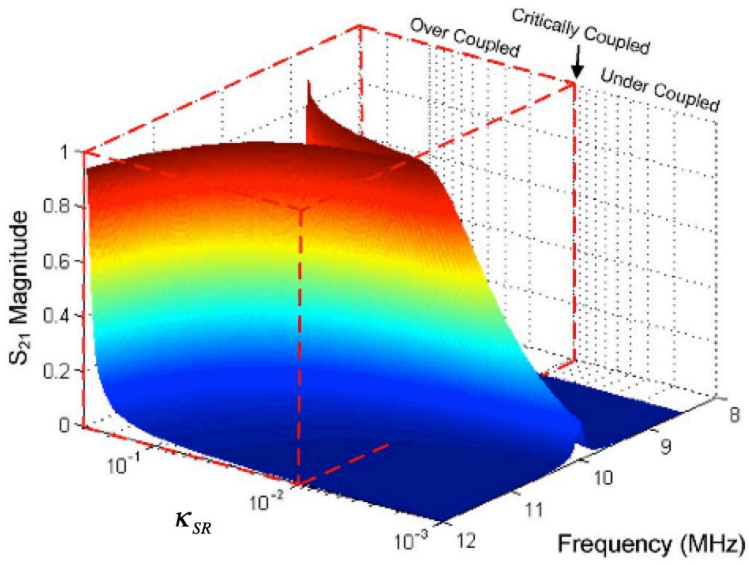

Figure 2-10 An example of frequency splitting in 4-coil magnetic resonance coupling WPT system [64].

The extension of transmission distance of magnetic resonance coupling does not come without its price compared to inductive coupling method. Since it is based on maximum power transfer theorem, the total efficiency cannot exceed 50%, no matter how high the transfer efficiency is between Sending and Receiving resonator coils [16].

Relay resonators between Sending and Receiving resonator coils can also be used to further extend transmission distance and improve transfer efficiency [68] [69].

Reducing the wire's AC resistance, thus reducing the ohmic loss, is another important aspect for both inductive coupling and magnetic resonance coupling WPT system operating above megahertz. Lee *et al.* [70] proposed a new spatial layout of winding coils that achieved 95% total efficiency over a distance of 30cm. And by coating the wire with magnetic thin film, Mizuno *et al.* [71] reduced the AC resistance by 40% at 12MHz.

2.2.4 Microwave Beamforming

While electromagnetic induction and magnetic resonance coupling use the near field of EM waves, microwave beam WPT utilizes the far field component of EM waves. To achieve a high efficiency over long range, a high gain antenna or an antenna array is used for transmission. On the receiver side, a rectenna or an rectenna array is used to convert microwave energy into DC electricity.

William C. Brown was the pioneer of microwave beam power transmission. In 1963 he invented the rectenna, rectifying antenna which he named, and achieved 50% efficiency at output 4W [72] In 1969, he managed to power supply a free-flying helicopter using microwave beam [73]. In 1975, the overall DC-DC total efficiency of 54% was experimentally obtained. Later on in 1975, his team conducted an experiment at the Venus Site of JPL Goldstone Facility where they received 30 kilowatts DC power over a distance of 1 mile, as shown in Figure 2-11, and the rectifying efficiency was raised to 82.5% [74].

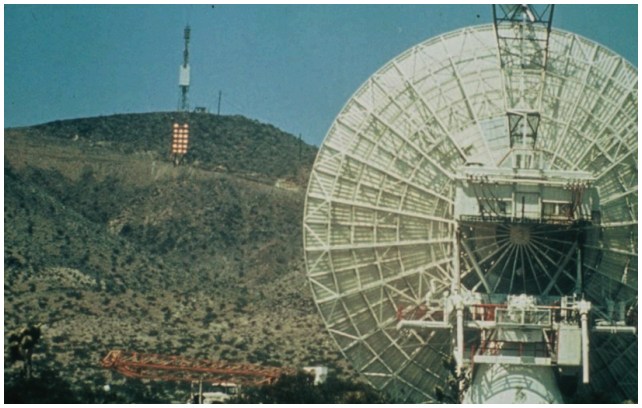

Figure 2-11 First ground-to-ground microwave beam wireless power transmission experiment in 1975 at the Venus Site of JPL Goldstone Facility [74].

Based on W. C. Brown's work, Peter Glaser proposed a Solar Power Satellite (SPS) in 1968 [75]. A satellite with gigantic solar panel in geostationary orbit collects sun

energy and converts it into electrical energy. The phased array antenna on the satellite then transmits the energy using microwave beam toward the rectenna array on the ground. A pilot signal is sent from the ground station to guide the power beam.

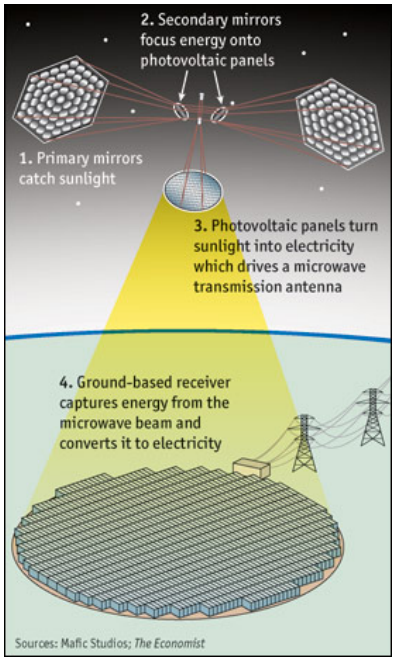

Figure 2-12 Concept of Solar Power Satellite (SPS).

Since then there were a lot of research and small-scale demonstration of this idea [72] [76]. In 1980s, Japanese scientists carried out the first microwave beam power transfer experiment called MINIX (Microwave Ionosphere Nonlinear Interaction eXperiment) in 1983 and ISY-METS (International Space Year –Microwave Energy Transmission in Space) in 1993 [77]. In 1987, Canadian group experimented a fuel-free airplane called SHARP (Stationary High Attitude Relay Platform) powered by microwave beam at 2.45GHz [78].

Figure 2-13 MINIX experiment in 1983 [77].

However, the geostationary orbit is about 35,000 kilometers above the earth. To achieve the desired narrow beam width and the high beam collecting efficiency, the dimensions of both transmitting and receiving antenna array are on the order of kilometers [79]. Also the cost of launching and re-assembling the array in the space prohibits its realization in the near future [79]. But research is still being continued to improve the technology and reduce the cost [80].

Recent research about microwave beam WPT focuses more on short-range (compared to SPS's range it is short, but the distance is in order of meters) and small-scale applications such as electronic devices, electric vehicle, and RFID [81]. In September 2013, a startup called *Ossia* demonstrated a prototype product that can transmit 1 watt power to the receiver over a distance of 30 feet using 200 transmitting elements [82].

Figure 2-14 Cota Wireless Charging System demonstration by Ossia [82].

2.2.5 Laser

When the frequency of the EM waves is in the region of visible light (several hundred of terahertz), power can be transmitted using a laser beam and collected by photovoltaic cells [17]. Compared to a microwave beam, the laser has much better directional property because of its collimated monochromatic wavefront propagation. This allows very narrow beam cross-section area for transmission over large distances [18].

However, laser radiation is hazardous, and even low power level can blind people or animals. High power level can even kill through localized spot heating. So laser beam is mostly explored in military weapons [19] [20] and aerospace [21].

Figure 2-15 Laser beam power transmission.

Commercial applications are also under development now. NASA demonstrated an unmanned aerial vehicle (UAV) powered by laser beam in 2003 [83]. At the same time, Steinseik *et al.* [84] developed a rover vehicle that was solely powered via laser with an output of 5W. The rover can travel to a distance of 200 meters. The laser transmitter system is designed to automatically find and track the target, also the receiver is equipped with a micro-controller that adjusts the photoelectric panel to the direction of laser beam.

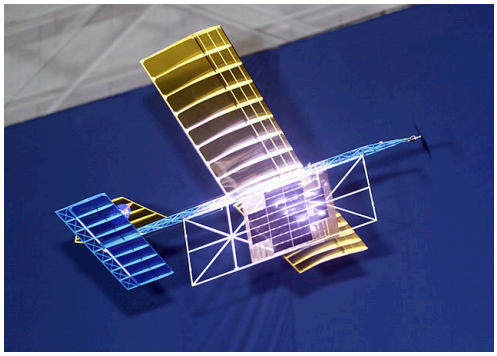

Figure 2-16 NASA's UAV powered by laser beam [83].

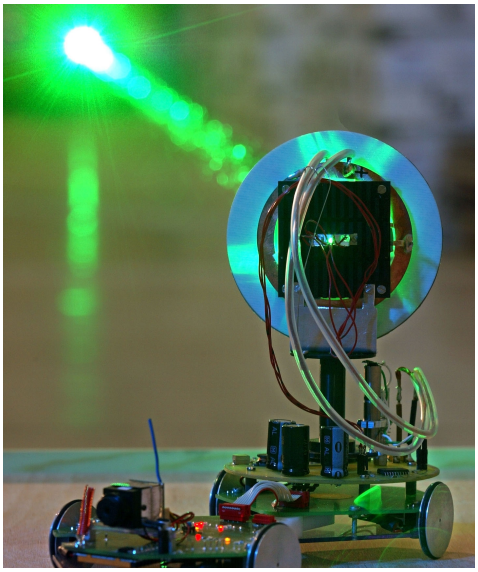

Figure 2-17 EADS developed fully laser powered autonomous rover vehicle [84].

2.3 Microwave Beamforming Methods

Retro-reflection is commonly used in microwave beam power transmission to focus beam on the receiver. Contrast to mirror reflection, retro-reflection reflects the wave back to the incident direction, thus it is able to automatically redirect the wave back to the source origin without prior knowledge of its location. There are several ways to realize retro-reflection. Corner reflector is one example [34], as shown in Figure 2-18. But more often retro-reflection is realized using a retro-reflective (also called retro-directive) antenna array.

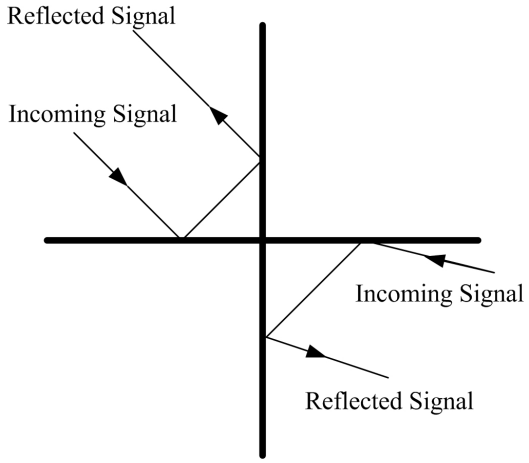

Figure 2-18 Corner reflector [34].

2.3.1 Van Atta Array

Van Atta array is one way of achieving retro-reflection, which was proposed by Van Atta [80]. Pairs of antennas are equally spaced on the same plane, and interconnected by transmission lines of the same length or multiple wavelength difference. Figure 2-19 shows two types of Van Atta array, one is passive and the other is active by inserting bi-directional amplifiers in the transmission lines [33]. The signal received by one antenna is reradiated by its pair. Because the transmission lines have the same length, the phase difference between the pairs is flipped. The reverse of phase

difference creates the outgoing wavefront same as the incoming one, so that the reradiated signal is retro-reflected back to the incident direction.

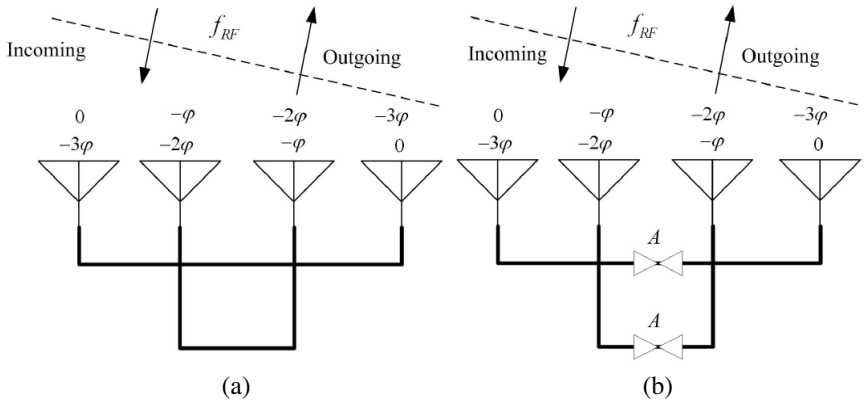

Figure 2-19 Schematic of Van Atta array and the relative phase for received and re-transmitted signals [34]. (a) Passive Van Atta array, (b) active Van Atta array.

When the interconnecting transmission lines have the same length, the Van Atta array can be made for wideband application by using broadband antennas. However, the Van Atta array is restricted to planar wavefront and planar arrangement, thus not very spatially efficient for realizing retro-reflectivity on many applications [34].

2.3.2 Phase Conjugate Array

Phase-conjugate array using heterodyne scheme is a more popular way to realize retro-reflection [35]. It reverses phase at each antenna instead of its pair in Van Atta array. In this way, the antenna elements are not restricted to planar placement of equally distance. There are two major heterodyne schemes of phase-conjugate array: (1) using local oscillator (LO) at twice of the radio frequency (RF) [36], and (2) using a small intermediate frequency (IF).

2.3.2.1 Heterodyne scheme using LO at twice of RF frequency

The diagram of this scheme is shown in Figure 2-20. The incoming and outgoing antennas can be served by one physical antenna through a circulator or a directional coupler. The output signal of the mixer at the IF port is shown in Equation (2.2). The component at frequency ($3\omega_{RF}$) is filtered out by the following low pass filter. It can be seen that the phase of incoming signal is reversed.

$$\begin{aligned} V_{IF} &= V_{RF}\cos\left(\omega_{RF}t+\phi\right)V_{LO}\cos\left(\omega_{LO}t\right) \\ &= \frac{1}{2}V_{RF}V_{LO}\left\{\cos\left[\left(\omega_{LO}-\omega_{RF}\right)t-\phi\right]+\cos\left[\left(\omega_{LO}+\omega_{RF}\right)t+\phi\right]\right\} \\ &= \frac{1}{2}V_{RF}V_{LO}\left\{\cos\left(\omega_{RF}t-\phi\right)+\cos\left(3\omega_{RF}t+\phi\right)\right\} \\ &= \frac{1}{2}V_{RF}V_{LO}\cos\left(\omega_{RF}t-\phi\right) \end{aligned} \tag{2.2}$$

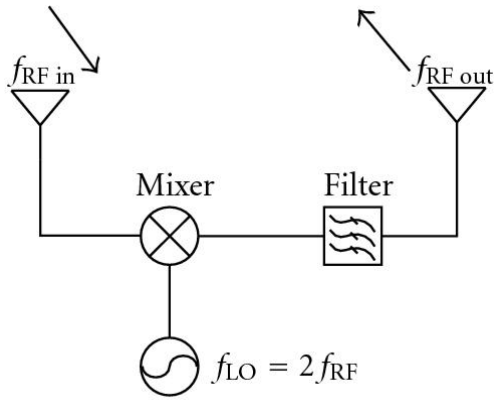

Figure 2-20 Schematic of heterodyne phase-conjugate array using an LO at twice of RF frequency [34].

The advantage of this scheme is simplicity (using only one LO and one mixer). Sometimes the filter is not necessary if the antenna does not resonant at the triple RF frequency. However, the retransmitted IF signal and the received RF signal have the same frequency, so they are very difficult to isolate. This problem can be mitigated by low

frequency offset between received and retransmitted signals [85], directional coupler [86], orthogonal polarizations [87], and balanced mixers [88].

2.3.2.2 Heterodyne scheme using small IF

In this configuration, two LOs and two mixers are used, as shown in Figure 2-21. The RF signal is down-converted to an IF frequency by a LO signal at frequency ($\omega_{RF} \pm \omega_{IF}$), and then the IF signal is up-converted to RF frequency by a LO signal at frequency ($\omega_{RF} \mp \omega_{IF}$). The down-conversion is expressed mathematically by Equation (2.3):

$$\begin{aligned} V_{IF} &= V_{RF}\cos\left(\omega_{RF}t+\phi\right)V_{LO1}\cos\left(\omega_{LO1}t\right) \\ &= \frac{1}{2}V_{RF}V_{LO1}\left\{\cos\left[\left(\omega_{LO1}-\omega_{RF}\right)t-\phi\right]+\cos\left[\left(\omega_{LO1}+\omega_{RF}\right)t+\phi\right]\right\} \\ &= \frac{1}{2}V_{RF}V_{LO1}\left\{\cos\left(\omega_{IF}t-\phi\right)+\cos\left[\left(2\omega_{RF}+\omega_{IF}\right)t+\phi\right]\right\} \\ &= \frac{1}{2}V_{RF}V_{LO1}\cos\left(\omega_{IF}t-\phi\right) \end{aligned} \tag{2.3}$$

The component at frequency ($2\omega_{RF}+\omega_{IF}$) is filtered by low pass filter. The up-conversion is expressed in Equation (2.4):

$$\begin{aligned} V_{RF} &= V_{IF}\cos\left(\omega_{IF}t-\phi\right)V_{LO2}\cos\left(\omega_{LO2}t\right) \\ &= \frac{1}{2}V_{IF}V_{LO2}\left\{\cos\left[\left(\omega_{LO2}+\omega_{IF}\right)t-\phi\right]+\cos\left[\left(\omega_{LO2}-\omega_{IF}\right)t+\phi\right]\right\} \\ &= \frac{1}{2}V_{IF}V_{LO2}\left\{\cos\left(\omega_{RF}t-\phi\right)+\cos\left[\left(\omega_{RF}-2\omega_{IF}\right)t+\phi\right]\right\} \\ &= \frac{1}{2}V_{IF}V_{LO2}\cos\left(\omega_{RF}t-\phi\right) \end{aligned} \tag{2.4}$$

The component at frequency ($\omega_{RF}-2\omega_{IF}$) is filtered by a band pass filter or high pass filter.

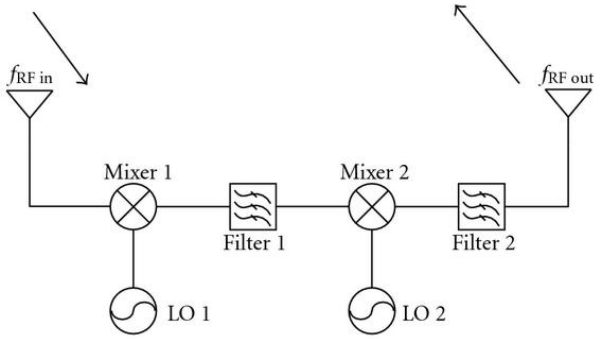

Figure 2-21 Schematic of heterodyne phase-conjugate array using an IF frequency [34].

The benefit of this configuration is its capability of full-duplex communication, because it is simple to apply modulation to the retransmitted signal, allowing the transmission of information [89], but adding more LO, mixer and filter make the system costly and bulky.

There are also some other techniques that achieve phase conjugation. Fusco *et al.* [90] designs a phase-conjugating locked loop (PCLL) to ensure that the retransmitted phase is locked to the conjugation of received signal's phase, as shown in Figure 2-22. This technique offers a better conversion efficiency and RF-to-IF isolation.

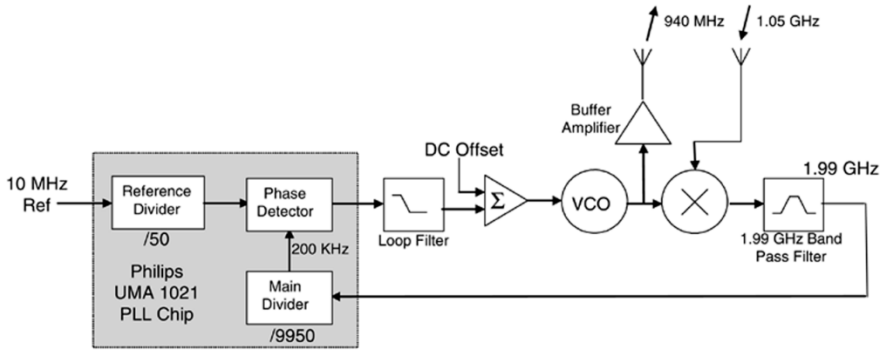

Figure 2-22 Phase-conjugating locked loop configuration [90].

All these heterodyne scheme phase-conjugate arrays suffer one problem for wireless power transmission, which is that they can only respond to the incoming signal but not transmit signal by themselves.

2.3.3 Phase Detection And Phase Shifting

Phase detection and phase shifting is used in [38], where a two-element receiving antenna array is used to detect the angle of incidence. The detected angle information is used to control a phase shifter of transmitting antenna array to direct the beam back to the source origin, as shown in Figure 2-23. Unlike all the phase-conjugate method mentioned above, this method is not only capable of full-duplex communication, but can also maintain a constant retransmitting power level, which is critical for wireless power transmission. However, similar to Van Atta array, this method also requires a planar wavefront, a planar arrangement and equal spacing of antenna elements.

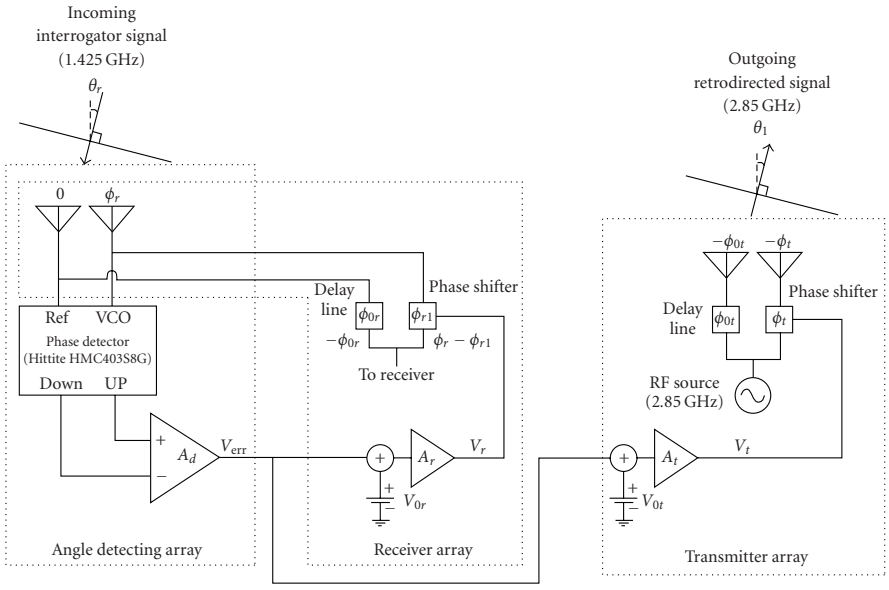

Figure 2-23 Schematic of a retrodirective antenna array using angle detection and phase shifting [38].

A similar idea is proposed by Akagi *et al.* [90]. The transmitter array detects the pilot signal power level by electronically steering the scanning angle of a conventional phased array, as shown in Figure 2-24. By reciprocity, the direction of maximum received power is the same as that of maximum transmitting power.

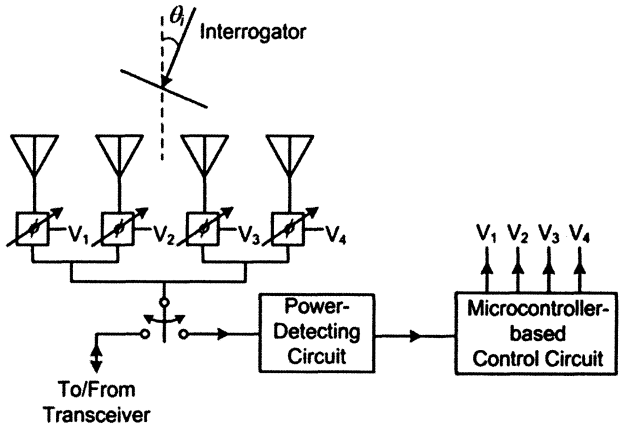

Figure 2-24 Schematic of self-steering array using power detection and phase shifting [90].

2.3.4 Try-and-Error Brute Force

In this method, the transmitting antenna array keeps adjusting the phase shifter of each antenna until the receiver reports maximum power is received [39]. At the beginning, the phase of first transmitter is fixed, and the second transmitter adjusts its phase until the receiver reports back maximum power is received. Then the second transmitter is turned off and the third transmitter adjusts its phase till the received power is maximized. The procedure is repeated until all transmitters' phases are synchronized with respect to the first transmitter. After this tune-up, all transmitters are turned on to transmit power to the receiver. This method guarantees that the received power is maximized with little communication overhead. But it is not efficient. If the receiver keeps moving, the method takes a lot of time to synchronize, especially when the number of

antenna is large, and large number of antenna is required to increase the transmission efficiency. So this limits the mobility of the receiver.

Chapter 3

Description of Retro-reflective Antenna Array Wireless Power Transmission

For wireless power transmission, there are several requirements. The most important one is a constant retransmitting power. This requires a phase shifter for each antenna or antenna sub-array so that the system can continuously transmit power and the receiver only needs to send pilot signal when necessary. The second requirement is isolation between received pilot signal (carries information) and retransmitted signal (carries power). The retransmitted signal is usually several order of magnitude higher than received signal so the received signal can be easily overwhelmed by leakage from retransmitted signal. Frequency offset or time division multiplexing or the combination of the two methods is often used to ensure system performance [85]. Sidelobe is another consideration in wireless power transmission. It is not only a waste of energy, but also potential interference to other wireless technologies. In single frequency power transmission, beam shaping techniques are usually adopted to reduce sidelobes [40], but the maximum gain of the antenna array remains the same, instead the main beam width is increased. In other words, the focal area is larger. In some applications, this could improve the transmission efficiency if the receiving antenna or array is large enough. Another way to reduce the sidelobe is to use ultra-wideband (UWB) retro-reflective beamforming [41]. In this method, the main beam width and maximum gain remain the same, but the sidelobes are smaller because their energy goes to the nulls in the radiation pattern. The numerical simulation in [41] shows that the sidelobes (or multiple focal points) are greatly reduced when 30 frequencies in an ultra-wideband are used. The system architecture is illustrated in **Error! Reference source not found.**. Each antenna element in the retro-reflective array has its own power transmitter.

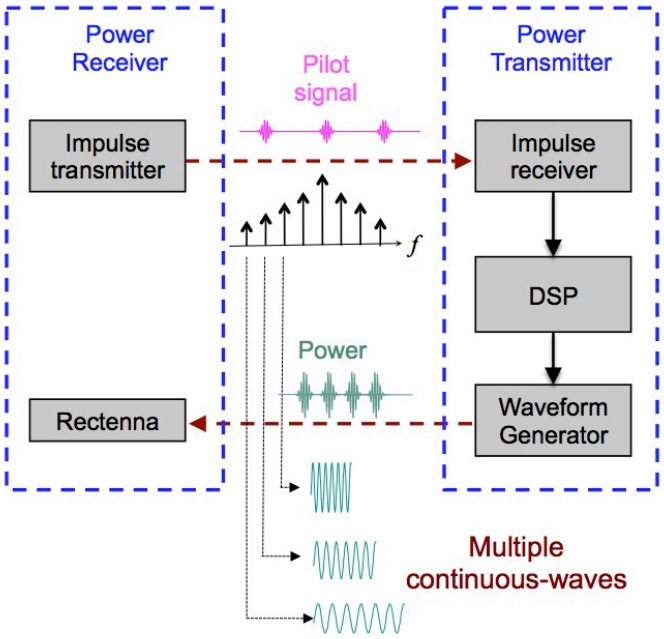

Figure 3-1 Architecture of the UWB WPT system.

The wireless power transmission process is described as follows. First, the power receiver sends pilot signals to notify the power transmitters its presence and request for power transmission. Second, all the power transmitters receive the pilot signals and perform phase-conjugate in DSP. Also the power levels of received pilot signals will be monitored. If the power level is lower than a certain criterion, which indicates the link between receiver and transmitter is possibly blocked by some object (for example, humans), then the transmitter will turn off. This is not only a safety procedure, but also saves power for the transmitter. Third, the active power transmitters transmit the phase-conjugate version of the pilot signals they receive. By using the phase conjugate technique, the microwave beam from each power transmitter will spatially focus on the power receiver [41]. Finally, a rectifier in the power receiver converts the received RF energy into DC electricity.

The numerical model of the WPT application is shown in Figure 3.2, and described as follows [41]. Eight base stations (retro-reflective antenna array) are deployed over a circle with a radius 3 meter in the xy-plane. Each base station comprises of a 5-by-5 z-oriented dipole array with equal spacing of 12cm. Two power receivers reside around the center of the circle. They transmit short impulses as pilot signals, which covers frequency band [4GHz, 6GHz]. The model in Figure 3.2 is simulated by the Method of Moments.

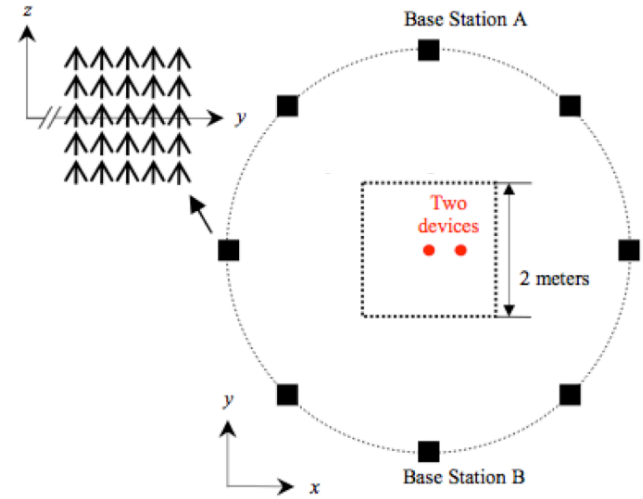

Figure 3-2 Numerical model of the UWB wireless power transmission [41].

Simulated Ez field distribution in a 2m by 2m region around the two power receivers are presented in Figure 3.3 [41]. When only one power receiver sends pilot signals and single frequency (4.09GHz) is used for power transmission, the field distribution is shown in Figure 3.3(a). Many unwanted focal points (resembles sidelobes of regular antenna array) appear besides the power receiver's location. When the number of frequency is chosen to be 30, only one focal point at the receiver's location is left, as shown in Figure 3.3(b).

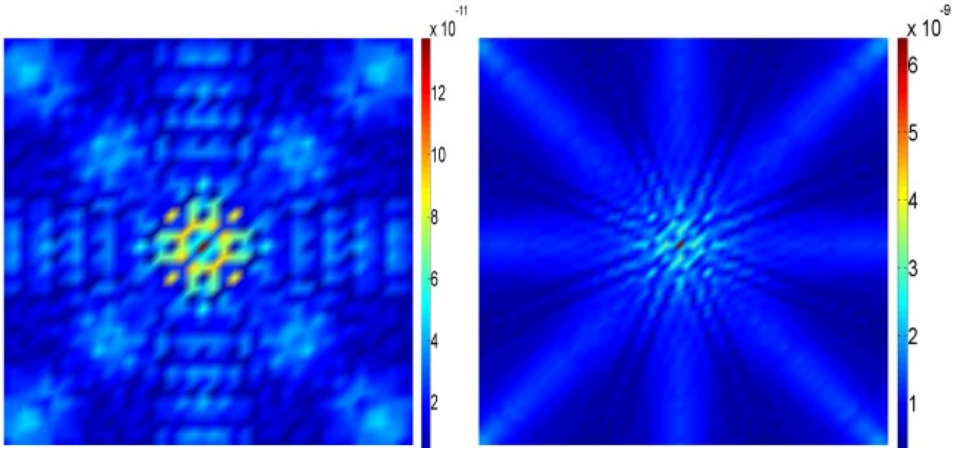

(a) (b)

Figure 3-3 Simulated field distribution of the UWB WPT system [41]. (a) One power receiver and single frequency power transmission, (b) one power receiver and 30 frequencies power transmission.

Chapter 4

Design, Simulation and Experimental Results

4.1 Single Frequency Wireless Power Transmission

4.1.1 Retro-reflective Antenna Array Design

The retro-reflective antenna array based on proposed phase-conjugate method is shown in Figure 4.1. In this figure, the receiving and transmitting antenna pair share one physical antenna through a directional coupler or a single-pole-double-throw (SPDT) switch. 4 antenna elements are just shown for illustration purpose. In real application the number of antenna can be increased or decreased. The retro-reflective antenna array works as follows. First, the pilot signal received at each antenna is amplified by a low noise amplifier (LNA) and then down-converted to an IF frequency by a local oscillator (LO). One LO is shared by all antennas so that the phase error introduced by the LO is the same. The phase errors caused by LNA and mixer are negligible. Second, the IF signals are simultaneously sampled by multi-channel ADCs. Because the ADCs are synchronized, the phase difference between all antennas are preserved. Third, Fourier transform is applied to the sampled data to find the magnitude and phase of the received pilot signal at each antenna. The steps are shown mathematically in Equation (4.1),

$$\begin{aligned} g_i(t) &= f_i(t)\cos(\omega_{LO}t+\phi) \\ &= A_i\cos(\omega_{RF}t+\phi_i)\cos(\omega_{LO}t+\phi) \\ &= \frac{A_i}{2}\left\{\cos\left[(\omega_{RF}+\omega_{LO})t+\phi_i+\phi\right]+\cos\left[(\omega_{RF}-\omega_{LO})t+\phi_i-\phi\right]\right\} \\ &= \frac{A_i}{2}\cos(\omega_{IF}t+\phi_i-\phi) \end{aligned} \quad (4.1)$$

where $f_i(t)$ is the pilot signal received by antenna i, and A_i is its magnitude. ϕ is the phase error of LO. In the equation, the gain of LNA and conversion loss of mixer is neglected because they are the same for each antenna. The relative phase differences between

antennas are important rather than absolute phase of each antenna, so we can set the phase of the first antenna as a reference then calculate the phase difference between them. Assume $\phi_1^{'} = \phi_1 - \phi = 0$, then $\phi_i^{'} = (\phi_i - \phi) - (\phi_1 - \phi) = \phi_i - \phi_1$. It can be seen that the phase error of LO is cancelled. Same as the receiving mode mentioned above, one LO is also shared by all antennas in the transmitting mode, so that LO will not introduce phase difference between antennas. Finally, the conjugated phase $-\phi_i^{'}$ is applied to the phase shifter for each antenna through DACs. The retransmitted signals are amplified by power amplifier (PA) before transmission. Because the phases at all antennas are detected individually and simultaneously, the antennas are not limited to equal spacing and planar arrangement. Instead, they can be placed arbitrarily. In the implementation, PA can also be replaced by variable-gain amplifier (VGA) to enable beam shaping, but the system complexity is increased. In our experiments, PA is used for simplicity.

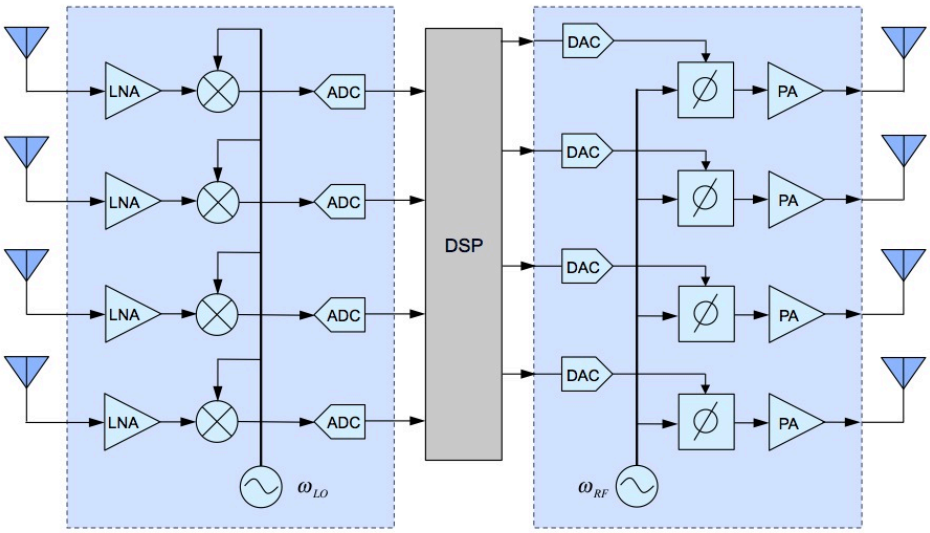

Figure 4-1 Circuit diagram of proposed retro-reflective antenna array.

4.1.2 Experiment Setup

The schematic of experiment setup is shown in Figure 4-2. On the transmitter side, a PC functions as DSP to process the data and control the phase shifters. The processing circuits represent the circuits in Figure 4-1 for simplicity. On the receiver side, the receiving antenna is connected to a LO when it sends pilot signal, or a power meter when it receives power. The distance between the transmitter and receiver is 50cm when the receiving antenna faces the center of antenna array (x=0cm). To demonstrate the focusing and tracking capability of the antenna array, the power receiver sends the pilot signal at position x=0cm, x=-10cm, x=-20cm and x=-30cm respectively. Then the power receiver moves along x-axis from x=-50cm to x=+50cm in the step size of 2.5cm, to measure the received power.

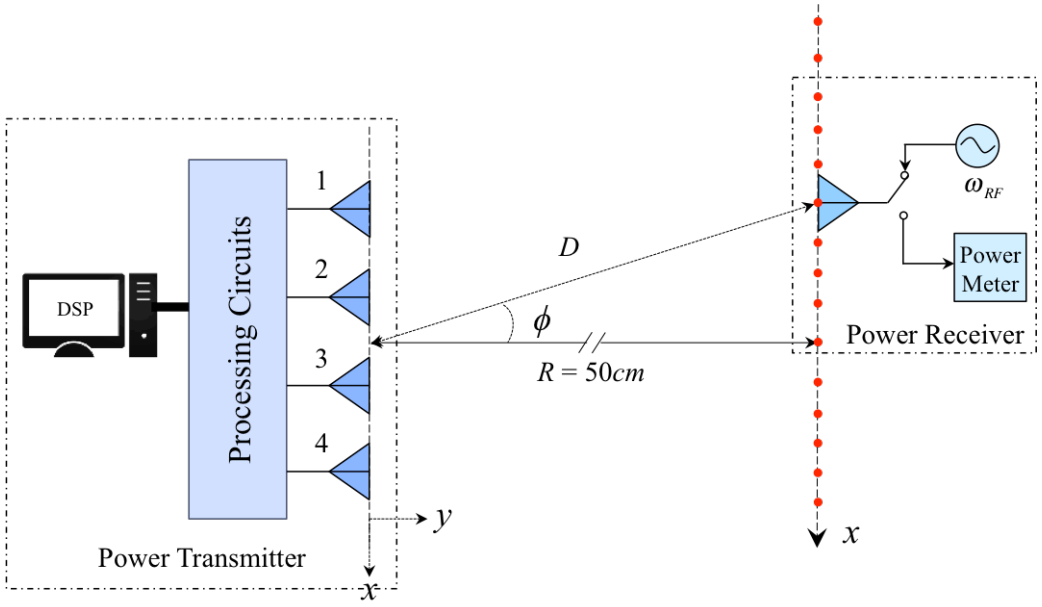

Figure 4-2 Schematic of experiment setup.

Table 4-1 lists all the circuit components used in the system implementation. ADCs are 40MS/s 12-bit 4-channel simultaneous data acquisition card, and DACs are 100KS/s 16-bit 8-channel simultaneous analog output card, both are made by Beijing Art

Technology Development Co. The VCO in the power receiver is the same as that in the power transmitter. The power meter is NRP-Z21 made by Rohde and Schwarz Inc. Because the experiments are not in real time, the switch is not used in the power receiver. We just connect the antenna to the VCO when it transmits pilot signal and to the power meter when it receives power.

Table 4-1 Circuit Components Used in The Power Transmitter

Components	Model	Manufacturer
LNA	ADL5523	Analog Devices
Mixer	ADL5365	Analog Devices
VCO	ADF4360-1	Analog Devices
ADC	PCI8502	Beijing Art Technology Development Co., ltd.
DAC	PCI8250	Beijing Art Technology Development Co., ltd.
Phase shifter	HMC928LP5E	Hittite
PA	ADL5323	Analog Devices

4.1.3 Antenna Design

The design of the antenna is not the focus of this dissertation, so a microstrip patch antenna is used in the single frequency WPT experiment, since it is low-profile, low weight, and easy to fabricate. The principle and design of the microstrip antenna is classical and can be found in [107], so the design procedure and details are omitted here. A 4-element rectangular microstrip patch antenna array is designed for the power transmitter, and a circular patch antenna is designed for power receiver. The antennas are simulated using commercial software HFSS. Both antennas are designed to resonate at 2.1GHz using FR4 (ε_r = 4.6). The thickness of substrate is 2.5mm. Dimensions of the array and circular patch are shown in Figure 4-3 and Figure 4-4, respectively, and summarized in Table 4-2.

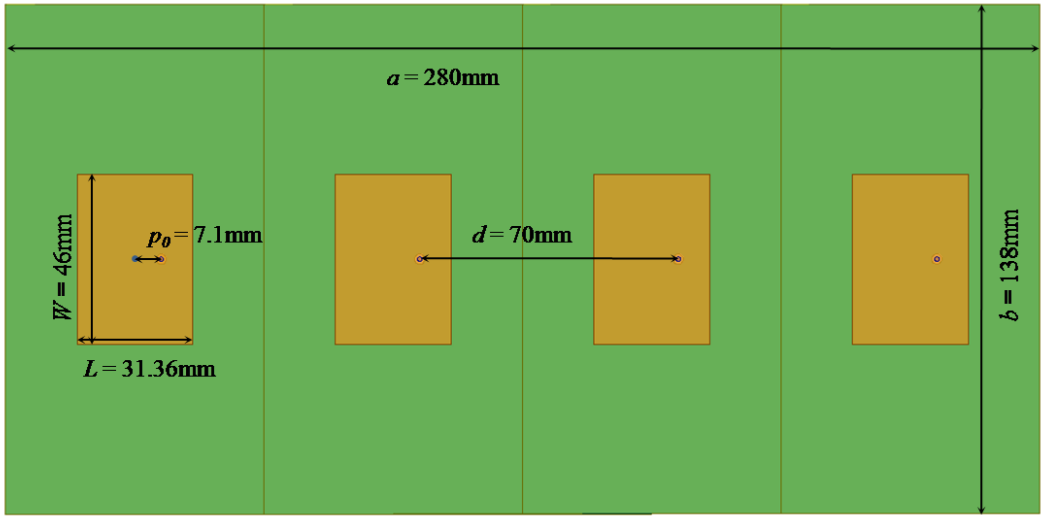

Figure 4-3 Dimensions of 4-element rectangular patch antenna array.

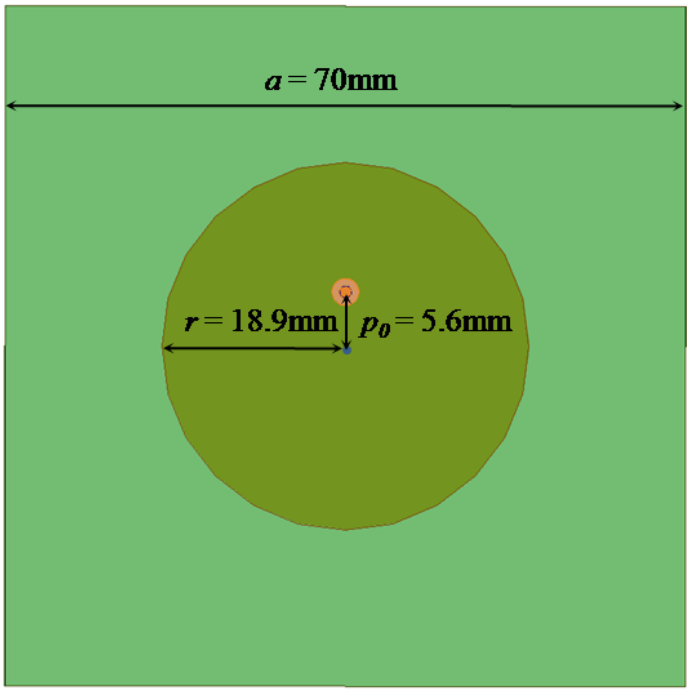

Figure 4-4 Dimensions of circular patch receiving antenna.

Return losses of the antennas are measured using Agilent N5230C. The results for the circular patch antenna and 4-element array are shown in Figure 4-6 and Figure 4-5, respectively. The measured resonant frequencies are lower than the simulation

results. The reason is that the dielectric constant of FR4 material is not exactly 4.6 due to fabrication tolerance. Changing the dielectric constant to 4.7 will better match the simulation results to measured ones. The photos of the fabricated antenna array and circular patch antenna are shown in Figure 4-7 and Figure 4-8, respectively.

Table 4-2 Antenna Design Parameters

Description	Symbol	Dimensions
4-element array		
Patch width	*W*	46 mm
Patch length	*L*	31.36 mm
Feed position from patch center	p_0	7.1 mm
Antenna spacing	*d*	70 mm
Ground length	*a*	280 mm
Ground width	*b*	138 mm
Circular patch		
Patch radius	*r*	18.9 mm
Feed position from patch center	p_0	5.6mm
Ground width	*a*	70 mm

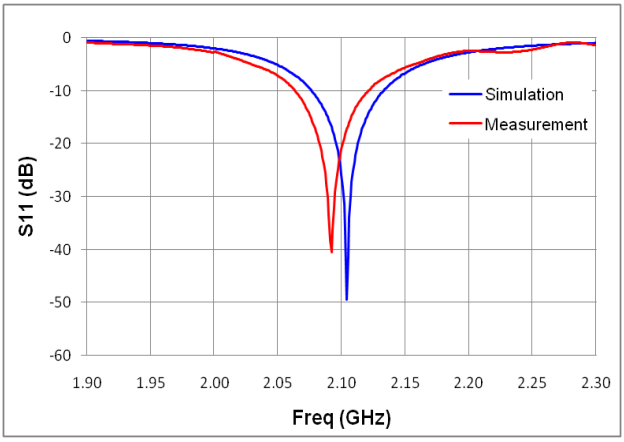

Figure 4-5 Return loss of the circular patch antenna.

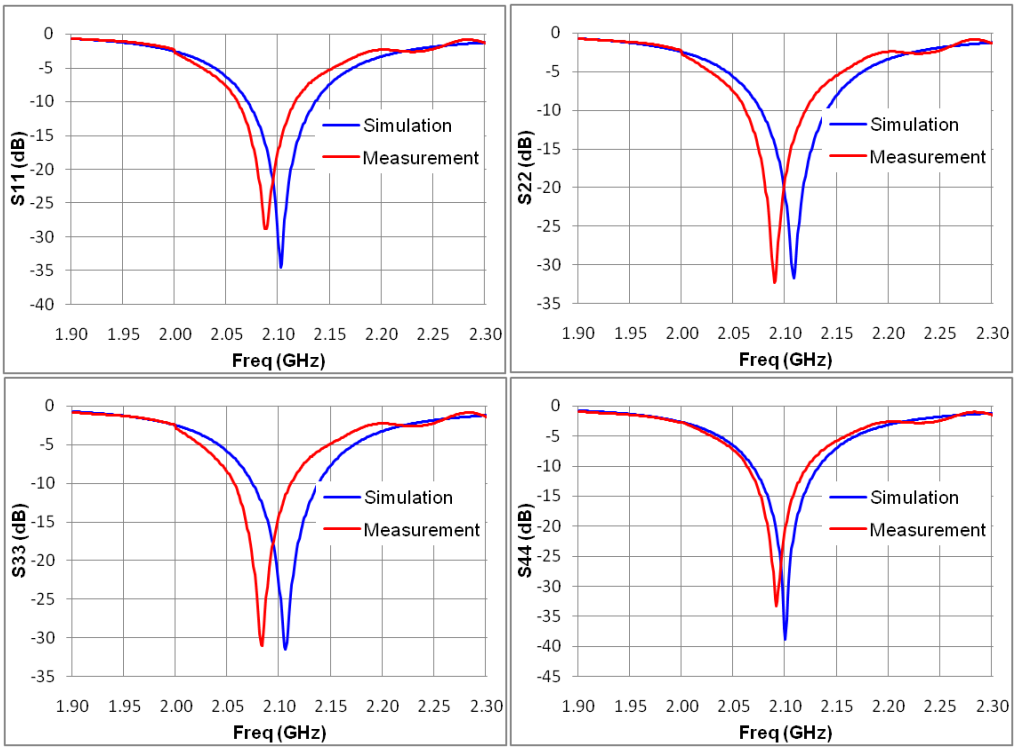

Figure 4-6 Return loss of the 4-element antenna array.

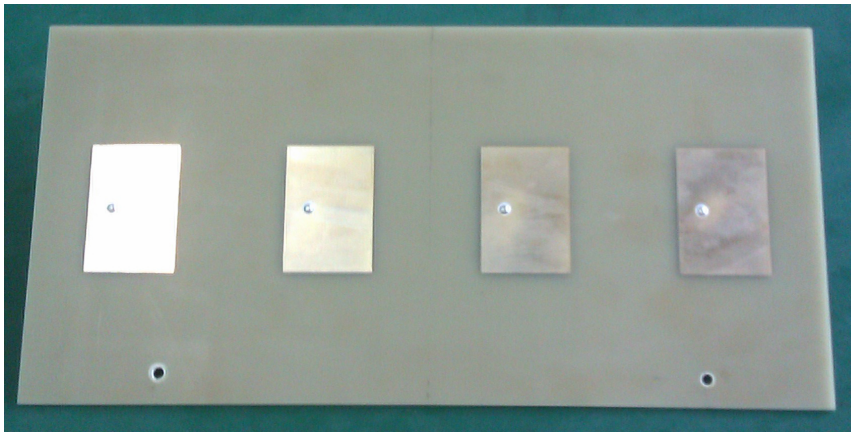

Figure 4-7 Photo of the fabricated 4-element antenna array.

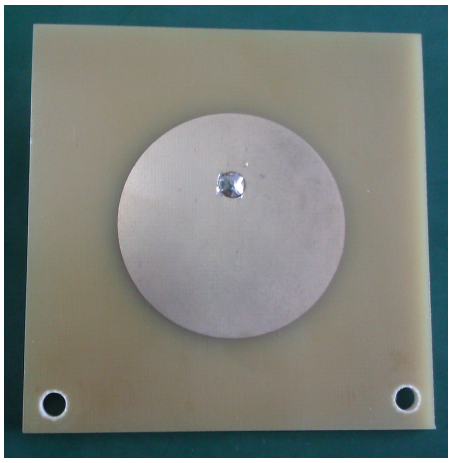

Figure 4-8 Photo of the fabricated circular patch antenna.

4.1.4 Calculation of Transmission Efficiency

The efficiency of the wireless power transmission can be calculated theoretically using Friis transmission equation,

$$\eta = \frac{P_r}{P_t} = G_t\left(\theta_t,\phi_t\right)G_r\left(\theta_r,\phi_r\right)\left(\frac{\lambda}{4\pi D}\right)^2 \tag{4.2}$$

where $G_t\left(\theta_t,\phi_t\right)$ is the gain of transmitting antenna in the direction of $\left(\theta_t,\phi_t\right)$, $G_r\left(\theta_r,\phi_r\right)$ is the gain of receiving antenna in the direction of $\left(\theta_r,\phi_r\right)$, λ is the wavelength of operation, and *D* is the distance between antennas (center-to-center). In our cases, the receiving antenna is always facing -*y* direction as shown in Figure 4-2, which mean $\left(\theta_t,\phi_t\right)=\left(\theta_r,\phi_r\right)$. Also both antenna are in the *xy*-plane, or $\theta_t=\theta_r=90^o$. In equation (4.2) we assume there is no polarization mismatch and the antennas are perfectly matched to the following circuits. Equation (4.3) is then simplified to,

$$\eta = G_t\left(\phi\right)G_r\left(\phi\right)\left(\frac{\lambda}{4\pi D}\right)^2 \tag{4.3}$$

It will be more convenient by expressing equation (4.3) in dB scale,

$$\begin{aligned}\eta_{dB} &= 10 \bullet \log_{10}\left\{ G_t(\phi) G_r(\phi) \left(\frac{\lambda}{4\pi D} \right)^2 \right\} \\ &= G_{t,dB}(\phi) + G_{r,dB}(\phi) + 20 \bullet \log_{10}\left(\frac{\lambda}{4\pi D} \right)\end{aligned} \tag{4.4}$$

According to the setup in Figure 4-2, direction ϕ and distance D can be calculated by,

$$\begin{aligned} D &= \sqrt{R^2 + x^2} \\ \phi &= \tan^{-1}\left(\frac{x}{R} \right)\end{aligned} \tag{4.5}$$

The gains for the receiving antenna in different angles are found by simulating the radiation pattern in HFSS. For the antenna array, the radiation pattern is the multiplication of array factor and single-element radiation pattern. For the uniform linear array with equal excitation, the array factor (AF) can be found in [108],

$$AF = \sum_{n=1}^{N} e^{j(n-1)\psi} = \frac{\sin\left(N\frac{\psi}{2} \right)}{\sin\left(\frac{\psi}{2} \right)} e^{j(N-1)\frac{\psi}{2}} \tag{4.6}$$

where $\psi = kd\sin\phi + \beta$, $k = 2\pi / \lambda$ is wave number, d is antenna spacing, β is the phase difference between adjacent elements, and *N* is number of elements. The maximum values of the array factor $|AF|$ occur when

$$\psi = kd\sin\phi_{\max} + \beta = \pm 2m\pi,\ m = 0,1,2,... \tag{4.7}$$

where ϕ_{max} is the main beam direction. So given the desired main beam direction, we can find the phase difference β by,

$$\beta = -kd\sin\phi_{\max} \pm 2m\pi,\ m = 0,1,2,... \tag{4.8}$$

Once the antenna gains are available, the transmission efficiency can be calculated by equation (4.3). The calculated efficiencies for 2-element array are listed in Table 4-3. It can be seen the efficiency drops as the receiver moves away from the center. This is largely due to the decrease of the gain as the incident angle increases. The gain and efficiency increase slightly as the operating frequency goes higher.

Table 4-3 Calculation of Transmission Efficiency for 2-element Antenna Array.

x (cm)	ϕ (deg)	D (cm)	G_t (dB)	G_r (dB)	η (%)
2.06GHz					
0	0	50	6.56	3.92	0.60
-10	-11	51	5.94	3.70	0.48
-20	-22	54	5.32	3.12	0.32
-30	-31	58	5.77	2.40	0.26
2.08GHz					
0	0	50	6.74	3.95	0.63
-10	-11	51	6.21	3.74	0.51
-20	-22	54	5.63	3.17	0.35
-30	-31	58	5.94	2.46	0.28
2.108GHz					
0	0	50	6.97	4.00	0.67
-10	-11	51	6.52	3.80	0.56
-20	-22	54	5.96	3.24	0.38
-30	-31	58	6.11	2.53	0.29

The radiation patterns of the 2-element array for different scanning angles are plotted in Figure 4-9, Figure 4-10 and Figure 4-11 for frequency of 2.06GHz, 2.08GHz, and 2.108GHz, respectively. However, the main beam is too wide, so the focusing effect is not obvious. Also, the beam pointing error (BPE), which is the difference between the desired beam direction and actual beam direction, is too large.

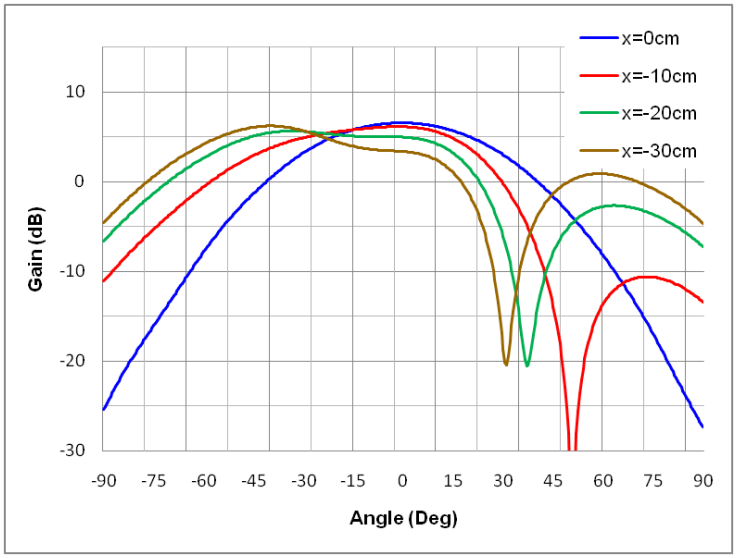

Figure 4-9 Radiation patterns of 2-element antenna array at 2.06GHz.

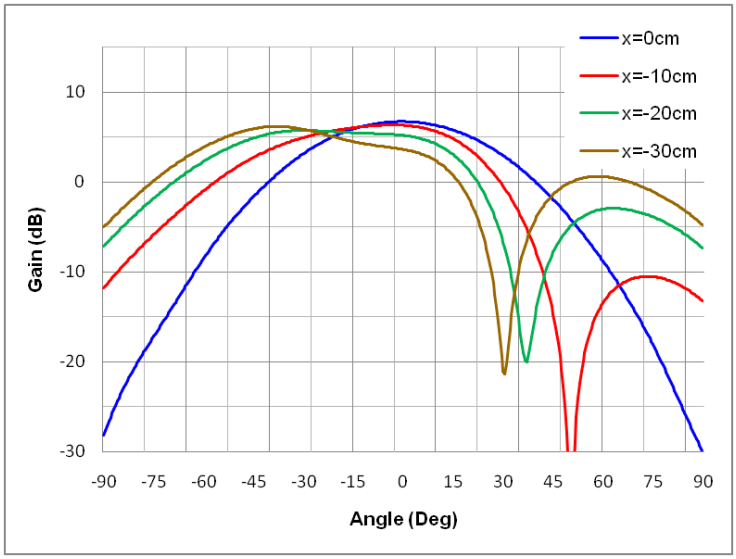

Figure 4-10 Radiation patterns of 2-element antenna array at 2.08GHz.

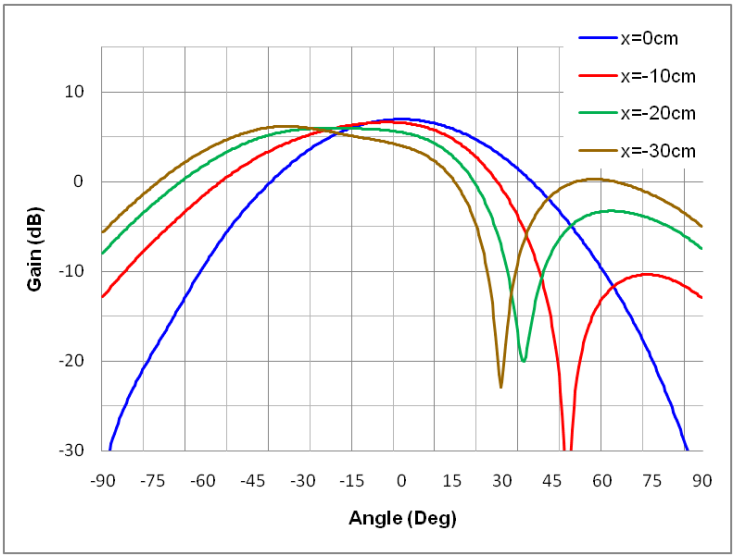

Figure 4-11 Radiation patterns of 2-element antenna array at 2.108GHz.

The beam pointing error can be improved by increasing the number of elements [108]. The simulation results for 4-element array are plotted in Figure 4-12, Figure 4-13, and Figure 4-14. Compared to 2-element array, the BPEs are greatly reduced, and the main beam width becomes narrower. The maximum gain also increases.

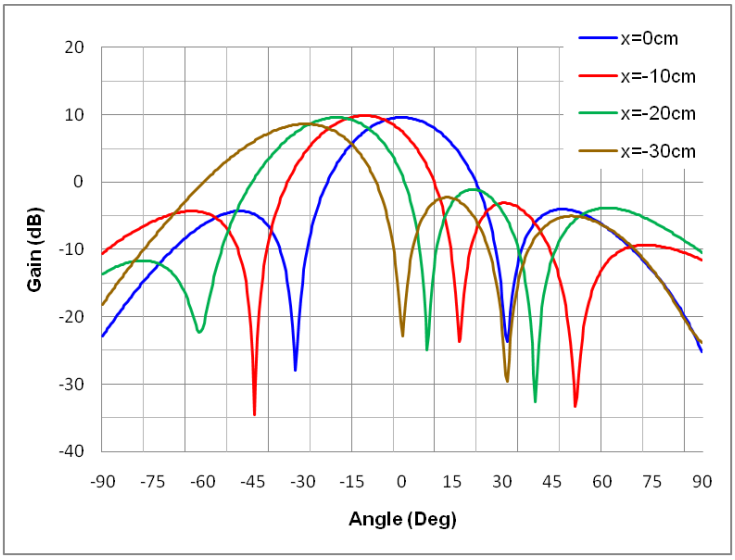

Figure 4-12 Radiation patterns of 4-element antenna array at 2.06GHz.

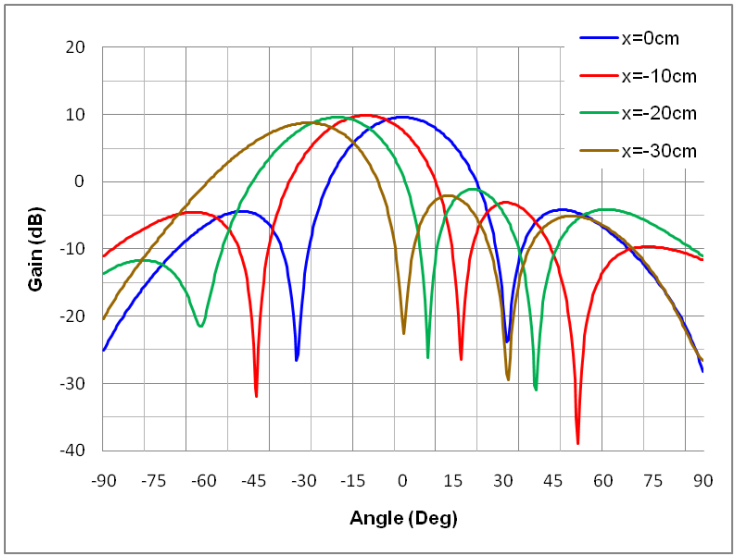

Figure 4-13 Radiation patterns of 4-element antenna array at 2.08GHz.

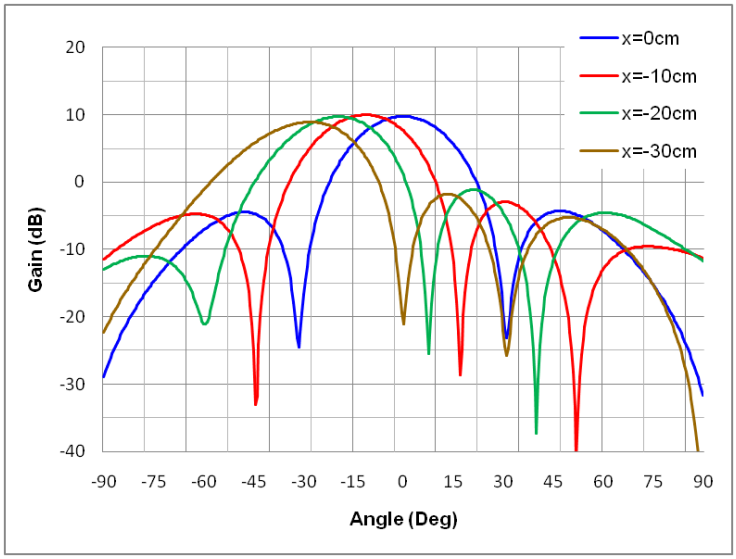

Figure 4-14 Radiation patterns of 4-element antenna array at 2.108GHz.

The transmission efficiency for 4-element array is calculated in Table 4-4. Compared to the 2-element array, the efficiencies for all cases are increased. Theoretically, the efficiency will increase linearly with respect to the number of antenna

element, however, the mutual couplings between antenna elements limit the total gain of the array.

Table 4-4 Calculation of Transmission Efficiency for 4-element Antenna Array.

x (cm)	ϕ (deg)	D (cm)	G_t (dB)	G_r (dB)	η (%)
2.06GHz					
0	0	50	9.54	3.92	1.19
-10	-11	51	9.86	3.70	1.17
-20	-22	54	9.48	3.12	0.84
-30	-31	58	8.61	2.40	0.50
2.08GHz					
0	0	50	9.63	3.95	1.23
-10	-11	51	9.92	3.74	1.20
-20	-22	54	9.55	3.17	0.86
-30	-31	58	8.70	2.46	0.52
2.108GHz					
0	0	50	9.74	4.00	1.27
-10	-11	51	9.98	3.80	1.23
-20	-22	54	9.62	3.24	0.89
-30	-31	58	8.80	2.53	0.54

4.1.5 Simulation of Transmission Efficiency

More rigorous simulations are performed using HFSS. The setup in Figure 4-2 is modeled in HFSS, as shown in Figure 4-15. Perfect Matched Layer (PML) boundary condition is used in the simulation instead of radiation boundary condition because it has no reflection for incidence from any angle. For better accuracy, all PMLs are placed at least 50mm (about 1/3 wavelength) away from any radiating object, and the thickness of PML layers is 100mm. Lumped ports with 50 ohm impedance are used for excitations of antennas. Port 1 to 4 are assigned to transmitting antennas, and port 5 is assigned to the receiving antenna. In this setup, the transmission efficiency is calculated using transmission coefficients between antennas. Assume the pilot signal is $f(t) = \cos(\omega t)$, the signal receiver at antenna *i* will be,

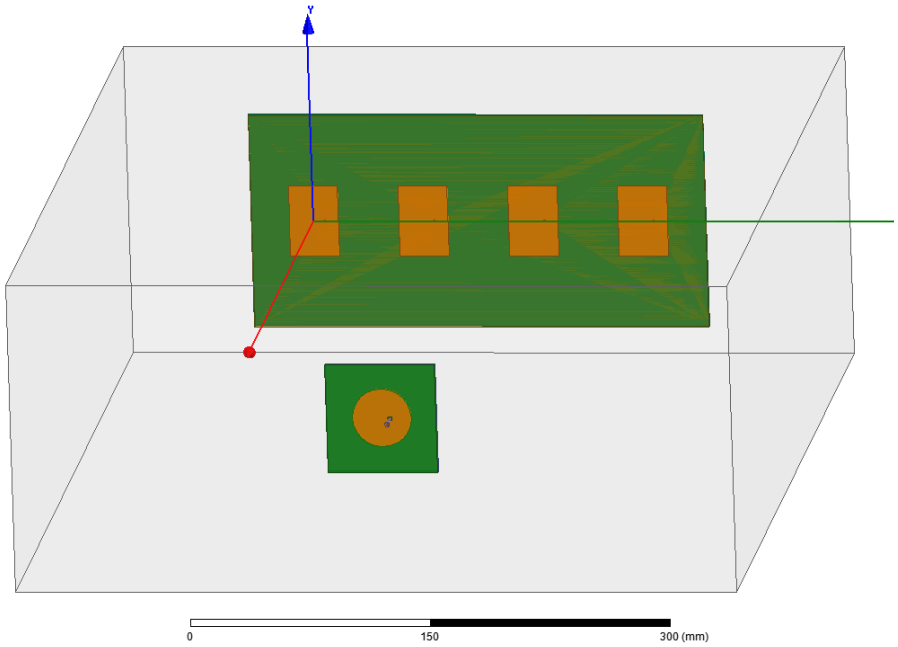

Figure 4-15 HFSS model of experiment setup.

$$\begin{aligned} g(t) &= \mathrm{Re}\left\{ f(t)S(i,5) \right\} = \mathrm{Re}\left\{ \cos(\omega t)\left|S(i,5)\right| e^{j\phi_i} \right\} \\ &= \cos(\omega t + \phi_i)\left|S(i,5)\right| \end{aligned} \tag{4.9}$$

where S(*i*,5) represents transmission coefficient from antenna 5 to antenna *i*. When phase-conjugate and amplification are applied, the retransmitted signal from each antenna of the transmitting array will be,

$$\hat{g}(t) = A\cos(\omega t - \phi_i) = \mathrm{Re}\left\{ A\cos(\omega t)e^{-j\phi_i} \right\} \tag{4.10}$$

where *A* is the amplitude of the retransmitted signal. Because of reciprocity, the transmission coefficient from antenna i to antenna *5 S(5,i)* is equal to *S(i,5)*, so the signal received at antenna *5* from antenna *i* is,

$$\begin{aligned}\hat{f}(t) &= \mathrm{Re}\left\{\hat{g}(t)S(5,i)\right\} = \mathrm{Re}\left\{A\cos(\omega t)e^{-j\phi_i}S(5,i)\right\} \\ &= \mathrm{Re}\left\{A\cos(\omega t)e^{-j\phi_i}\left|S(5,i)\right|e^{j\phi_i}\right\} \\ &= \mathrm{Re}\left\{A\cos(\omega t)\left|S(5,i)\right|\right\} \\ &= A\cos(\omega t)\left|S(5,i)\right|\end{aligned} \tag{4.11}$$

Thus the waves from each transmitting antenna will add up constructively at the receiver. The transmission efficiency is then calculated by,

$$\eta = \frac{\left(A\sum_{i=1}^{N}\left|S(5,i)\right|\right)^2}{NA^2} = \frac{\left(\sum_{i=1}^{N}\left|S(5,i)\right|\right)^2}{N} \tag{4.12}$$

Table 4-5 lists the simulated transmission efficiencies. The calculated transmission efficiencies are also included for comparison. For the 2-element antenna array, only antennas in the center (antenna 2 and 3) are used. The simulation results agree with the calculations, but are smaller in all cases because they take into account of the impedance mismatch and polarization mismatch.

Table 4-5 Comparisons of Transmission Efficiency Between Calculation and Simulation.

2-element Array						
	2.06GHz		2.08GHz		2.108GHz	
x (cm)	Calculation	Simulation	Calculation	Simulation	Calculation	Simulation
0	0.60	0.45	0.63	0.58	0.67	0.58
-10	0.48	0.41	0.51	0.52	0.56	0.51
-20	0.32	0.28	0.35	0.36	0.38	0.36
-30	0.26	0.20	0.26	0.24	0.29	0.23
4-element Array						
	2.06GHz		2.08GHz		2.108GHz	
x (cm)	Calculation	Simulation	Calculation	Simulation	Calculation	Simulation
0	1.19	0.86	1.23	1.09	1.27	1.09
-10	1.17	0.85	1.20	1.04	1.23	1.00
-20	0.84	0.66	0.86	0.80	0.69	0.78
-30	0.50	0.43	0.52	0.51	0.54	0.47

The electrical field distributions at 2.08GHz different receiver positions are shown in Figure 4-16, Figure 4-17, Figure 4-18 and Figure 4-19. The field distributions at other frequencies are similar and not shown here. Antenna 1 and 4 are disabled (excitation is set zero) in the 4-element array to simulate the 2-element antenna array. It can be seen that the waves propagate in the direction of receiver location, and the beam width of the 4-element array is much narrower than that of the 2-element array.

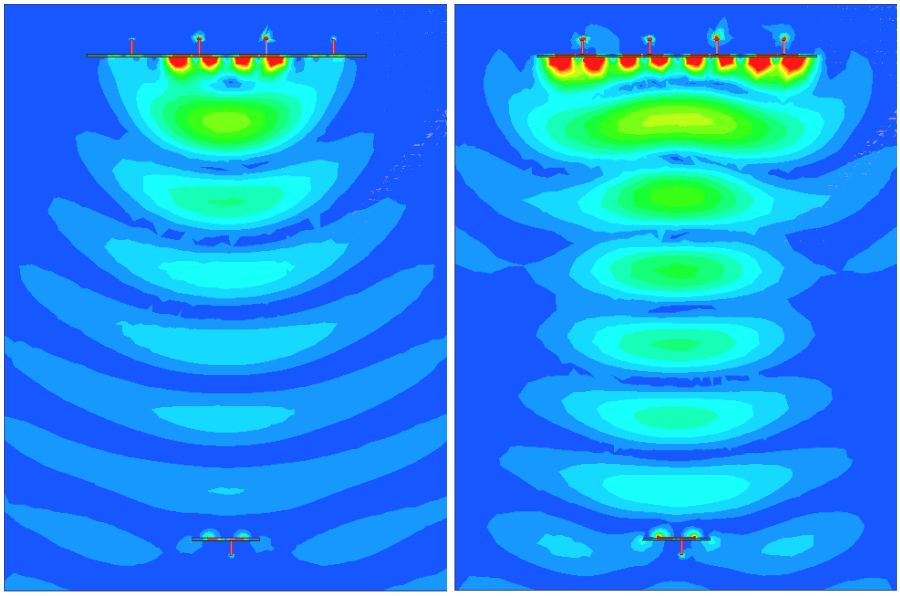

(a) (b)

Figure 4-16 Electric fields distributions for receiver at x=0cm. The fields are plotted on xy-plane at 2.08GHz. (a) 2-element array, (b) 4-element array.

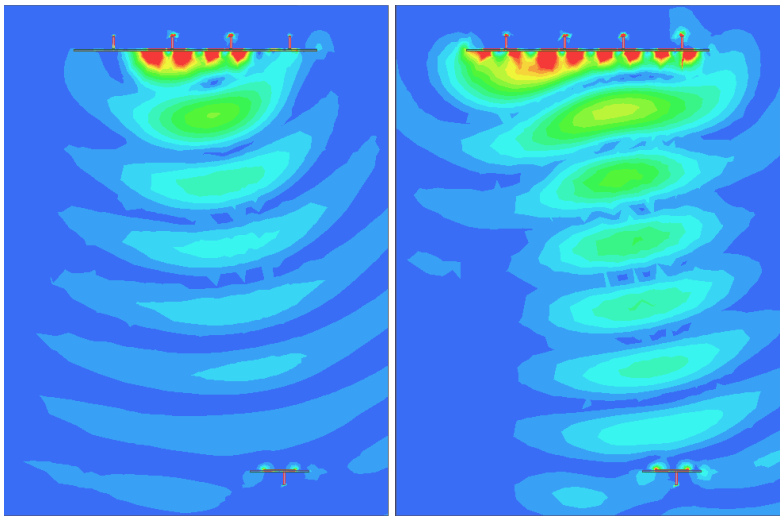

(a) (b)

Figure 4-17 Electric fields distributions for receiver at x=-10cm. The fields are plotted on xy-plane at 2.08GHz. (a) 2-element array, (b) 4-element array.

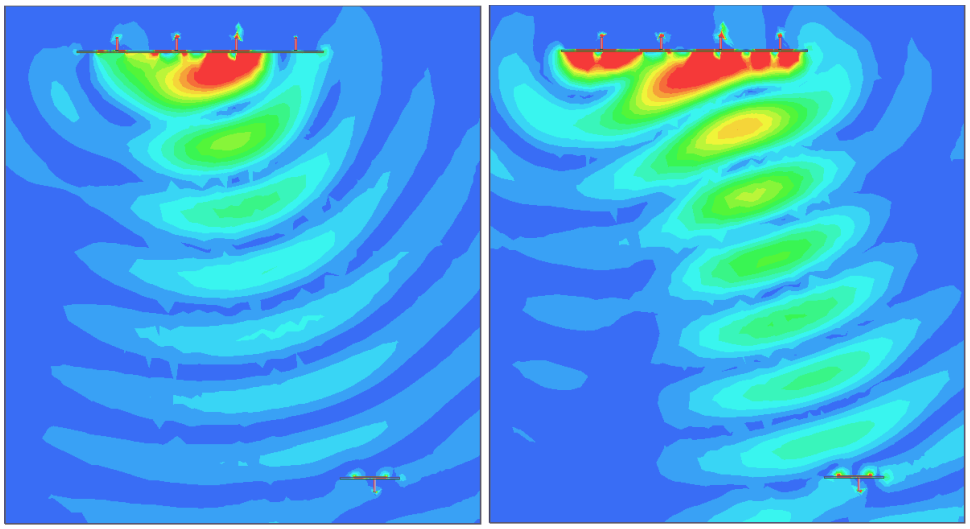

(a) (b)

Figure 4-18 Electric fields distributions for receiver at x=-20cm. The fields are plotted on xy-plane at 2.08GHz. (a) 2-element array, (b) 4-element array.

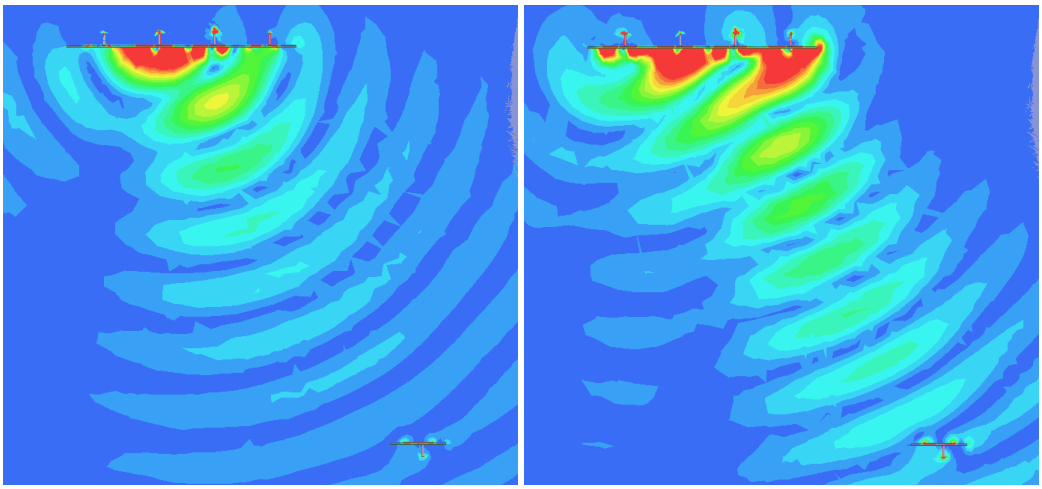

(a) (b)

Figure 4-19 Electric fields distributions for receiver at x=-30cm. The fields are plotted on xy-plane at 2.08GHz. (a) 2-element array, (b) 4-element array.

4.1.6 Experiment Results of Transmission Efficiency

The photo of the experiment setup in power transmission mode is shown in Figure 4-20. The input power for each antenna is about 23dBm measured by power meter. The received powers measured along the x-axis at different frequencies are plotted in Figure 4-21, Figure 4-22 and Figure 4-23. The results show good agreement with the simulated radiation patterns in Figure 4-9, Figure 4-10 and Figure 4-11. However, as predicted by simulation, the beam width is too wide and the beam pointing error is very large too.

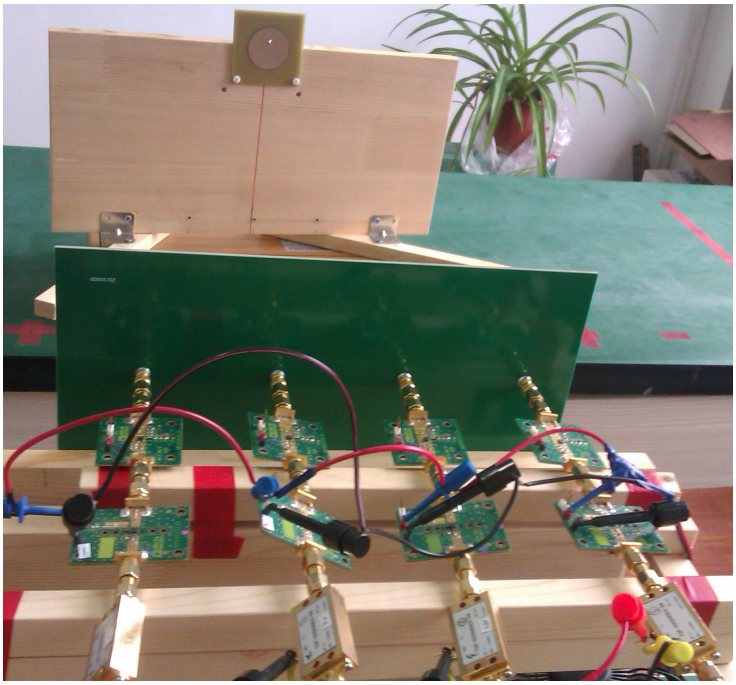

Figure 4-20 Photo of experiment setup in power transmission mode.

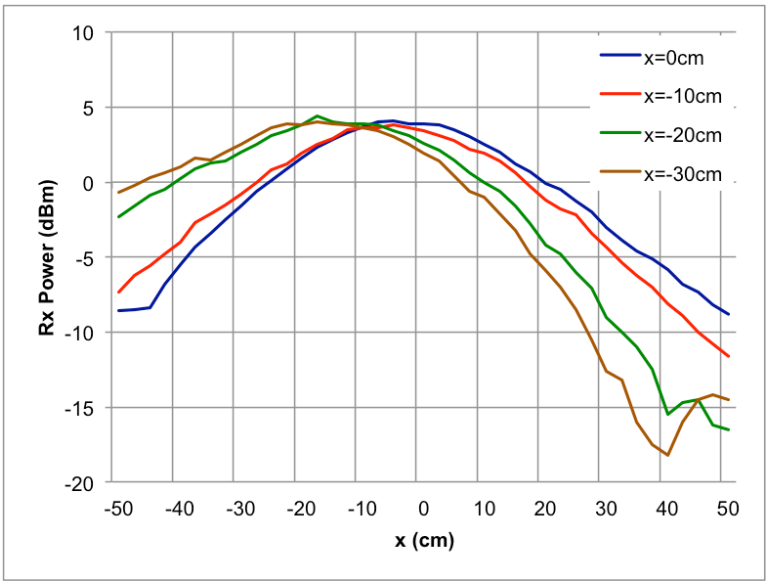

Figure 4-21 Measurement of received power of 2-element antenna array for different pilot signal positions at 2.06GHz.

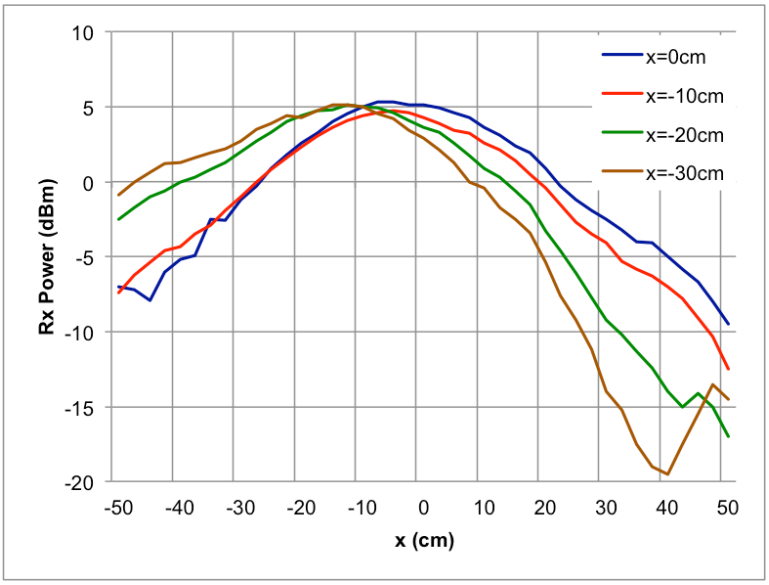

Figure 4-22 Measurement of received power of 2-element antenna array for different pilot signal positions at 2.08GHz.

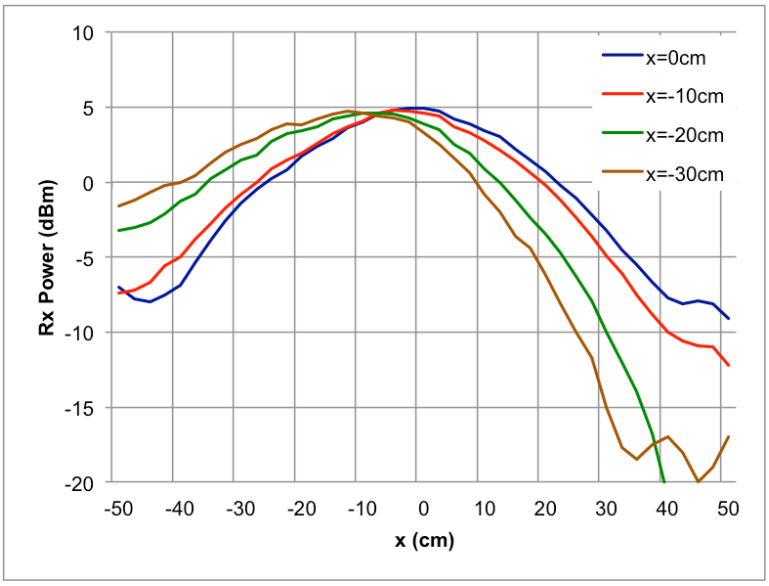

Figure 4-23 Measurement of received power of 2-element antenna array for different pilot signal positions at 2.108GHz.

The measurement results for 4-element array are plotted in Figure 4-24, Figure 4-25 and Figure 4-26. The results also agree with simulated radiation patterns. Knowing the combined transmitting power for 4 antennas is about 29dBm, we can easily calculate the transmission efficiency. The comparisons of transmission efficiency between calculation, simulation and test results are summarized in Table 4-6. The test results are higher than the calculation and simulation. One reason is that the measurements were not done in the anechoic chamber, so the multipath reflection could cause fluctuation of received power. Also the power meter measures the total power in a wide bandwidth, thus the interference and noise in the environment add to the received power. The measured transmission efficiency between 2-element array and 4-element array are compared in Figure 4-27, Figure 4-28 and Figure 4-29, at frequency 2.06GHz, 2.08GHz and 2.108GHz respectively. The average improvement of transmission efficiency is about 70% at 2.06GHz, 91% at 2.08GHz and 168% at 2.108GHz.

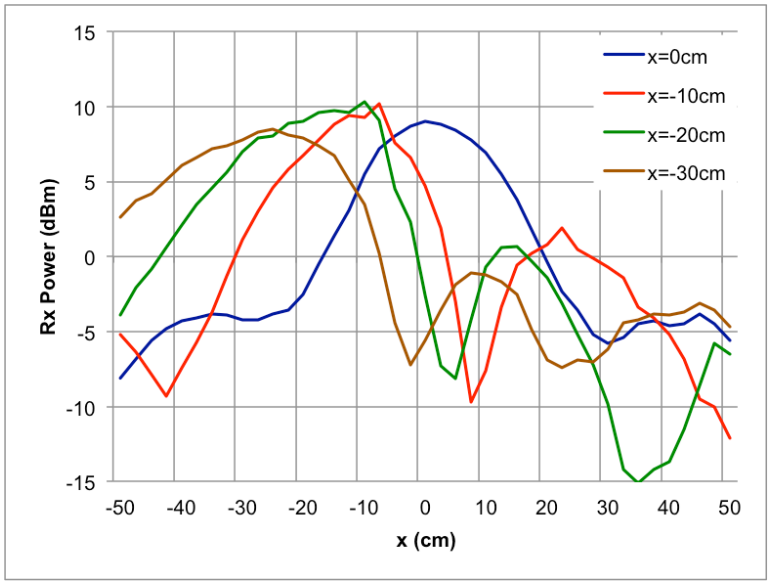

Figure 4-24 Measurement of received power of 4-element antenna array for different pilot signal positions at 2.06GHz.

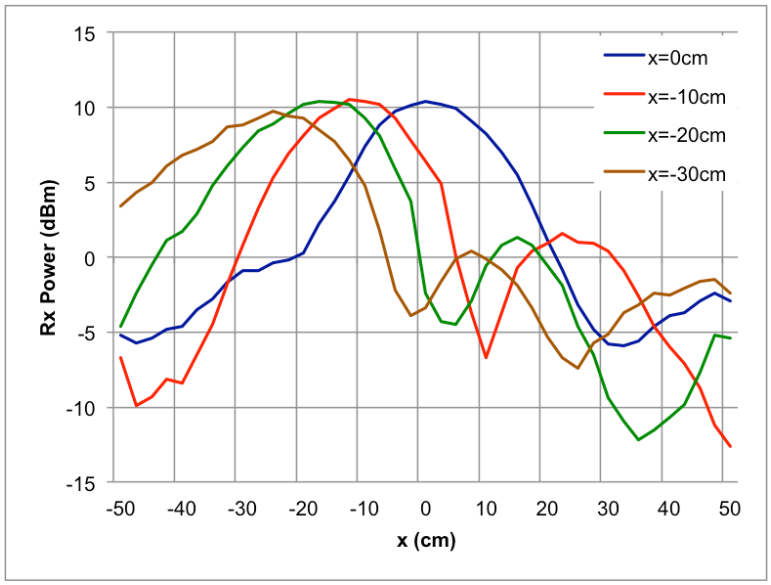

Figure 4-25 Measurement of received power of 4-element antenna array for different pilot signal positions at 2.08GHz.

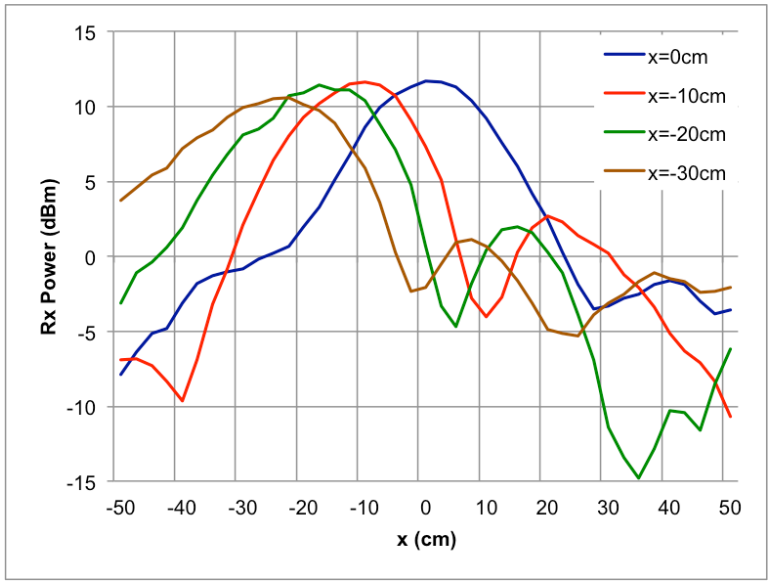

Figure 4-26 Measurement of received power of 4-element antenna array for different pilot signal positions at 2.108GHz.

Table 4-6 Comparisons of Transmission Efficiency Between Calculation, Simulation and Experiment.

2-element Array					
		x=0cm	x=-10cm	x=-20cm	x=-30cm
2.06GHz	Calculation	0.60	0.48	0.32	0.26
	Simulation	0.45	0.41	0.28	0.20
	Test	0.62	0.58	0.60	0.45
2.08GHz	Calculation	0.63	0.51	0.35	0.26
	Simulation	0.58	0.52	0.36	0.24
	Test	0.81	0.69	0.69	0.47
2.108GHz	Calculation	0.67	0.56	0.38	0.29
	Simulation	0.58	0.51	0.36	0.23
	Test	0.79	0.65	0.55	0.45
4-element Array					
		x=0cm	x=-10cm	x=-20cm	x=-30cm
2.06GHz	Calculation	1.19	1.17	0.84	0.50
	Simulation	0.86	0.85	0.66	0.43
	Test	1.00	1.07	1.00	0.76
2.08GHz	Calculation	1.23	1.20	0.86	0.52
	Simulation	1.09	1.04	0.80	0.51
	Test	1.38	1.38	1.32	0.95
2.108GHz	Calculation	1.27	1.23	0.69	0.54
	Simulation	1.09	1.00	0.78	0.47
	Test	1.86	1.82	1.55	1.23

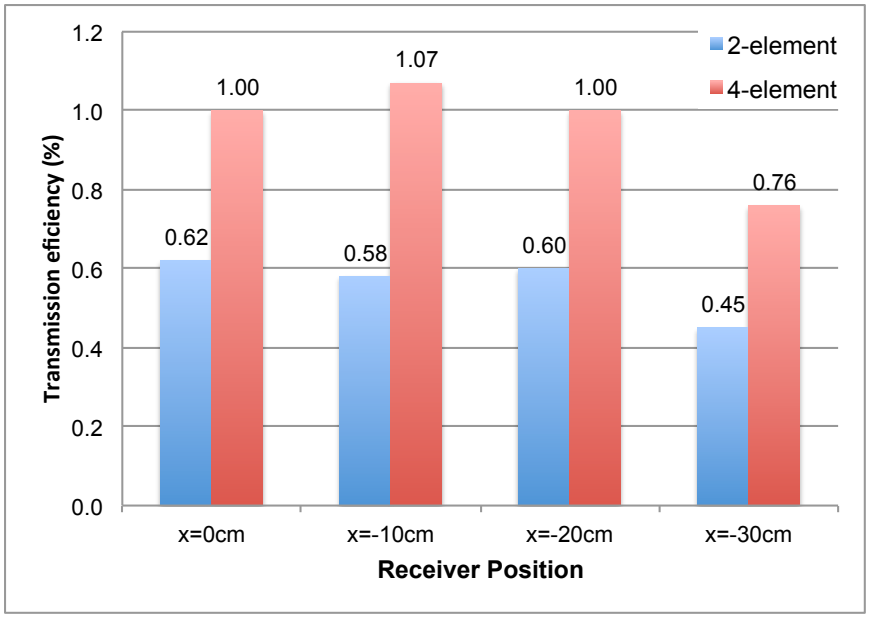

Figure 4-27 Comparison of measured transmission efficiency between 2-element and 4-element arrays at 2.06GHz.

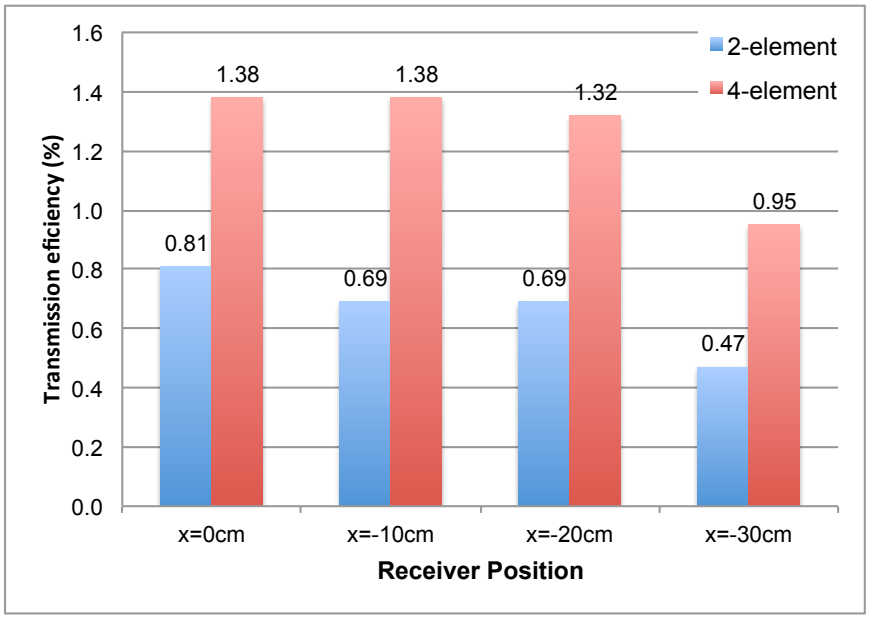

Figure 4-28 Comparison of measured transmission efficiency between 2-element and 4-element arrays at 2.08GHz.

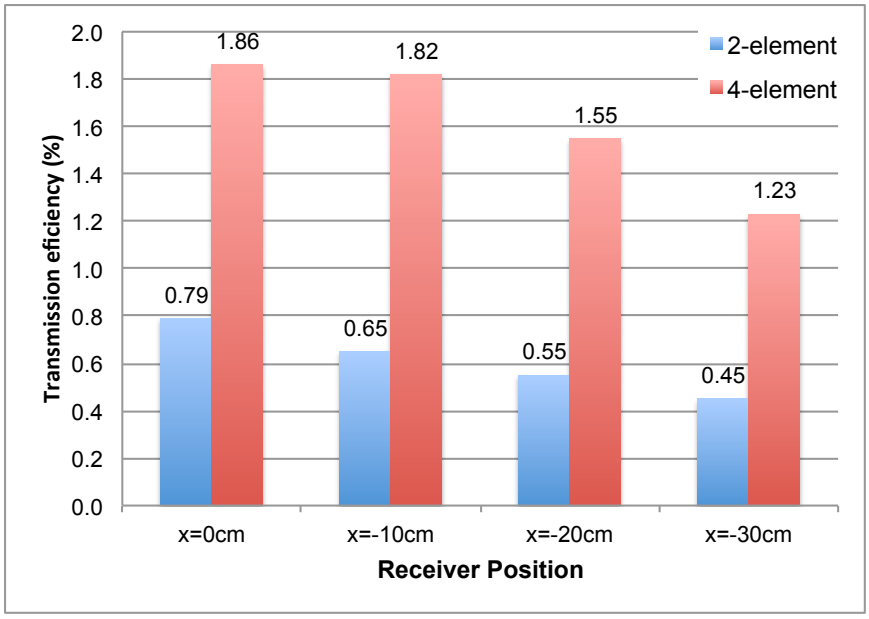

Figure 4-29 Comparison of measured transmission efficiency between 2-element and 4-element arrays at 2.108GHz.

4.2 Rectenna

A rectenna is the combination of Rectifier and Antenna. It is used to convert RF energy into DC energy. It usually consists of four subsystems, as shown in Figure 4-30, (1) antenna, (2) impedance matching, (3) rectification and (4) filtering.

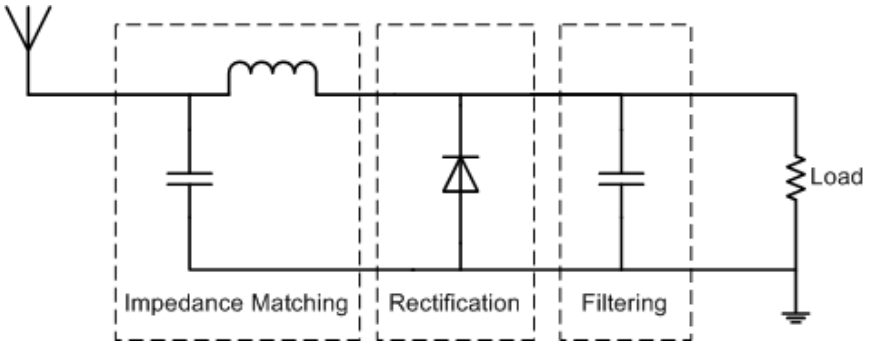

Figure 4-30 Basic rectenna system.

4.2.1 Antenna

The antenna is used to receive the RF energy. Depending on the applications, the antenna may have high gain or omni-directional property, broadband or narrow band. Polarization can be linear, dual, or circular, depending on the polarization of transmitting antennas. However, high efficiency, low weight and small size is always desirable.

4.2.2 Impedance Matching

The impedance matching serves two purposes. Primarily it matches the antenna input impedance to the input impedance of rectification circuit so that maximum power captured by antenna will be transferred to the next stage. The impedance matching can also serves as a filter to prevent the reradiation of high order harmonics produced by rectifying diode. This not only suppresses the interference to other around devices, but also increases the conversion efficiency by reflecting the harmonics back to the rectifier.

Depending on the geometry, the antenna itself can also function as a filter. For example, the rectangular patch antenna resonates at the fundamental frequency and its harmonic frequencies. The harmonics generated by the diode coincide with the resonant frequencies of rectangular patch antenna. However, for a circular patch antenna, its resonant frequencies correspond to the root of first kind Bessel function, which is not a multiple integer of fundamental frequency, therefore suppressing the reradiation of high order harmonics.

4.2.3 Rectification

The heart of a rectenna is rectification. This is where the RF energy is converted DC energy. The basic principle of rectification is analogous to diode clamping circuit [97]. The conversion efficiency of a diode depends on the input power level. The general relationship is shown in Figure 4-31, where V_j, V_{br}, and R_L are the forward voltage drop (or turn-on voltage), reverse breakdown voltage, and the DC load resistance,

respectively. The efficiency is small when the power is low because the voltage across the diode is smaller than or comparable with the forward voltage drop of the diode. As the power level increases the efficiency increases as well, but the rate of increase becomes smaller because the generation of stronger high order harmonics. The efficiency decreases when the power is too large that the voltage at the diode exceeds the reverse breakdown voltage. The critical input power where the breakdown effect becomes dominant is expressed as $V_{br}^2 / 4R_L$.

The equivalent circuit model of a diode is shown in Figure 4-32. It consists of a series resistor R_s, a nonlinear junction resistor R_j described by the I-V characteristic curve, and a nonlinear junction capacitance C_j. The cutoff frequency of a diode is determined by Equation (4.13) [97], where C_{j0} is zero-bias junction capacitance,

$$f_{cutoff} = \frac{1}{2\pi R_s C_{j0}} \tag{4.13}$$

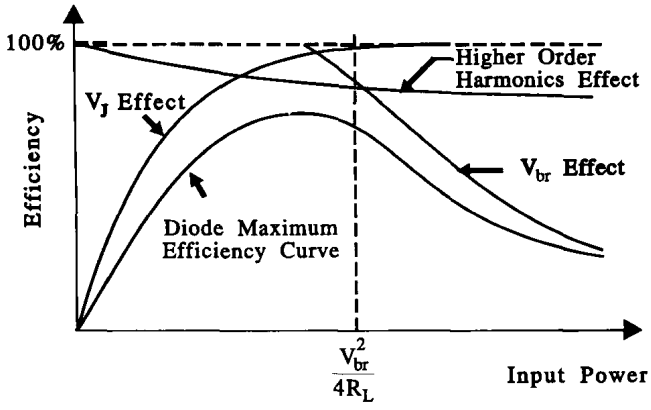

Figure 4-31 General relationship between diode conversion efficiency and input power [97].

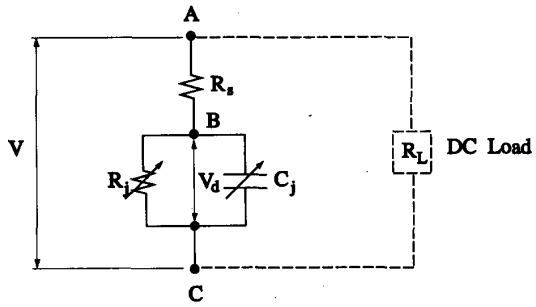

Figure 4-32 Equivalent circuit of diode [97].

Theoretical close-form equation for the power conversion efficiency can be found in [97]. In general the efficiency is defined by:

$$\eta = \frac{P_{out}}{P_{in}} = \frac{V_{DC}^2 / R_L}{P_{in}} \times 100\% \tag{4.14}$$

Where V_{DC} is DC output voltage at load R_L, and P_{in} is input power.

To achieve high efficiency, a diode with low forward voltage drop, high reverse breakdown voltage, low capacitance and series resistance is desirable. But these parameters are related to each other due to the diode material properties, for example, lower forward voltage drop usually means lower reverse breakdown voltage. When the RF power is low, the output voltage is usually small and not enough to drive other circuit components, so the voltage multiplier is often used to boost the output voltage. A voltage doubler is shown in Figure 4-33. Assume the diode is ideal, i.e., the forward voltage drop is zero. Let the input AC voltage has a peak amplitude V_{ac}. During the negative half-cycle of the input signal, D1 will be open and C1 is charged to the peak of input voltage V_{ac}. During the following positive half cycle of input, D1 is turned off and D2 is open. The voltage across C1 remains unchanged and adds on to the input, so that the voltage at position 1 will be $V_1 = V_{in} + V_{ac}$. Since D2 is open now, C2 will be charged to peak voltage $2V_{ac}$. The output voltage can be further increased by adding more stages of rectification.

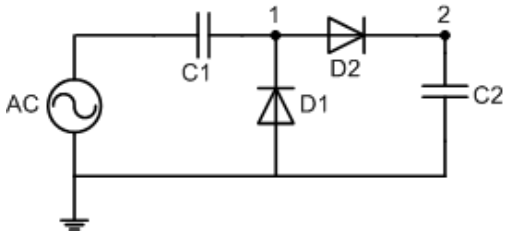

Figure 4-33 Voltage doubler.

4.2.4 Filtering

After rectification, the RF energy is converted into large DC component with small harmonic components. These harmonic components have to be filtered before feeding to the load. Usually a parallel-connected capacitor is enough.

4.2.5 Rectifier Design and Simulations

For the 4-element array, the received powers at the pilot signal locations are between 7dBm to 12dBm. A rectenna is designed and optimized for that input power range. The antenna is already designed in previous section, which is a circular patch antenna. Circular patch antenna is preferred over rectangular patch antenna because it can suppress reradiation of higher order harmonics generated by the diodes. Schottky diode SMS7630-079LF made by Skyworks Inc. is chosen here, because it has low forward voltage drop. The package model of SMS7630-079LF is shown in Figure 4-34. The SPICE model for the diode is listed in Table 4-7 [109].

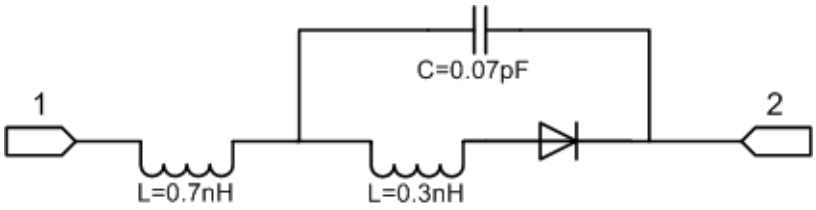

Figure 4-34 Package model of Skyworks SMS7630-079LF.

Table 4-7 SPICE Parameters of Diode SMS7621-079LF.

Parameters	Symbol	SMS7630-079LF
Reverse breakdown voltage	B_v	2 V
Current at B_v	I_{Bv}	1E-4 A
Energy bandgap	E_G	0.69 eV
Zero-bias junction capacitance	C_{j0}	0.18 pF
Saturation current	I_s	3E-6 A
Ideal factor	N	1.06
Series resistance	R_s	25 Ω
Junction potential	$P_B(V_J)$	0.35 V
Saturation-current temperature exponent	P_T(XTI)	2
Grading coefficient	M	0.5

Because of the low reverse breakdown voltage of the diode, 6-stage voltage multiplier multiplier architecture is adopted to boost the output voltage. The schematic of the rectifier is shown in Figure 4-35, and the values of the components are listed in

. L1 and C1 form an L matching network, and C7 functions as a single-pole low pass filter for the load. The circuit is simulated in Advanced Design System (ADS). Because of the nonlinear characteristics of the diode, Harmonic Balance (HB) simulation (ip to the 3rd harmonic) is used to calculate the steady-state response. The parasitic parameters of PCB at RF frequencies cannot be neglected, so Momentum EM Simulator is used to model the PCB layout. Also, in the circuits, Murata surface mount (SMT) capacitors (GQM18 series, size 0603) and inductors (LQG18H series, size 0603) are used instead of ideal components. The PCB is made of FR4 with relative dielectric constant of 4.4 and loss tangent of 0.02. The thickness is 1.6mm. Top layer and bottom layer of PCB are connected through vias. The input of rectifier is coplanar waveguide with ground (CPWG) with characteristic impedance of 50Ω to match the antenna. The layout of circuit is shown in Figure 4-36.

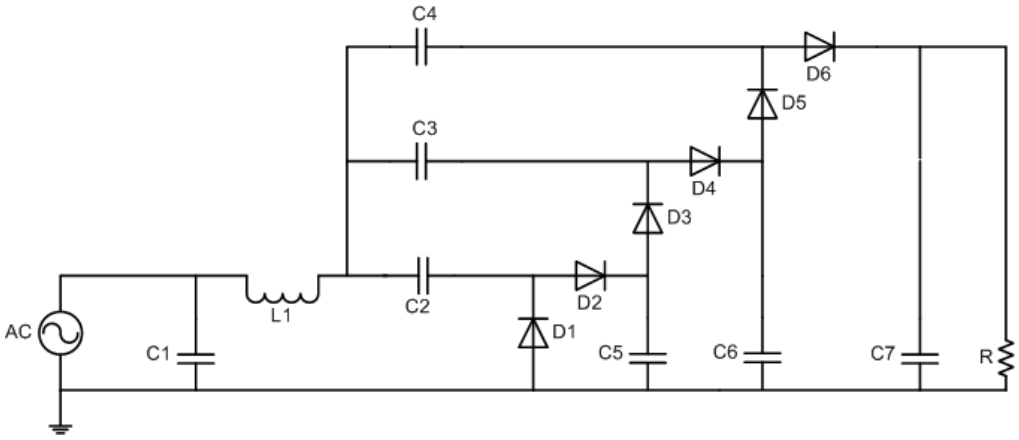

Figure 4-35 Schematics of the rectifier.

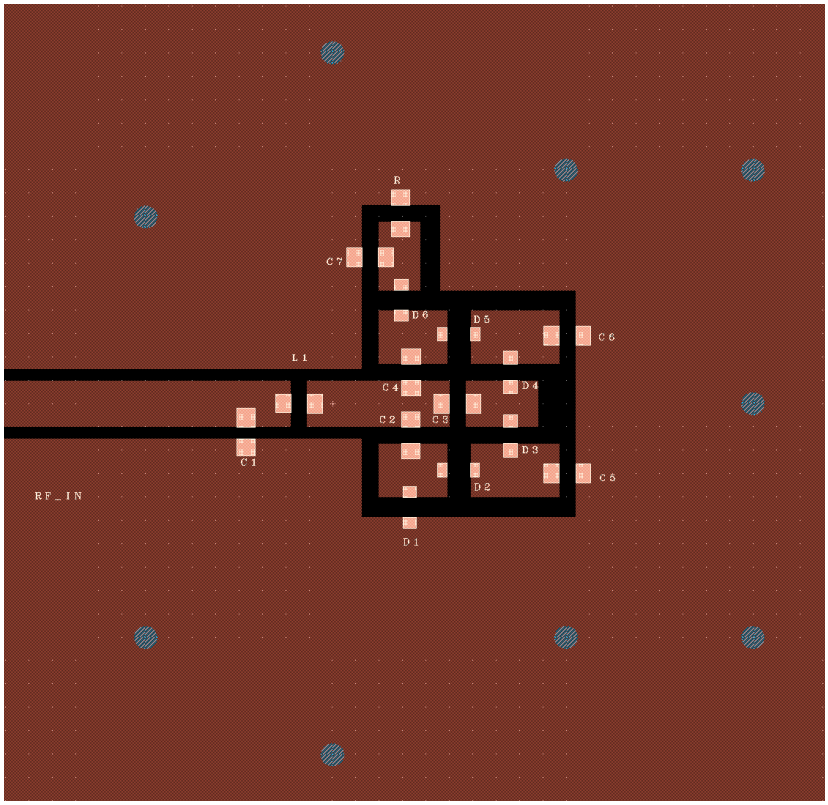

Figure 4-36 Layout of the rectifier.

Table 4-8 Values of Circuit Components.

Components	Value
C1	1 pF
L1	1.6 nH
C2	15 pF
C3	15 pF
C4	15 pF
C5	330 pF
C6	220 pF
C7	120 pF
R	1.8 kΩ

4.2.6 Measurement Results of Rectifier

The photo of the fabricated rectifier is shown in Figure 4-37. Due to the limitation of the test equipment, the input power is measured up to 10dBm. The simulated and measured DC output voltages are plotted in Figure 4-38, Figure 4-39 and Figure 4-41. And the conversion efficiencies are plotted in Figure 4-41, Figure 4-42 and Figure 4-43. The measurement result shows excellent agreement with simulation result. For 10dBm input power, the measured efficiencies are 43.9%, 47.4% and 45.4% for 2.06GHz, 2.08GHz and 2.108GHz respectively. And the simulated efficiencies are 51.7%, 52.8% and 53.4% for 2.06GHz, 2.08GHz and 2.108GHz respectively. The difference between measurement and simulation is expected, as the real diodes do not behave exactly as the SPICE model, and the values of capacitor and inductor have about ±5% tolerance and the fabrication of PCB also has process variance. Also the discontinuity between the SMA connect and CPWG transmission line causes additional reflection. The return losses for 10dBm input power are plotted in Figure 4-44. The measured reflection coefficients are less than -9dB for all frequencies, which is acceptable.

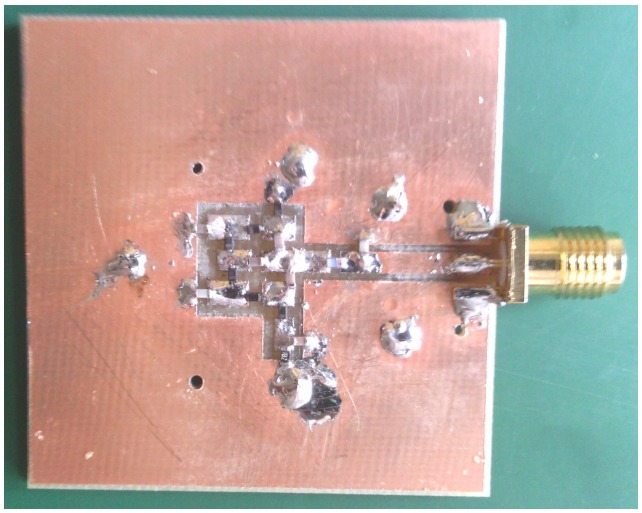

Figure 4-37 Photo of the fabricated rectifier.

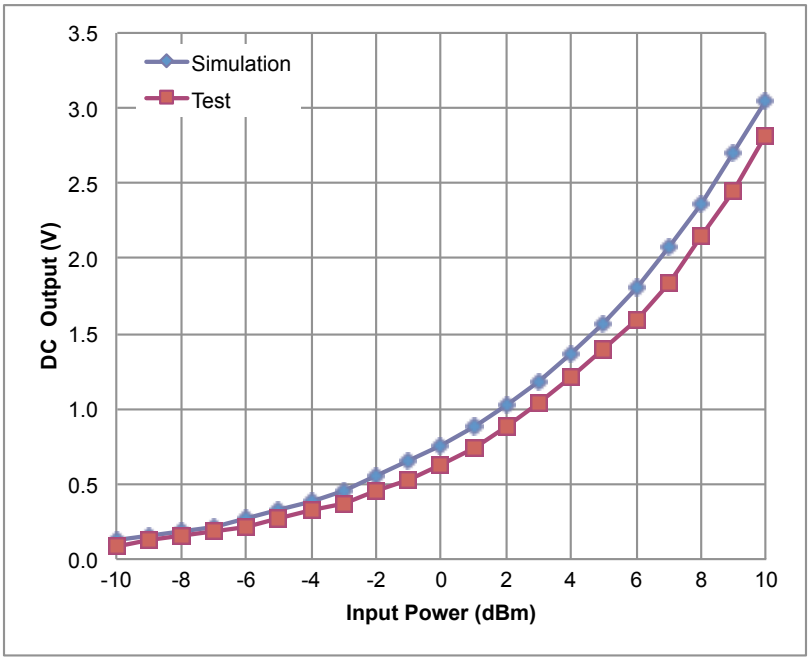

Figure 4-38 DC output voltage of the rectifier at 2.06GHz.

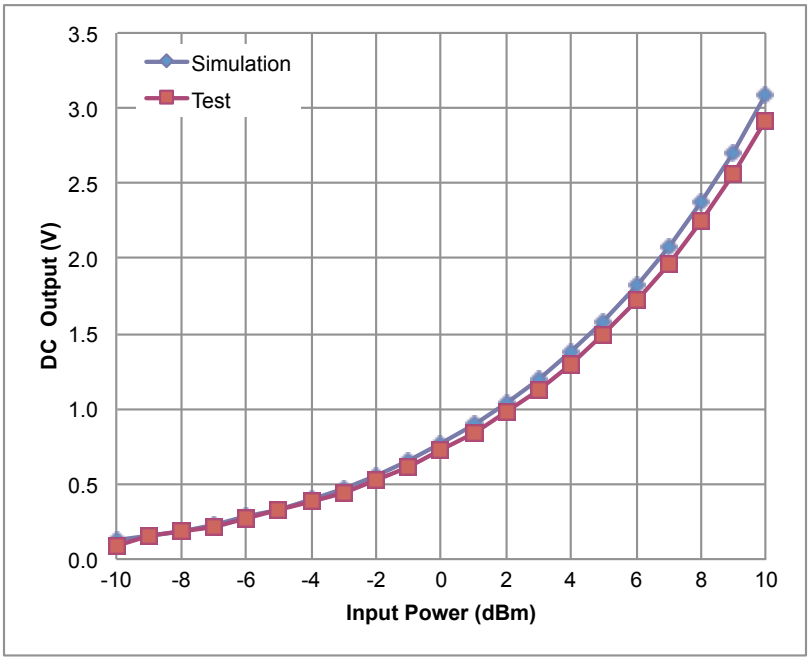

Figure 4-39 DC output voltage of the rectifier at 2.08GHz.

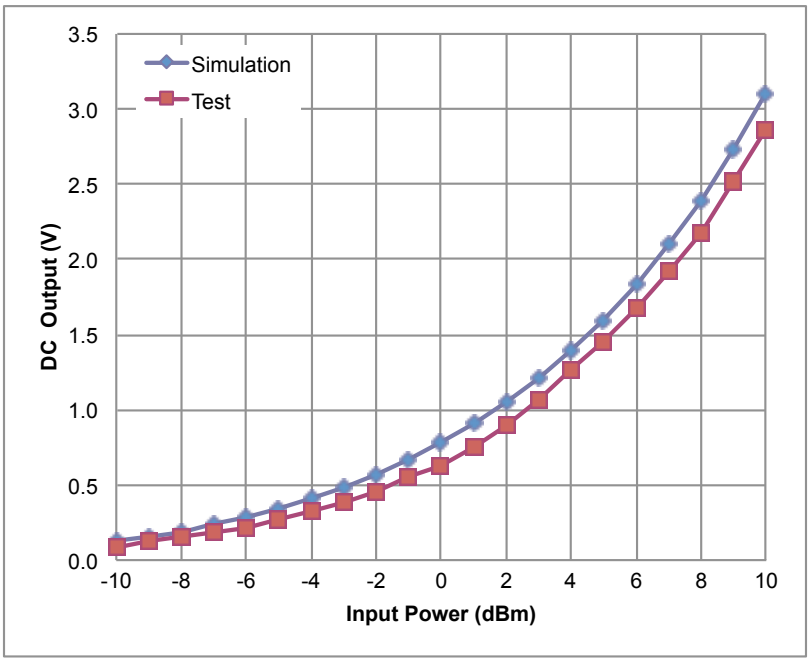

Figure 4-40 DC output voltage of the rectifier at 2.108GHz.

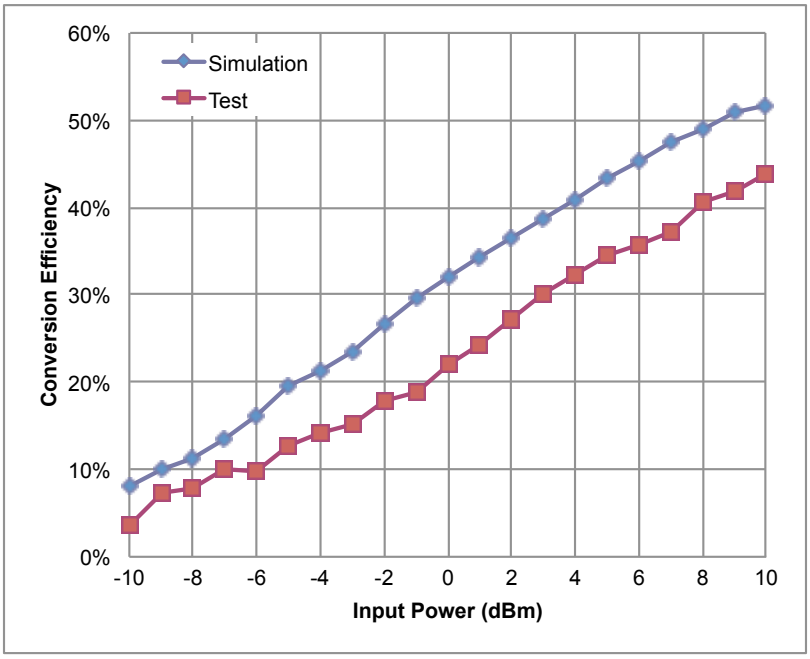

Figure 4-41 Conversion efficiency of the rectifier at 2.06GHz.

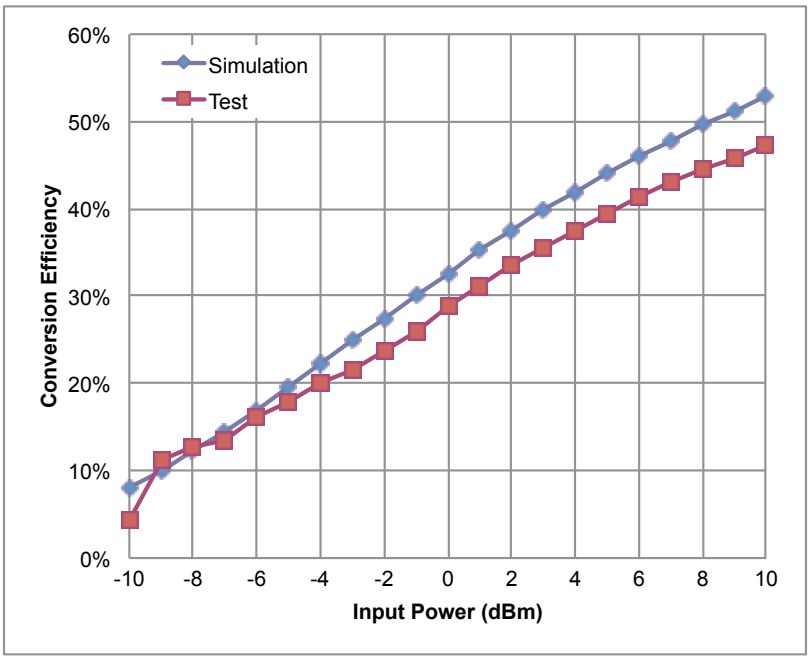

Figure 4-42 Conversion efficiency of the rectifier at 2.08GHz.

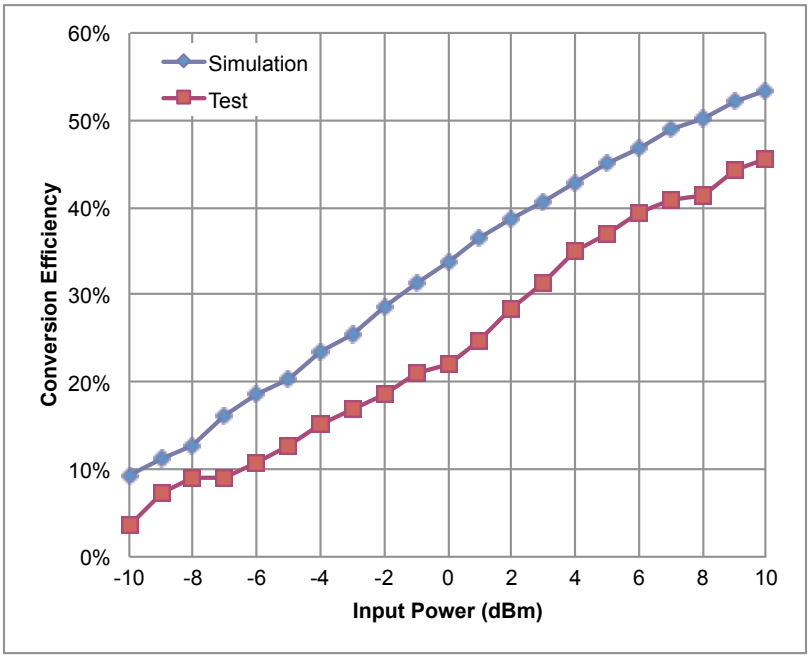

Figure 4-43 Conversion efficiency of the rectifier at 2.108GHz.

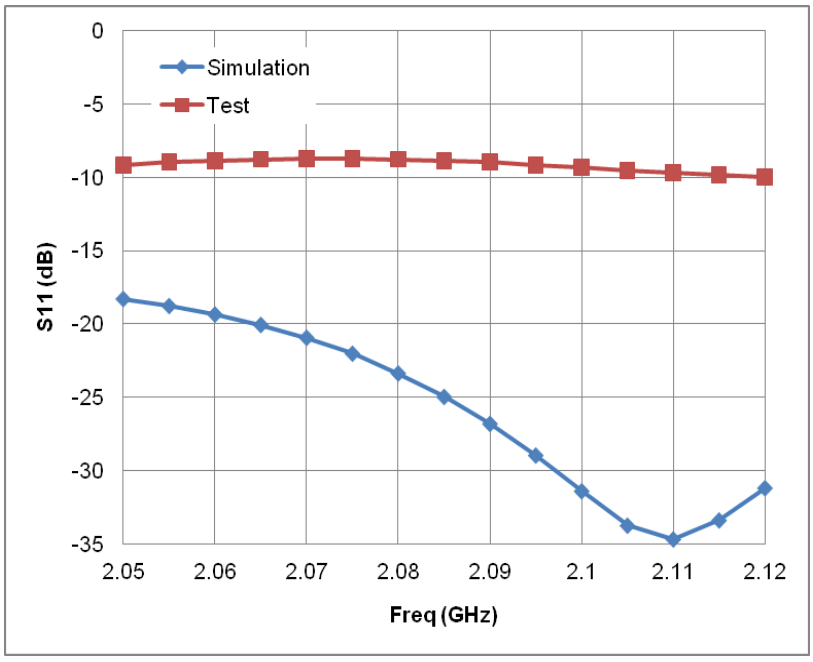

Figure 4-44 Return loss of the rectifier at 10dBm input power.

4.3 System Design of Ultra-wideband Retro-reflective Antenna Array

The experiments confirm that the sidelobe level is high for single frequency WPT. In the 4-element array experiments, the first sidelobe is only about 10dB low than the main beam. As suggested in [41], ultra-wideband retro-reflective beamforming can reduce the sidelobe level. In this dissertation, an architecture is proposed to implement the power transmitter as shown in Figure 3-1. The architecture is based on frequency-domain sampling method and sub-band technique. The circuit diagram of proposed power transmitter is shown in Figure 4-45. Compared to the circuit diagram in [31] (shown in Figure 4-46), the architecture proposed here is much simpler, because one set of LO, mixer and band pass filter can extract the spectra of multiple frequencies, but system in [31] requires one set for each frequency sample.

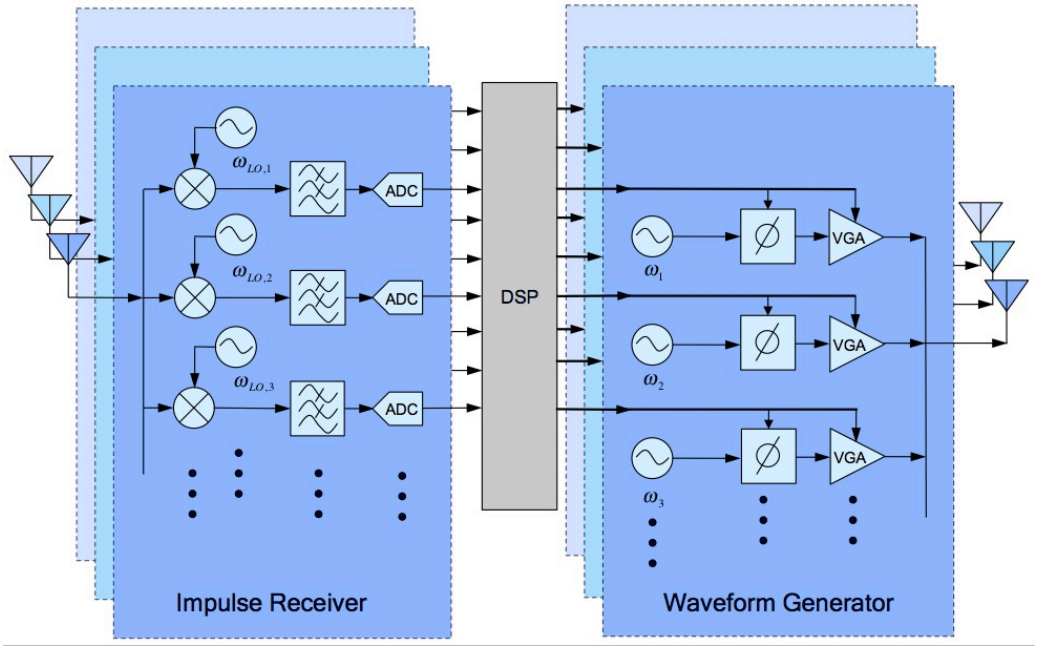

Figure 4-45 Circuit diagram of proposed power transmitter.

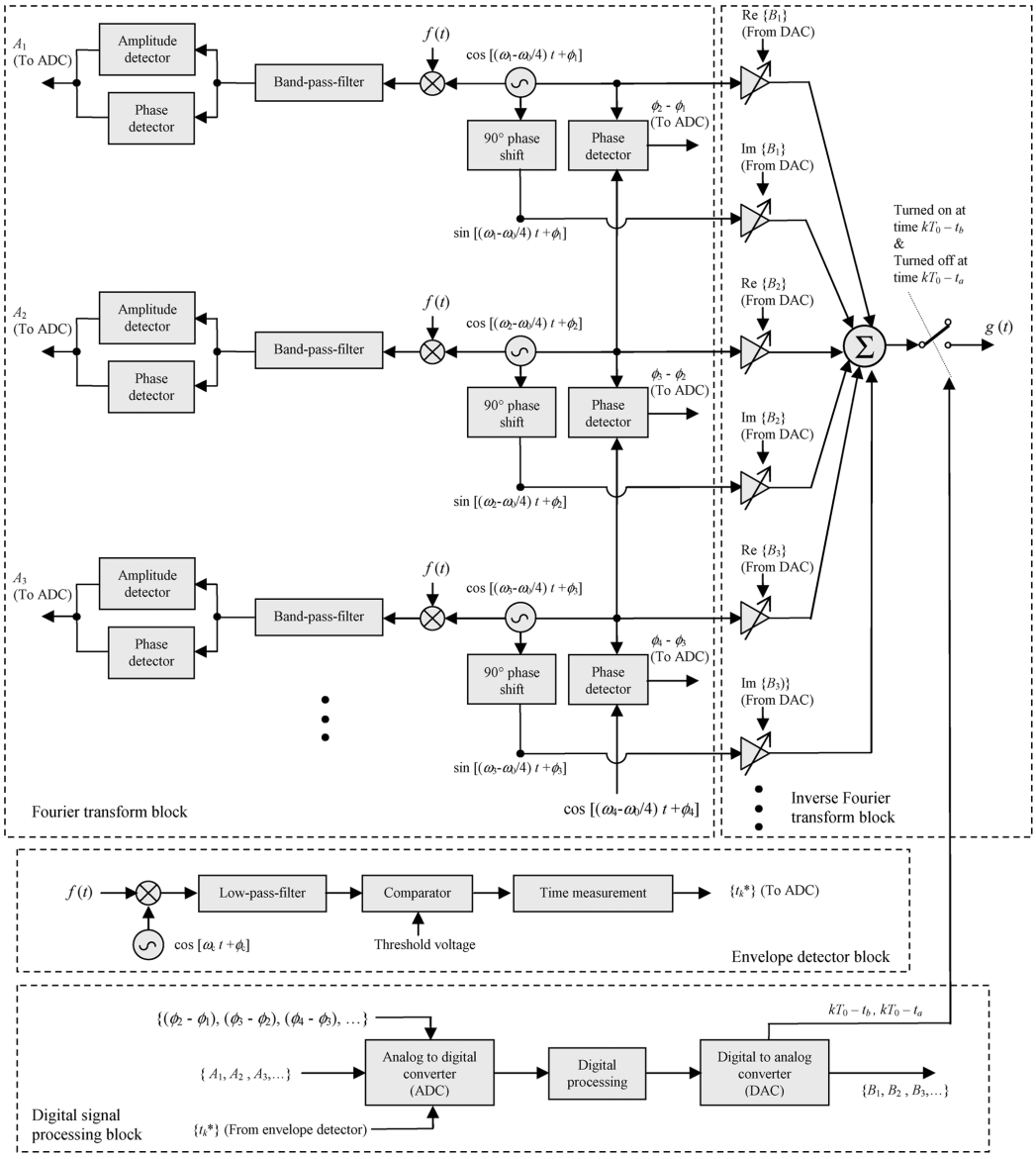

Figure 4-46 Circuit diagram of the system in [31].

4.3.1 Impulse Receiver

In order to completely retrieve the spectrum of the UWB pilot signal sent by the power receiver, the straightforward way is to sample the signals using analog-to-digital converters (ADCs) and carry out Fourier transform subsequently. Obviously, wideband

impulses call for ADCs with high sampling rates, which are well known to be expensive and difficult to realize [98]. Although "time-interleaved sampling" can relieve the high-sampling-rate difficulty, it requires precise and complicated time delay control [99] [100]. As alternatives to direct digitizing in the time domain, some researchers resorted to frequency-domain methods to achieve low-cost receivers for wideband impulses. Hoyos *et al.* [101] and Thirugnanam *et al.* [102] attempt to capture the impulses' spectral components using correlators and resonators, respectively. Although theoretically elegant, both the correlator and resonator approaches meet certain intricacies in practical implementation. For instance, since the correlators rely on integral (i.e., direct current) outputs, they are sensitive to various interferences such as the coupling between the radio-frequency (RF) port and local-oscillator (LO) port of the mixers, and, the passive resonators with high quality factor at RFs are difficult to accomplish in practice. In [103] [104] [105], the input signal's spectrum is decomposed into several sub-bands, so that sampling rates for each sub-band can be lowered. But the sub-band technique is designed to estimate the information bit carried in the UWB signal, not to perfectly extract the spectrum. However, the spectrum, especially the phase information, is very important in the retro-reflective antenna array to focus the beam automatically on the receiver.

The proposed architecture [106] adopts frequency-domain sampling method, and uses the sub-bands topology to lower the required sampling rate. But in our architecture, the adjacent sub-bands have overlapping region and an algorithm is developed to seamlessly reconstruct the whole spectrum from sub-bands' spectra. First, the input signal is divided into multiple channels by LOs at different frequencies. Each channel processes a small portion of the input's spectrum with the aid of low pass filters (LPFs); in other words, each channel serves as a narrow-band receiver. Overlapping bands are designated in between every two adjacent channels. Second, the signal in each channel

is sampled by ADC and processed by DSP to find the narrow band spectrum. Finally, the DSP reconstructs the wideband spectrum using the algorithm explained as follows.

Assume the received UWB signal is $f(t)$ with period T_0, starting time t_a and ending time t_b. Then $f(t)$ can be represented by Fourier series as:

$$f(t) = \sum_{m=-\infty}^{+\infty} A_m e^{jm\omega_0 t} \tag{4.15}$$

where $\omega_0=2\pi/T_0$, and

$$A_m = \frac{1}{T_0}\int_0^{T_0} f(t)e^{-jm\omega_0 t}\,dt \tag{4.16}$$

As can be seen from Figure 4-47, the spectrum of the periodic signal is discrete with spacing ω_0 (or frequency domain resolution) between two spectral lines.

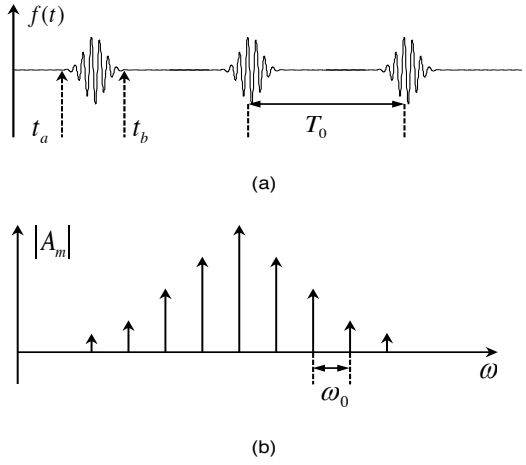

Figure 4-47 Illustration of periodic pulses as pilot signal. (a) Time domain signal, (b) frequency domain spectrum.

Then the received signal *f(t)* is processed by *N* parallel branches, and each branch behaves as a down-converter, as shown in Figure 4-48. Specifically, *N* local oscillators and N mixers are used to down-convert $f(t)$ to *N* intermediate-frequency (IF)

channels. In this illustration, N=3. The LO frequencies are chosen to be $\omega_0/4$ less than the frequency of the first spectral line in each IF channels. Each channel is followed by a low pass filter with a cutoff frequency at $(M+3/4)\omega_0$. Then the IF channel outputs are sampled by ADCs and processed by DSP to obtain the magnitude and phase information of each spectral line.

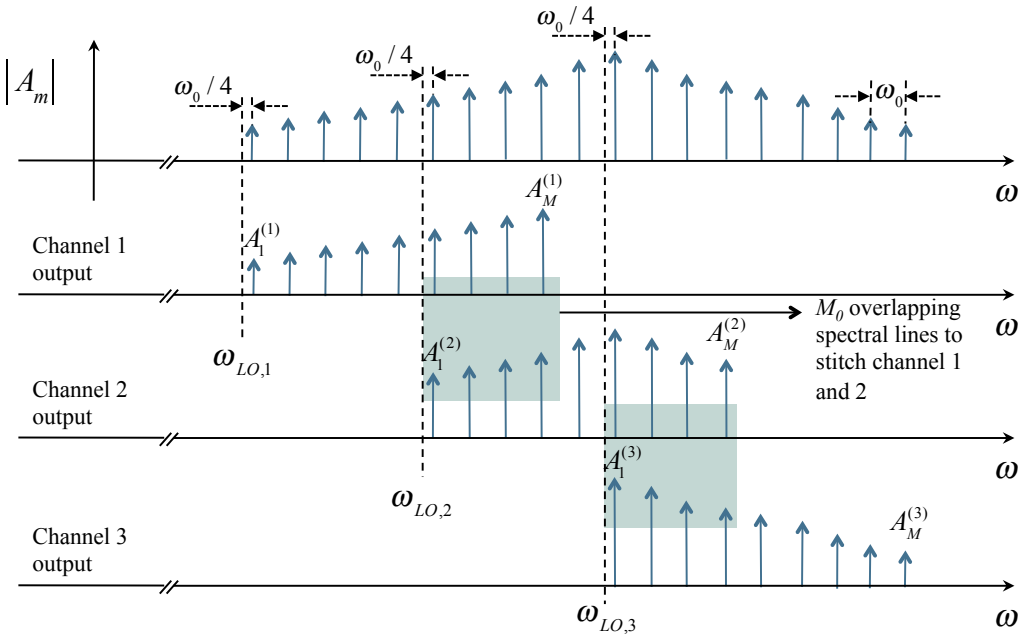

Figure 4-48 Illustration of how impulse receiver processes periodic pulses.

Let the complex values of the spectral lines in each sub-band are denoted by $A_m^{(n)}$, with m = 1, 2, …, M, and n = 1, 2, …, N. In the overlapping bands (marked by shaded areas), there are M_0 spectral lines. To be specific, the following two groups of data originate from the same spectral samples of $f(t)$:

$$\begin{aligned} &\left\{A_{M-M_0+1}^{(n)}, A_{M-M_0+2}^{(n)}, \ldots, A_M^{(n)}\right\} \\ &\left\{A_1^{(n+1)}, \quad A_2^{(n+1)}, \quad \ldots, A_{M_0}^{(n+1)}\right\} \end{aligned} \tag{4.17}$$

With the same origin, the only possible differences between these two groups of data are different time delays from the antenna port to the ADC inputs, and the phase errors introduced by LOs. When the sampling time is short, the phase error in each group introduced by the LO can be considered as a constant. As a consequence, the phase difference between them should be linear with respect to frequency. This fact triggers the following algorithm to stitch the two adjacent sub-bands, which consists of three steps:

Step 1) At the post-processing stage, a vector is constructed as

$$\begin{bmatrix} \angle A_{M-M_0+1}^{(n)} - \angle A_1^{(n+1)} \\ \angle A_{M-M_0+2}^{(n)} - \angle A_2^{(n+1)} \\ \vdots \\ \angle A_M^{(n)} - \angle A_{M_0}^{(n+1)} \end{bmatrix} \tag{4.18}$$

Where the operator "$\angle\cdot$" takes the phase of its argument.

Step 2) A linear function $a + b\omega$ is used to fit the data in (4.18). To be specific, unknowns a and b are obtained by minimizing the least squares error between $a + b\omega$ and the data in (4.18). When the least squares error is calculated, the phase data in (4.18) are weighed according to the corresponding magnitude data in (4.17). Also, additional care needs to be taken in the curve fitting process as the phase is 2π-periodic, i.e., ϕ and $\phi + 2\pi$ are indistinguishable by the "$\angle\cdot$" operator.

Step 3) When the phases of either $\left\{A_1^{(n)}, A_2^{(n)}, ..., A_M^{(n)}\right\}$ or $\left\{A_1^{(n+1)}, A_2^{(n+1)}, ..., A_M^{(n+1)}\right\}$ is corrected (i.e., subtracted or added) by $a + b\omega$, the outcomes of IF channels n and n+1 are merged.

After the aforementioned algorithm is carried out for all the neighboring channels, narrow-band outcomes from the N channels are "stitched" into the entire spectrum. It is noted that "stitching error" could propagate from channel to channel. In our

implementation, we always start with the two channels with the strongest spectral magnitudes in order to minimize the error propagation.

4.3.2 DSP

Some functions of DSP block are explained in previous section, which is reconstructing the entire spectrum from sub-band spectra using the algorithm aforementioned. Then phase-conjugate is implemented by changing the sign of phase for each spectral line:

$$\angle A_i^* = -\angle A_i \ , i = 1,2,...,M_0 + N(M - M_0) \tag{4.19}$$

The phase information is transformed to control voltage of phase shifter in waveform generator block according to the data sheet provided by the phase shifter manufacturer. The magnitude of the spectrum is used to control the gain of amplifier in waveform generator for beam shaping.

The safety procedure is also implemented in DSP. The maximum received power level of each antenna array (or maybe only one array) is compared to a preset criterion, if it is smaller than the preset value, which means a significant path loss, then the antenna array will be shut off. It not only saves the power, but also prevents over-exposure of EM energy to humans or other living animals.

4.3.3 Waveform Generator

The waveform generator in the power transmitter is essentially an inverse Fourier transform block, where multiple discrete frequencies are synthesized into a time domain signal. The magnitude and phase for each discrete frequency are adjusted through the variable gain amplifier (VGA) and phase shifter, respectively.

Because the spacing between two adjacent spectral lines $\omega_0=2\pi/T_0$ is inverse proportional to the period T_0 of pulses in time domain, increasing ω_0 by a factor χ will decrease the period by the same factor, where χ is undersampling factor.

$$\chi\omega_0 = \frac{2\pi}{T_0/\chi} \tag{4.20}$$

In other words, if we sample the spectrum every χ spectral lines, then in the same period, we shall have χ pulses. This undersampling idea is illustrated in Figure 4-49. By undersampling in frequency domain (less number of discrete frequencies), the required number of LOs for reconstructing the time-domain signal is reduced, thus the system complexity is reduced. Also the power transmission is more continuous. In an extreme case, only one frequency is selected, then the reconstructed signal becomes a continuous wave (CW).

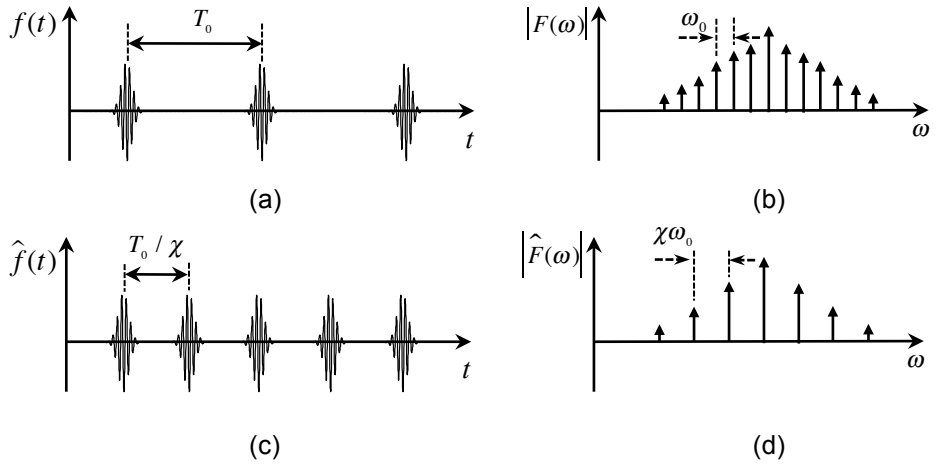

Figure 4-49 Illustration of frequency domain undersampling. (a) Original time domain periodic signal with period of T_0, (b) spectrum of signal in (a) with spacing of ω_0, (c) inverse Fourier transform of undersampled spectrum in (d), now the period is T_0/χ, (d) undersampled spectrum of (b) by a factor of χ.

4.3.4 Experiment Results of Impulse Receiver

Figure 4-50 shows the experimental setup to verify the impulse receiver proposed in previous section. Periodic impulses are generated by National Instrument PXI-5610; The impulses have carrier frequency 2.1 GHz and period T_0=0.5us. Two standard horn antennas are used to establish a wireless link. One antenna is connected to the PXI-5610 as the transmitting antenna. The other is connected to the impulse receiver as the receiving antenna. The received signal *s*(*t*) is fed to the circuit shown through a power divider. In our implementation, we used two physical branches to represent all the logical branches by reconfiguring the frequencies of two oscillators. The two local oscillators are synthesizer ADF4360-1 and the two mixers are ADL5365, all made by Analog Devices Inc. The two synthesizers are locked by one external 10-MHz reference clock, so that their outputs will keep in phase, or by a constant phase difference. The frequencies of the synthesizers are set to {…, 2.0975, 2.0995, 2.1015, 2.1035, …} GHz sequentially. Because the synthesizer's frequency is tuned to be ω_0/4 to the left of a certain spectral line of *s*(*t*), the fundamental frequency of the IF channel is 0.5MHz. In our experiments, all IF channels are recorded by an Agilent 54621A storage oscilloscope with 200-MHz sampling rate, and digital processing is used to emulate all the filters. In this section, results from the circuit in Figure 4-50 are termed from "frequency-domain approach." For the purpose of verifying the results from Figure 4-50, the received signal *s(t)* is directly measured by a Lecroy WavePro 760Zi oscilloscope with 40GHz sampling rate. Results measured by the high-speed oscilloscope and processed afterwards are termed from "time-domain approach".

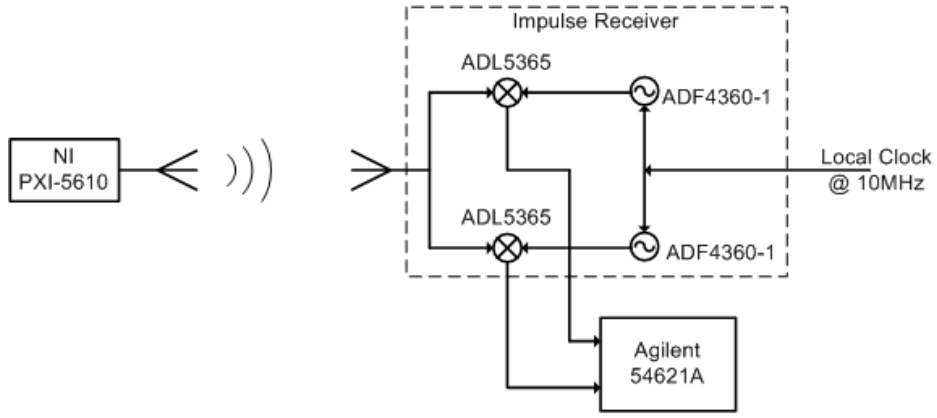

(a)

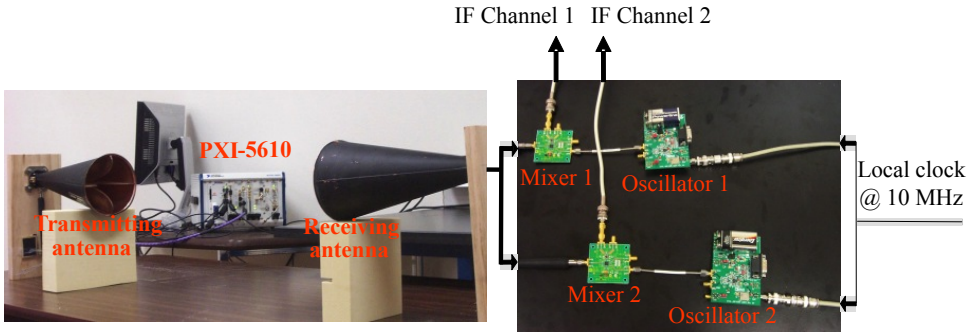

(b)

Figure 4-50 Experiment setup and circuit implementation of impulse receiver. (a) Schematic of experiment setup, (b) Photo of experiment setup.

The impulse signal measured by the time-domain approach is plotted in Figure 4-51. Its time-average power is roughly 0dBm, measured by power meter. Normalized discrete spectra of $s(t)$ from frequency- and time-domain approach are compared in Figure 4-52. It is observed that amplitudes from the two approaches match each other very well. And the phase difference between two approaches follows by a straight line, which is due to different arriving times of the pulses with respect the starting time t = 0 *us*. The phase error is large at the frequencies whose magnitudes are small. It is expected as

they are more susceptible to noise. Spectral data from the frequency-domain approach can be inverse Fourier transformed to reconstruct the signal $s(t)$. In our implementation, the following reconstruction is carried out using Matlab.

$$\hat{s}(t) = \alpha \,\mathrm{Re}\left\{ \sum_{m=1}^{N} A_m e^{j\omega_m t} \right\} \tag{4.21}$$

where A_m is the spectrum at frequency ω_m, and N is the total number of spectral lines. The constant α scales the reconstructed waveform to have a normalized peak voltage. In Figure 4-53, the reconstructed signal with N = 17 is plotted.

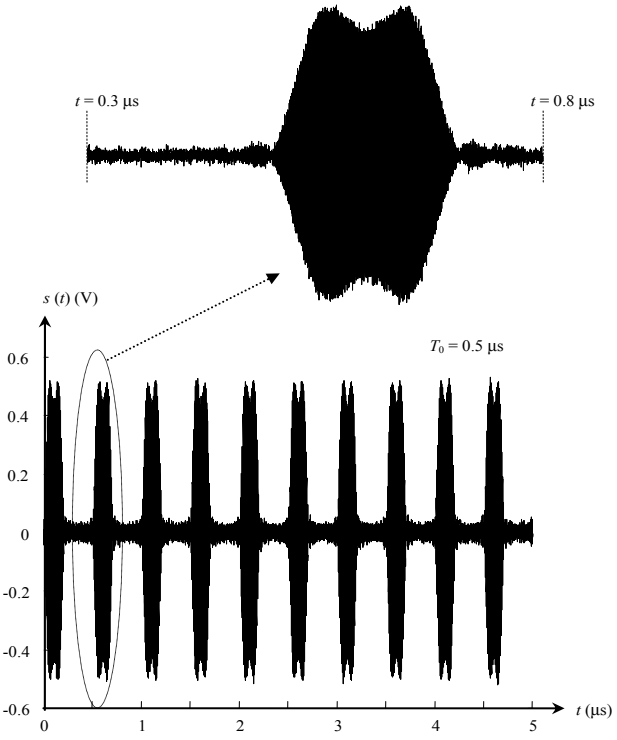

Figure 4-51 Received impulse signal from time-domain approach, with transmitting power at 0dBm.

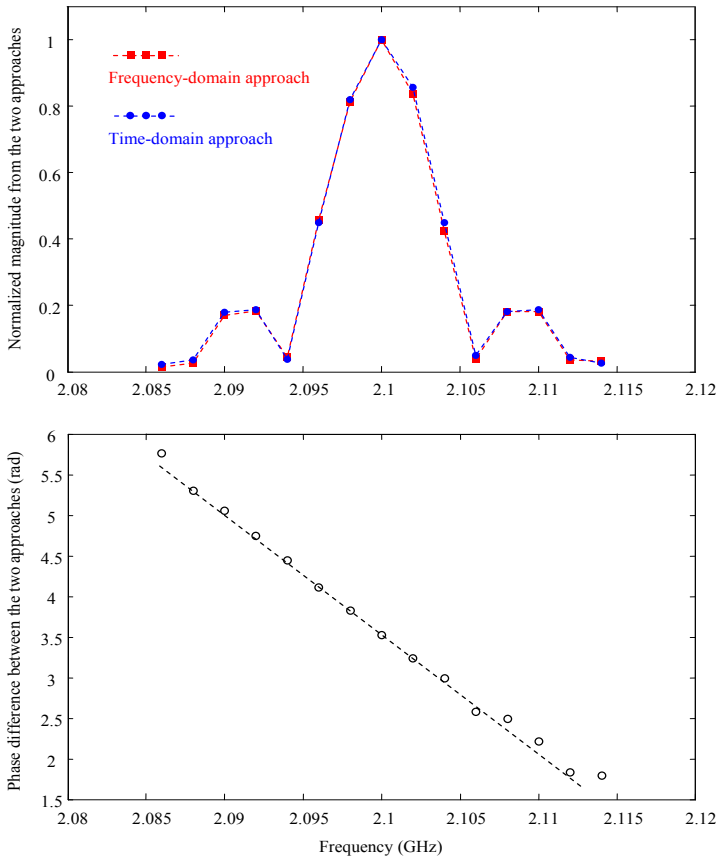

Figure 4-52 Spectrum of the received impulse signal with transmitting power of 0dBm.

When the impulse signals are transmitted with various transmitting power (0dBm, -10dBm, -30dBm), the received signals measured by spectrum analyzer are shown in Figure 4-54. The signal's power, which is the summation of the spectral lines' power, is calculated to be −33dBm, -43dBm, and -63dBm, respectively. Meanwhile, the noise power density is read to be −95dBm per 30kHz, since the signal's bandwidth is about 30MHz, the total noise power is −65dBm. As a result, the SNR in Figure 4-54 are about 32dB, 22dB and 2dB, respectively. The measurement results for the 22- and 2-dB-SNR scenarios are shown in Figure 4-55 and Figure 4-56, respectively. It is clear that the impulse's spectrum can be retrieved reliably, even when the SNR is as poor as 2dB.

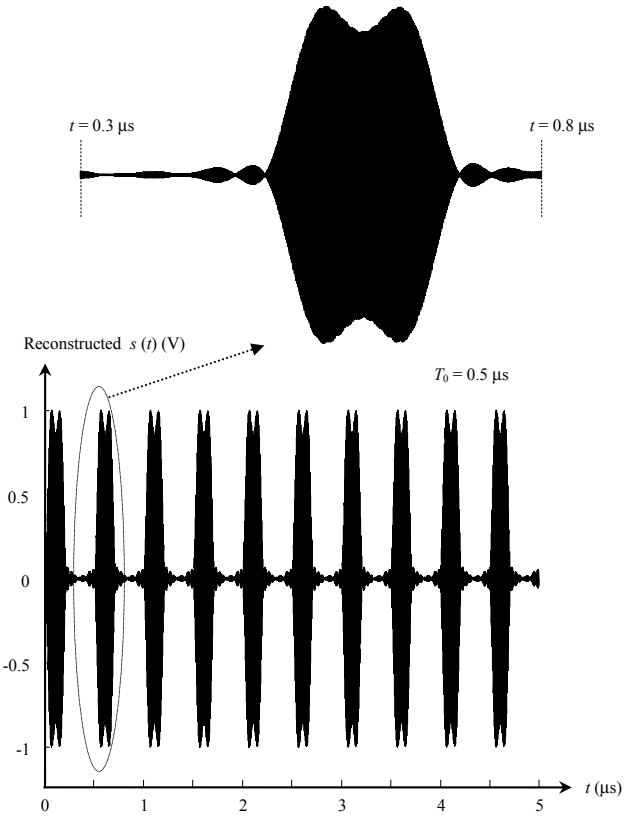

Figure 4-53 Reconstructed impulse signal from time-domain approach, with transmitting power at 0dBm.

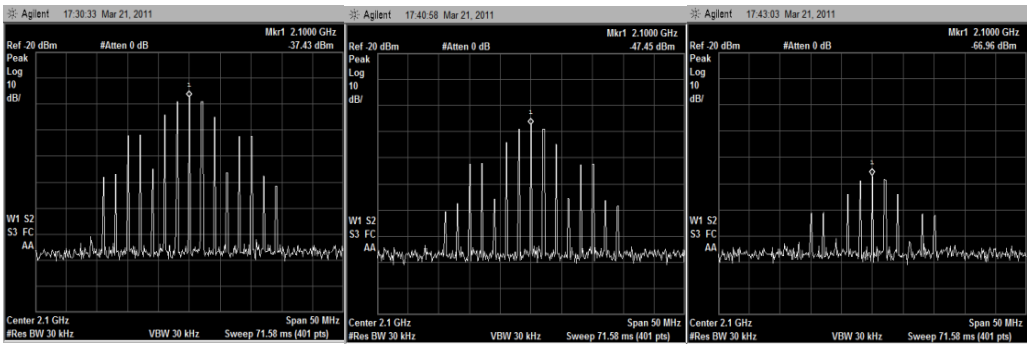

(a) (b) (c)

Figure 4-54 Received impulse signals measured by spectrum analyzer. (a) Transmitting power of 0dBm, (b) transmitting power of -10dBm, (c) transmitting power of -30dBm.

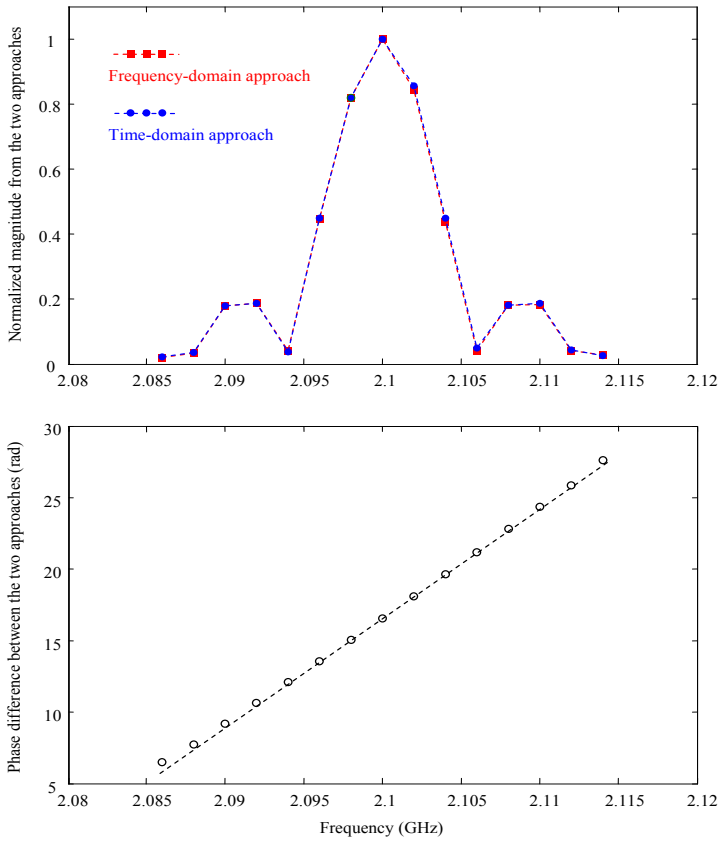

Figure 4-55 Spectrum of the received impulse signal with transmitting power of -10dBm.

The relative error between frequency-domain approach and time-domain approach (as the reference) is calculated by:

$$\varepsilon = \frac{\left\| \mathbf{A}^{\mathbf{FD}} - \mathbf{A}^{\mathbf{TD}} \right\|}{\left\| \mathbf{A}^{\mathbf{TD}} \right\|} = \frac{\sqrt{\sum_{m=1}^{N} \left| A_m^{FD} - A_m^{TD} \right|^2}}{\sqrt{\sum_{m=1}^{N} \left| A_m^{TD} \right|^2}} \tag{4.22}$$

where operator "||·||" takes the Euclidean norm of the argument. $\mathbf{A}^{\mathbf{FD}}$ and $\mathbf{A}^{\mathbf{TD}}$ are vectors of spectra obtained by frequency-domain and time-domain approach, respectively. Table 4-9 lists the measurement errors for the proposed architecture. The results shows the measurement error is very low (3.73%) for SNR = 32 dB and it does

not deteriorate substantially (6.08%) even the SNR reduces by 30dB. This is because the periodic signal's spectrum consists of discrete spectral lines. So the magnitudes and phase at these discrete frequencies add constructively for all pulses, but he noise power spectrum is uniformly distributed all over the frequency band, and does not add constructively.

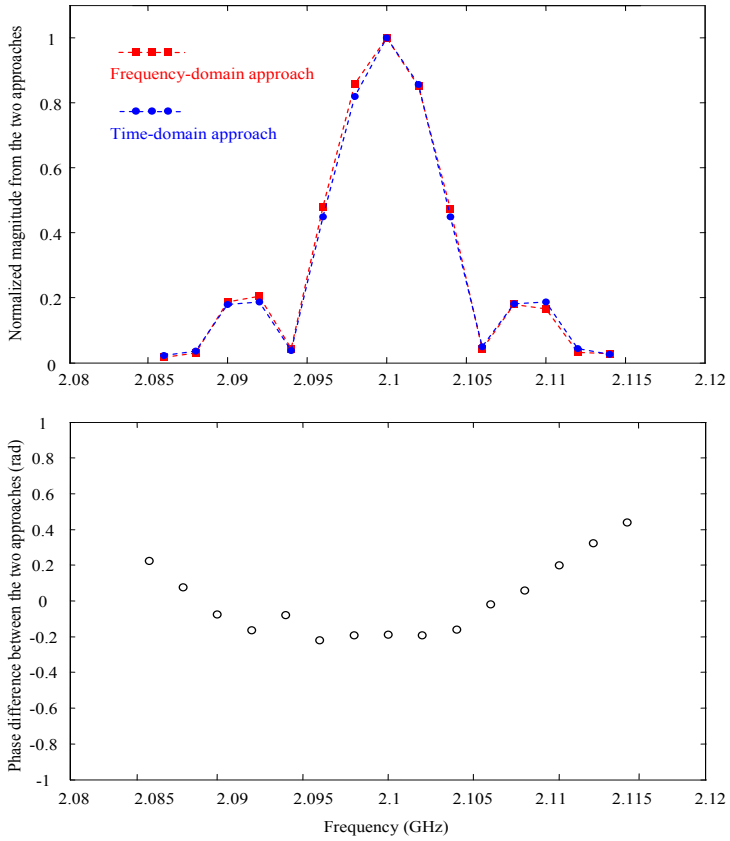

Figure 4-56 Spectrum of the received impulse signal with transmitting power of -30dBm.

Table 4-9 Measurement Errors with Three SNRs

Transmitting power	0 dBm	-10 dBm	-30 dBm
SNR at the receiving antenna	32 dB	22 dB	2 dB
Measurement error	3.73%	4.79%	6.08%

Chapter 5

Conclusions and Future Works

Wireless power transmission (WPT) has been a hot research topic in the past decade. Different technologies are investigated for WPT, such as ultrasonic, inductive coupling, magnetic resonance coupling, microwave beamforming and laser. Each technology has its own advantages and disadvantages. Thus, choosing proper applications for each technology is critical, for example, through-metal WPT can only be done using ultrasonic because EM waves cannot penetrate metals; inductive coupling is very efficient for short-range WPT, such as wireless charging for mobile devices and electrical vehicles; and laser beam can transmit over very long distance with good overall efficiency. Compared to other technologies, microwave beamforming has fast tracking capability, multiple receivers tracking capability, good penetration through objects and also works in multipath environment.

There are many microwave beamforming methods, but retro-reflective antenna array is preferred because it can automatically reflect the incident wave back to the source origin without prior knowledge of source location. Retro-reflective antenna array can be implemented in various ways, such as Van Atta array and phase-conjugate array using heterodyne scheme. But these two methods can only retransmit the incoming signals, but cannot transmit signal to the receiver by themselves. A phase detection and phase shifting method is investigated in reference [38], but it requires a planar wavefront, a planar arrangement and an equal spacing of antenna elements. In reference [39], a try-and-error brute force method is proposed to maximize the received power by adjusting phase shifters in the transmitters, but this method takes a lot of time to synchronize all transmitters and thus limits the mobility of receiver. In this dissertation, a new phase conjugate method is proposed to realize the retro-reflective antenna array. The phase of

the received pilot signal at each antenna element is detected simultaneously using heterodyne receiver, then the conjugated phase is applied to the phase shifter of each antenna for retransmission. Because the phase-conjugate is performed at each antenna individually, the antenna element can be placed arbitrarily, which offers high construction flexibility. Also, the phase shifters enable the antenna array transmit power to the receiver continuously, so the receiver only need to send pilot signal when it moves or in a low repetition rate.

Single frequency WPT experiments are conducted to verify the proposed retro-reflective antenna array. The experimental results show that the retro-reflective antenna array is able to track the receiver when it moves. The tracking error, also called beam pointing error, can be reduced by increasing the antenna number. Also, with more antenna element, the main beam is narrow and the transmission efficiency would be higher. A 2-element array and a 4-element array are compared in the experiments. Results show that the transmission efficiencies are improved by 70%, 91% and 168% for frequency 2.06GHz, 2.08GHz and 2.108GHz respectively. A rectenna is also designed to rectify the received RF energy. A 6-stage voltage multiplier architecture is used to boost the DC output voltage. Measured results show excellent agreement with the simulation. The conversion efficiencies for 10dBm input power are measured to be 43.9%, 47.4% and 45.4% for 2.06GHz, 2.08GHz and 2.108GHz respectively on a load resistance of 1.8kΩ. They are slightly lower than the simulated efficiencies because of the circuit components tolerance and PCB fabrication variance.

Sidelobe is another consideration in wireless power transmission. It is not only a waste of energy, but also potential interference to other wireless technologies. In single frequency power transmission, beam shaping techniques are usually adopted to reduce sidelobes. An ultra-wideband (UWB) retro-reflective beamforming is proposed in [41] to

reduce the sidelobes or multiple focal points. In this dissertation, an improved hardware system is proposed to reduce the number of local oscillator and mixer, thus reducing the system complexity, compared to the system in [31]. Impulse receiver is used to extract the spectrum of UWB signal. Time-domain method requires a high speed ADC, which is very expensive. Frequency-domain sampling method with sub-band technique are investigated to reduce the ADC sampling speed. But existing sub-band technique can only estimate the information bit carried in the UWB signal, but not extract the complete spectrum. In this dissertation, the sub-band technique is improved by assigning overlapping regions to the adjacent sub-bands and an algorithm is developed to seamlessly merge the sub-band spectra into a wideband spectrum.

Experimental results show that the proposed impulse receiver can extract the wideband spectrum of periodic impulses with little distortion. The measurement error for SNR=32dB is as low as 3.73% and it does not deteriorate substantially when the SNR reduces. For SNR=2dB, the measurement error is only increased by less than 3% (6.08%).

Future works include two aspects. One is to improve the performance of single frequency retro-reflective antenna array, for example, using more antenna elements to increase the transmission efficiency, and integrating all circuit components to reduce the system size. Real time implementation is also planned in the future, so that the system can track the receiver without human assistance. The rectenna will also be improved to achieve higher efficiency. The other aspect is to implement the ultra-wideband retro-reflective antenna array. The impulse receiver is already finished. The next step is to implement the waveform generator and integrate the impulse receiver and waveform generate into a complete system using DSP. To receive the UWB signal, ultra-wideband antenna and rectenna have to be designed too.

References

[1] Ishiyama, Toshihiko, Yasuyuki Kanai, Junichi Ohwaki, and Masato Mino. "Impact of A Wireless Power Transmission System Using An Ultrasonic Air Transducer for Low-Power Mobile Applications." *Ultrasonics, 2003 IEEE Symposium on*, vol. 2, pp. 1368-1371, 2003.

[2] Waffenschmidt, Eberhard, and Toine Staring. "Limitation of Inductive Power Transfer for Consumer Applications." In Power Electronics and Applications, 2009. EPE '09. 13th European Conference on, pp. 1-10, Sep, 2009.

[3] Imura, Takehiro, Hiroyuki Okabe, and Yoichi Hori. "Basic Experimental Study on Helical Antennas of Wireless Power Transfer for Electric Vehicles by Using Magnetic Resonant Couplings." In Vehicle Power and Propulsion Conference, 2009. VPPC '09. IEEE, pp. 936-940, 2009.

[4] McDonough, M.; Shamsi, P.; Fahimi, B., "Application of Multi-Port Power Electronic Interface for Contactless Transfer of Energy in Automotive Applications," Vehicle Power and Propulsion Conference (VPPC), 2011 IEEE, pp.1-6, Sept. 2011.

[5] Ghovanloo, Maysam, and Suresh Atluri. "A Wide-band Power-Efficient Inductive Wireless Link for Implantable Microelectronic Devices Using Multiple Carriers." Circuits and Systems I: Regular Papers, IEEE Transactions on, vol. 54, issue 10 pp. 2211-2221, Oct. 2007.

[6] Zhang, Fei, Xiaoyu Liu, Steven A. Hackworth, Robert J. Sclabassi, and Mingui Sun. "In Vitro and In Vivo Studies on Wireless Powering of Medical Sensors and Implantable Devices." In Life Science Systems and Applications Workshop, 2009. LiSSA 2009. IEEE/NIH, pp. 84-87. IEEE, 2009.

[7] Kiani, M.; Ghovanloo, M., "An RFID-based Closed-loop Wireless Power Transmission System for Biomedical Applications," Circuits and Systems II: Express Briefs, IEEE Transactions on, vol.57, no.4, pp. 260-264, April 2010.

[8] Gonalves, R., Carvalho, N.B., Pinho, P., "Increasing The RFID Readability Range Using Wireless Power Transmission Enhancements," Wireless Power Transfer (WPT), 2013 IEEE, pp.135-138, May 2013.

[9] N. Tesla, “System of Transmission of Electrical Energy”, Sept. 2, 1897, U.S. Patent No. 645,576, Mar. 20, 1900.

[10] N. Tesla, "World System of Wireless Transmission of Energy", Telegraph and Telephone Age, vol. 20, pp. 457-460, 1927.

[11] Wheeler, L.P., "II — Tesla's Contribution to High Frequency," Electrical Engineering, vol. 62, no.8, pp. 355-357, Aug. 1943.

[12] Roes, M.G.L., Duarte, J.L., Hendrix, M.A.M., Lomonova, E.A., "Acoustic Energy Transfer: A Review", Industrial Electronics, IEEE Transactions on, Volume: 60, Issue: 1, pp. 242-248, Jan. 2013.

[13] T. Imura and Y. Hori, “Maximizing Air Gap and Efficiency of Magnetic Resonant Coupling for Wireless Power Transfer Using Equivalent Circuit and Neumann Formula”, IEEE Transaction on Industrial Electronics, vol. 58, no. 10, pp. 4746-4752, Oct. 2011.

[14] S.H. Lee and R. D. Lorenz, “Development and Validation of Model for 95% Efficiency 220W Wireless Power Transfer over A 30-cm Air Gap”, IEEE Trans. Industry Applications, vol. 47, no. 6, pp. 2495-2504, Nov./Dec. 2011.

[15] Kurs, Andre, Aristeidis Karalis, Robert Moffatt, John D. Joannopoulos, Peter Fisher, and Marin Soljačić. "Wireless Power Transfer via Strongly Coupled Magnetic Resonances." Science, vol. 317, no. 5834, pp. 83-86, Jul. 2007.

[16] Hui, S., Zhong, W., Lee, C., "A Critical Review of Recent Progress in Mid-range Wireless Power Transfer," Power Electronics, IEEE Transactions on, vol. PP, no. 99, pp.1, 2013.

[17] Sahai, A., and D. Graham. "Optical Wireless Power Transmission at Long Wavelengths." In Space Optical Systems and Applications (ICSOS), 2011 International Conference on, pp. 164-170. IEEE, 2011.

[18] Dickinson, Richard M. "Wireless Power Transmission Technology State of The Art The First Bill Brown Lecture." Acta Astronautica, vol. 53, no. 4, pp. 561-570, 2003.

[19] Myrabo, Leik N. "World Record Flights of Beam-riding Rocket Lightcraft: Demonstration of 'Disruptive' Propulsion Technology." AIAA paper 3798, no. 2001 (2001): A01-34448.

[20] Cook, Joung R., and John R. Albertine. "The Navy's High-energy Laser Weapon System." In Photonics West'97, International Society for Optics and Photonics, pp. 264-271, 1997.

[21] Nayfeh, Taysir, Brian Fast, Daniel Raible, Dragos Dinca, Nick Tollis, and Andrew Jalics. "High Intensity Laser Power Beaming Architecture for Space and Terrestrial Missions." 2010 Advanced Space Propulsion Workshop, Colorado Springs, CO, Nov. 2011.

[22] Osepchuk, John M. "Health and Safety Issues for Microwave Power Transmission." Solar Energy, vol. 56, no. 1, pp. 53-60, Jan. 1996.

[23] Christ, Andreas, Mark G. Douglas, John M. Roman, Emily B. Cooper, Alanson P. Sample, Benjamin H. Waters, Joshua R. Smith, and Niels Kuster. "Evaluation of Wireless Resonant Power Transfer Systems with Human Electromagnetic

Exposure Limits." Electromagnetic Compatibility, IEEE Transactions on, vol. 55, issue 2, pp. 1-10, Apr. 2012.

[24] "ICNIRP Guidelines for Limiting Exposure to Time-varying Electric, Magnetic and Electromagnetic Fields (1Hz to 100kHz)", Health Physics, vol. 99, no. 6, pp. 818-836, Dec. 2010.

[25] "ICNIRP Guidelines for Limiting Exposure to Time-varying Electric, Magnetic and Electromagnetic Fields (up to 300GHz)", Health Physics, vol. 74, no. 4, pp. 494-522, 1998.

[26] IEEE Standard for Safety Levels with Respect to Human Exposure to Radio Frequency Electromagnetic Fields 3kHz to 300 GHz, IEEE 2006.

[27] Guidelines for the Safe Use of Ultrasound Part II – Industrial & Commercial Applications – Safety Code 24, Health Canada, ISBN 0-660-13741-0.

[28] "Health Effects of Exposure to Ultrasound and Infrasound." Health Protection Agency, UK, pp. 167–170, AGNIR (2010).

[29] H. Hoang and F. Bien, "Maximizing Efficiency of Electromagnetic Resonance Wireless Power Transmission Systems with Adaptive Circuits", in Wireless Power Transfer – Principles and Engineering Explorations, pp. 207-225, Jan. 2012.

[30] Sample, Alanson P., David A. Meyer, and Joshua R. Smith. "Analysis, Experimental Results, and Range Adaptation of Magnetically Coupled Resonators for Wireless Power Transfer." Industrial Electronics, IEEE Transactions on, vol. 58, issue 2, pp. 544-554, 2011.

[31] Huiqing Zhai; Shaoshu Sha; Shenoy, V.K.; Sungyung Jung; Mingyu Lu; Kyoungwon Min; Sungchul Lee; Ha, D.S., "An Electronic Circuit System for Time-Reversal of Ultra-Wideband Short Impulses Based on Frequency-domain

Approach," Microwave Theory and Techniques, IEEE Transactions on, vol.58, no.1, pp.74-86, Jan. 2010.

[32] G. Lerosey, J. de Rosny, A. Tourin, and M. Fink, "Focusing Beyond The Diffraction Limit with Far-field Time Reversal," Science, vol. 315, pp. 1120-1122, February 2007.

[33] Van Atta, Lester Clare. "Electromagnetic reflector." U.S. Patent 2,908,002, issued October 6, 1959.

[34] Guo, Yu-Chun, Xiao-Wei Shi, and Lei Chen. "Retrodirective Array Technology." Progress In Electromagnetics Research B, vol. 5, pp. 153-167, 2008.

[35] Pon, C. "Retrodirective Array Using The Heterodyne Technique." Antennas and Propagation, IEEE Transactions on, vol. 12, no. 2, pp. 176-180, 1964.

[36] M. Skolnik and D. King, “Self-phasing Array Antennas,” IEEE Transactions on Antennas and Propagation, vol. 12, pp. 142– 149, 1964.

[37] Chen, Lei, Yu Chun Guo, Xiao Wei Shi, and Tian Ling Zhang. "Overview on The Phase Conjugation Techniques of The Retrodirective Array." International Journal of Antennas and Propagation, vol. 2010, article 564357, 2010.

[38] G. S. Shiroma, R. Y. Miyamoto, and W. A. Shiroma, “A Full-duplex Dual-frequency Self-steering Array Using Phase Detection and Phase Shifting,” IEEE Transactions on Microwave Theory and Techniques, vol. 54, no. 1, pp. 128–133, 2006.

[39] Zeine, Hatem. "Wireless Power Transmission System." U.S. Patent 8,159,364, issued on April 17, 2012.

[40] Massa, Andrea, Giacomo Oliveri, Federico Viani, and Paolo Rocca. "Array Designs for Long-Distance Wireless Power Transmission: State-of-the-art and

Innovative Solutions." Proceedings of the IEEE, vol. 101, no. 6, pp. 1464-1481, Mar. 2013.

[41] Zhai, Huiqing, Helen K. Pan, and Mingyu Lu. "A Practical Wireless Charging System Based on Ultra-Wideband Retro-Reflective Beamforming." In Antennas and Propagation Society International Symposium (APSURSI), 2010 IEEE, pp. 1-4, Jul. 2010.

[42] H.M. Barlow, A.L. Cullen, “Surface Waves”, Proceedings of the IEE - Part III: Radio and Communication Engineering, Volume 100, Issue 68, Pages 329, 1953.

[43] http://en.wikipedia.org/wiki/Surface_plasmon

[44] N. Tesla, “Art of Transmitting Electrical Energy through The Natural Mediums”, May 16, 1900, U.S. Patent No. 787,412, Apr. 18, 1905.

[45] N. Tesla, “Apparatus for Transmitting Electrical Energy”, Jan. 18, 1902, U.S. Patent 1,119,732, Dec. 1, 1914.

[46] Schumann W. O., "Über Die Strahlungslosen Eigenschwingungen Einer Leitenden Kugel, Die Von Einer Luftschicht Und Einer Ionosphärenhülle Umgeben Ist". Zeitschrift und Naturfirschung 7a: 149–154, 1952.

[47] Simões, Fernando, Robert Pfaff, and Henry Freudenreich "Satellite Observations of Schumann Resonances in The Earth's Ionosphere." Geophysical Research Letters, vol. 38, no. 22, L22101, 2011.

[48] http://www.tfcbooks.com/articles/witricity.htm

[49] T. J. Lawry, G. J. Saulnier, J. D. Ashdown, K. R. Wilt, H. A. Scarton, S. Pascarelle, and J. D. Pinezich, “Penetration-free System for Transmission of Data And Power Through Solid Metal Barriers,” in Proc. MILCOM, pp. 389–395, Nov. 2011.

[50] Bao, Xiaoqi, Will Biederman, Stewart Sherrit, Mircea Badescu, Yoseph Bar-Cohen, Christopher Jones, Jack Aldrich, and Zensheu Chang. "High-power Piezoelectric Acoustic-electric Power Feedthru for Metal Walls." In The 15th International Symposium on: Smart Structures and Materials & Nondestructive Evaluation and Health Monitoring, pp. 69300Z-69300Z. International Society for Optics and Photonics, 2008.

[51] S. Ozeri, D. Shmilovitz, S. Singer, and CC. Wang, “Ultrasonic Transcutaneous Energy Transfer Using A Continuous Wave 650 Khz Gaussian Shaded Transmitter,” Ultrasonics, vol. 50, no. 7, pp. 666–674, Jun. 2010.

[52] S. Arra, J. Leskinen, J. Heikkilä, and J. Vanhala, “Ultrasonic Power and Data Link for Wireless Implantable Applications,” in Proc. 2nd ISWPC, pp. 567–571, Feb. 2007.

[53] J.O. Mur-Miranda, G. Fanti, Y. Feng, K. Omanakuttan, R. Ongie, A. Setjoadi and N. Sharpe, “Wireless Power Transfer Using Weakly Coupled Magnetostatic Resonators”, in Proc. ECCE, pp. 4179-4186, 2010.

[54] M. Pinuela, D. Yates, S. Lucyszyn and P.D. Mitcheson, “Maximising DC To Load Efficiency For Inductive Power Transfer”, IEEE Transaction on Power Electronics, vol. 28, no. 5, pp. 2437-2447, May 2013.

[55] F. Zhang, S.A. Hackworth, W. Fu, C. Li, Z. Mao, and M. Sun, “Relay Effect of Wireless Power Transfer Using Strongly Coupled Magnetic Resonances,” IEEE Transactions on Magnetics, vol. 47, no. 5, pp. 1478-1481, May 2011.

[56] C.K. Lee, W.X. Zhong and S.Y.R. Hui, “Effects of Magnetic Coupling of Non-adjacent Resonators on Wireless Power Domino-resonator Systems”, IEEE Trans. Power Electronics, vol. 27, no. 4, pp. 1905-1916, Apr. 2012.

[57] W.X. Zhong, C.K. Leeand, and S.Y.R. Hui, “Wireless Power Domino-resonator Systems with Noncoaxial Axes and Circular Structures”, IEEE Trans. Power Electronics, vol. 27, no. 11, pp. 4750- 4762, Nov. 2012.

[58] W.X. Zhong, C.K. Lee and S.Y.R. Hui, “General Analysis on the Use of Tesla's Resonators in Domino Forms for Wireless Power Transfer”, IEEE Trans. Industrial Electronics, vol. 60, no. 1, pp. 261-270, Jan. 2013.

[59] http://www.wirelesspowerconsortium.com

[60] Yilmaz, G.; Dehollaini, C., "An Efficient Wireless Power Link for Implanted Biomedical Devices via Resonant Inductive Coupling," Radio and Wireless Symposium (RWS), 2012 IEEE, pp. 235-238, Jan. 2012.

[61] Rui-Feng Xue; Basappa, K.P.; Hyouk-Kyu Cha; Yuanjin Zheng; Minkyu Je, "High-efficiency Transcutaneous Wireless Energy Transfer for Biomedical Applications," Defense Science Research Conference and Expo (DSR), 2011, pp.1-4, Aug. 2011.

[62] S. Cheon, Y.H. Kim, S.Y. Kang, M. L. Lee, J.M. Lee, and T. Zyung, “Circuit-Model-Based Analysis of A Wireless Energy-transfer System via Coupled Magnetic Resonances”, IEEE Transaction on Industrial Electronics, vol. 58, no. 7, pp. 2906-2914, Jul. 2011.

[63] Waffenschmidt, Eberhard, and Toine Staring. "Limitation of Inductive Power Transfer for Consumer Applications." In Power Electronics and Applications, 2009. EPE '09. 13th European Conference on, pp. 1-10, Sep, 2009.

[64] Sample, Alanson P., David A. Meyer, and Joshua R. Smith. "Analysis, Experimental Results, and Range Adaptation of Magnetically Coupled Resonators for Wireless Power Transfer." Industrial Electronics, IEEE Transactions on, vol. 58, issue 2, pp. 544-554, 2011.

[65] J. Park, Y. Tak, Y. Kim, Y. Kim, and S. Nam, “Investigation of Adaptive Matching Methods for Near-field Wireless Power Transfer”, IEEE Trans. Antennas and Propagation, vol. 59, no. 5, pp. 1769-1773, May 2011.

[66] Nam Yoon Kim; Ki Young Kim; Young-Ho Ryu; Jinsung Choi; Dong-Zo Kim; Changwook Yoon; Yun-Kwon Park; Sangwook Kwon, "Automated Adaptive Frequency Tracking System for Efficient Mid-range Wireless Power Transfer via Magnetic Resonance Coupling," Microwave Conference (EuMC), 2012 42nd European, pp. 221-224, Oct. 29 2012-Nov. 1 2012.

[67] W.S. Lee, W.I. Son, K.S. Oh and J.W. Yu, “Contactless Energy Transfer Systems Using Antiparallel Resonant Loops”, IEEE Trans. Industrial Electronics, vol. 60, no. 1, pp. 350-359, Jan. 2013.

[68] J.W. Kim, H.C. Son, K.H. Kim and Y.J. Park, “Efficiency Analysis of Magnetic Resonance Wireless Power Transfer with Intermediate Resonant Coil”, IEEE Antennas and Wireless Propagation Letters, vol. 10, pp. 389-392, 2011.

[69] M. Kiani, U.M. Jow and M. Ghovanloo, “Design and Optimization of a 3-coil Inductive Link for Efficient Wireless Power Transmission”, IEEE Trans. Biomedical Circuits and Systems, vol. 5, no. 6, pp. 579-591, Dec. 2011.

[70] S.H. Lee and R. D. Lorenz, “Development and Validation of Model for 95% Efficiency 220W Wireless Power Transfer over A 30-cm Air Gap”, IEEE Trans. Industry Applications, vol. 47, no. 6, pp. 2495-2504, Nov./Dec. 2011.

[71] T. Mizuno, S. Yachi, A. Kamiya and D. Yamamoto, “Improvement in Efficiency of Wireless Power Transfer of Magnetic Resonant Coupling Using Magnetoplated Wire”, IEEE Trans. Magnetics, vol. 47, no. 10, pp. 4445-4448, Oct. 2011.

[72] Brown, William C. "The History of Wireless Power Transmission." Solar Energy, vol. 56, no. 1, pp. 3-21, 1996.

[73] Brown, W. C. "Experiments Involving A Microwave Beam to Power and Position A Helicopter." Aerospace and Electronic Systems, IEEE Transactions on, vol. AES-5, issue 5, pp. 692-702, 1969.

[74] Brown W. C. “Combined Phase III and Final Report, Freespace Microwave Power Transmission Study,” Raytheon Report PT 4601. MSFC Contr. NAS-8-25374, 1975.

[75] Glaser, Peter E. "Power from The Sun: Its Future." Science, vol. 162, no. 3856, pp. 857-861, Nov. 1968.

[76] Matsumoto, Hiroshi. "Research on Solar Power Satellites and Microwave Power Transmission in Japan." Microwave Magazine, IEEE, vol. 3, no. 4, pp. 36-45, Dec. 2002.

[77] Matsumoto, H., et al., “MILAX Airplane Experiment and Model Airplane,” 12th ISAS Space Energy Symposium, Tokyo, Japan, March 1993.

[78] Schlesak, J. J., A. Alden and T. Ohno, “A Microwave Powered High Altitude Platform,” Microwave Symposium Digest, IEEE MTT-S International, vol. 1, pp. 283-286, May 1988.

[79] URSI White Paper on Solar Power Satellite (SPS) Systems, http://www.ursi.ca/SPS-2006sept.pdf

[80] Tanaka, K., Kenichiro, M., Takahashi, M., Ishii, T. and Sasaki, S. "Development of Bread Board Model for Microwave Power Transmission Experiment from Space to Ground Using Small Scientific Satellite." In Microwave Workshop Series on Innovative Wireless Power Transmission: Technologies, Systems, and Applications (IMWS), 2012 IEEE MTT-S International, pp. 191-194, 2012.

[81] Shinohara, Naoki. "Power Without Wires." Microwave Magazine, IEEE, vol. 12, no. 7, pp. S64-S73, Dec. 2011.

[82] http://techcrunch.com/2013/09/09/cota-by-ossia-wireless-power/

[83] Blackwell, T., “Recent Demonstrations of Laser Power Beaming at DFRC and MSFC.” AIP Conference Proceedings Beamed Energy Propulsion, Third International Symposium on Beamed Energy Propulsion, vol. 766, p.73-85, 2005.

[84] Frank Steinsiek, W. P. Foth, K. H. Weber, Christian Scha¨fer, and H. J. Foth. “Wireless Power Transmission Experiment as An Early Contribution to Planetary Exploration Missions.” In Proc. 54th International Astronautical Congress, Bremen, Germany, vol. 29, 2003.

[85] S. L. Karode and V. F. Fusco, “Frequency Offset Retrodirective Antenna Array,” Electronics Letters, vol. 33, no. 16, pp. 1350– 1351, 1997.

[86] C.W. Pobanz and T. Itoh, “A Conformal Retrodirective Array for Radar Applications Using A Heterodyne Phased Scattering Element,” in Proceedings of IEEE MITT-S International Microwave Symposium, vol. 2, pp. 905–908, May 1995.

[87] C. Luxey and J.-M. Laheurte, “A Retrodirective Transponder with Polarization Duplexing for Dedicated Short-range Communications,” IEEE Transactions on Microwave Theory and Techniques, vol. 47, no. 9, pp. 1910–1915, 1999.

[88] R. Y. Miyamoto, Y. Qian, and T. Itoh, “Retrodirective Array Using Balanced Quasi-Optical FET Mixers with Conversion Gain,” in Proceedings of the IEEE MTT-S International Microwave Symposium (MTT ’99), vol. 2, pp. 655–658, June 1999.

[89] Chen, Lei, Yu Chun Guo, Xiao Wei Shi, and Tian Ling Zhang. "Overview on The Phase Conjugation Techniques of The Retrodirective Array." International Journal of Antennas and Propagation, vol. 2010, article 564357, 2010.

[90] Akagi, Justin M., Alexis Zamora, Monte K. Watanabe, and Wayne A. Shiroma. "A Self-steering Array Using Power Detection and Phase Shifting." In Microwave Symposium Digest, 2008 IEEE MTT-S International, pp. 1325-1328, IEEE, 2008.

[91] T. Takahashi, T. Mizuno, M. Sawa, T. Sasaki, T. Takahashi, and N. Shinohara, ‘‘Development of Phased Array for High Accurate Microwave Power Transmission,’’ In Microwave Workshop Series on Innovative Wireless Power Transmission: Technologies, Systems, and Applications (IMWS), 2011 IEEE MTT-S International, pp. 157-160, 2011.

[92] A. K. M. Baki, K. Hashimoto, N. Shinohara, H. Matsumoto, and T. Mitani, ‘‘Comparison of Different Kinds of Edge Tapering System in Microwave Power Transmission,’’ IEICE Tech. Rep. SPS 2006-12, pp. 13–18, Dec. 2006.

[93] S. S. Shaposhnikov and V. N. Garmash, ‘‘Phase Synthesis of Antennas,’’ in Proc. IEEE Aerosp. Conf., vol. 2, pp. 891–900, 2002.

[94] V. Garmash, B. Z. Katsenelenbaum, S. S. Shaposhnikov, V. N. Tioulpakov, and R. B. Vaganov, ‘‘Some Peculiarities of The Wave Beams in Wireless Power Transmission,’’ IEEE Aerosp. Electron. Syst. Mag., vol. 13, no. 10, pp. 39–41, Oct. 1998.

[95] S. Takeshita, ‘‘Power Transfer Efficiency between Focused Circular Antennas with Gaussian Illumination in Fresnel Region,’’ IEEE Trans. Antennas Propag., vol. AP-16, no. 3, pp. 305–309, May 1968.

[96] Massa, Andrea, Giacomo Oliveri, Federico Viani, and Paolo Rocca. "Array Designs for Long-distance Wireless Power Transmission: State-of-the-Art and Innovative Solutions." Proceedings of the IEEE, vol. 101, no. 6, pp. 1464-1481, Mar. 2013.

[97] Yoo, T-W., "Experimental and Theoretical Study on 35 Ghz RF-to-DC Power Conversion Receiver for Millimeter-wave Beamed Power Transmission." Ph.D. Dissertation, Dept. of Electrical Engineering, Texas A&M University, Dec. 1993.

[98] H. Yin, Z. Wang, L. Ke, and J. Wang, “Monobit Digital Receivers: Design, Performance, and Application to Impulse Radio,” IEEE Trans. Commun., vol. 58, no. 6, pp. 1695–1704, Jun. 2010.

[99] C. R. Anderson, S. Venkatesh, J. E. Ibrahim, R. M. Buehrer, and J. H. Reed, “Analysis and Implementation of A Time-interleaved ADC Array for A Software-defined UWB Receiver,” IEEE Trans. Veh. Technol., vol. 58, no. 8, pp. 4046–4063, Oct. 2009.

[100] S. Lou and G. Bi, “Aliased Polyphase Sampling,” Signal Process., vol. 90, pp. 1323–1326, 2010.

[101] S. Hoyos and B. M. Sadler, “Frequency-domain Implementation of The Transmitted-reference Ultra-wideband Receiver,” IEEE Transaction on Microwave Theory and Techniques, vol. 54, no. 4, pp. 1745–1753, Jun. 2006.

[102] R. Thirugnanam and D. S. Ha, “A Feasibility Study on Frequency Domain ADC for Impulse-UWB Receivers,” Presented at the 4th Int. Conf. Circuits Systems Communications, Shanghai, China, 2008.

[103] S. Hoyos and B. M. Sadler, “UWB Mixed-signal Transform-domain Direct-sequence Receiver,” IEEE Trans. Wireless Commun., vol. 6, no. 8, pp. 3038–3046, Aug. 2007.

[104] M. E. Magana and Y. Chang, “A Channelized Digital Receiver Design for UWB Systems in A Multi-path Indoor Environment,” Wireless Pers. Commun., vol. 43, no. 4, pp. 1389–1397, Dec. 2007.

[105] A. Medi and W. Namgoong, “A High Data-rate Energy-efficient Interference-tolerant Fully Integrated CMOS Frequency Channelized UWB Transceiver for Impulse Radio,” IEEE J. Solid-State Circuits, vol. 43, no. 4, pp. 974–980, Apr. 2008.

[106] Sha, Shaoshu, Jinghong Chen, and Mingyu Lu. "Efficient Measurement of Impulses Based on Frequency-domain Approach." Instrumentation and Measurement, IEEE Transactions on, vol. 61, no. 6, pp. 1757-1764, 2012.

[107] Balanis, Constantine A. *Antenna theory: analysis and design*. 3rd Edition, John Wiley & Sons, 2012.

[108] Toh, Bee Yen, Vincent F. Fusco, and Niel B. Buchanan. "Assessment of Performance Limitations of PON Retrodirective Arrays." Antennas and Propagation, IEEE Transactions on, vol. 50, no. 10, pp. 1425-1432, Oct. 2002.

[109] http://www.skyworksinc.com/product.aspx?ProductID=511

Biographical Information

Shaoshu Sha received his Bachelor degree in Electrical Engineering, from Southeast University, Nanjing, China, in 2007, and Master degree in Electrical Engineering from University of Texas at Arlington, in 2009. After that, he worked as a research associate in the Wave Scattering Research Center in the University of Texas at Arlington. In August 2010, he joined the PhD program in the University of Texas at Arlington. His research areas include electromagnetics, antenna design, RF circuit design, and wireless charging.